

Universität Potsdam
Institut für Biochemie und Biologie

**Biocatalysis on Nanostructured Surfaces:
Investigation and Application of Redox Proteins using
Spectro-Electrochemical Methods**

**Dissertation
zur Erlangung des akademischen Grades
"doctor rerum naturalium"
(Dr. rer. nat.)
in der Wissenschaftsdisziplin "Analytische Biochemie"**

**eingereicht an der
Mathematisch-Naturwissenschaftlichen Fakultät
der Universität Potsdam**

**von
Stefano Frasca**

Potsdam, den 21. September 2011

Published online at the
Institutional Repository of the University of Potsdam:
URL <http://opus.kobv.de/ubp/volltexte/2012/5813/>
URN <urn:nbn:de:kobv:517-opus-58131>
<http://nbn-resolving.de/urn:nbn:de:kobv:517-opus-58131>

Table of Contents

List of Abbreviations	I
Abstract	III
Zusammenfassung	VI
Riassunto.....	IX
1 Introduction	1
1.1 Protein electrochemistry	1
1.1.1 Direct protein electrochemistry.....	2
1.1.2 Protein spectroelectrochemistry.....	3
1.1.3 Biosensors	4
1.2 Electrodes	7
1.2.1 Nanostructured electrode materials	7
1.3 Proteins	12
1.3.1 Cytochrome <i>c</i>	12
1.3.2 Mononuclear Molybdoenzymes	15
2 Aim of the work	28
3 Materials and Methods.....	29
3.1 Materials.....	29
3.1.1 Chemicals	29
3.1.2 Instruments	30
3.1.3 Buffers	35
3.2 Methods.....	35
3.2.1 Molar extinction coefficients.....	35
3.2.2 Spectroelectrochemical study of mesoporous materials	36
3.2.3 Electrochemical study of <i>h</i> SO on AuNPs.....	41
3.2.4 XDH spectroelectrochemical study	44
4 Results and Discussion.....	47

4.1	Mesoporous materials	47
4.1.1	Direct electron transfer of cyt <i>c</i> in mpITO.....	47
4.1.2	UV-Vis spectroelectrochemistry of cyt <i>c</i> in mpITO	51
4.1.3	Resonance Raman spectroelectrochemistry in mpITO.....	53
4.1.4	Spectroelectrochemical studies of cyt <i>c</i> in mpITBO	54
4.1.5	Superoxide biosensor	57
4.1.6	Reversible electro-system for biochemical switchable optical device ...	60
4.1.7	Spectroelectrochemical studies of <i>h</i> SO-HD in mpITO	64
4.1.8	Catalytic activity of <i>h</i> SO on planar ATO.....	66
4.2	Direct electrochemistry and catalytic activity of <i>h</i> SO on AuNP.....	70
4.2.1	Direct Electrochemistry of <i>h</i> SO	70
4.2.2	Surface enhanced resonance Raman spectroscopy.....	71
4.2.3	Catalytic activity of <i>h</i> SO	73
4.2.4	Sulfite biosensor	76
4.3	Direct electrochemistry of XDH and <i>m</i> AOH1.....	79
4.3.1	Direct Electrochemistry of immobilized proteins.....	79
4.3.2	Mediated spectroelectrochemical titration of XDHwt.....	82
5	Summary.....	85
6	References.....	93
7	List of publications	110
8	List of presentations.....	111
9	Acknowledgements.....	112

List of Abbreviations

ATO	Antimony doped tin oxide
Au	Gold
cSO	<i>Chicken</i> sulfite oxidase
CV	Cyclic Voltammetry
CVA	Cyclic voltabsorptogram
cyt c	Cytochrome c
DCVA	Derivative voltabsorptogram
DDAB	Didodecyldimethylammonium bromide
DET	Direct electron transfer
DNA	Deoxyribonucleic acid
E^0	Formal potential
EDC	N-Ethyl-N'-(3-dimethylaminopropyl)carbodiimide hydrochloride
EP-GC	Electrochemically pretreated glassy carbon
EPR	Electron paramagnetic resonance
ET	Electron transfer
k_{et}	heterogeneous electron transfer rate constant
K_m	Michaelis-Menten constant
GC	Glassy carbon
HD	Sulfite oxidase heme <i>b5</i> domain
HET	Heterogeneous electron transfer
<i>hSO</i>	<i>Human</i> sulfite oxidase
IET	Intramolecular electron transfer
IEP	Isoelectric point
ITO	Tin doped indium oxide
ITBO	<i>Tin rich</i> indium tin oxide
<i>mAOH1</i>	<i>Mouse</i> Aldehyde oxidase homolog 1
Moco	Molybdenum cofactor
MD	Sulfite oxidase Moco domain
MPT	Molybdopterin
MU	Mercapto-undecanol
MUA	Mercapto-undecanoic acid
NP	Nanoparticle
NHE	Normal hydrogen electrode
OTTLE	Optical transparent thin-layer electrochemical
PGE	Pyrolytic graphite electrode
PEI	Polyethylenimine
RRS	Resonance Raman spectroscopy
SAM	Self assembled monolayer
SDH	Sulfite dehydrogenase
SERRS	Surface enhanced resonance Raman spectroscopy
SHE	Standard hydrogen electrode
SOD	Superoxide dismutase
SWCNT	Single-walled carbon nanotubes
TMB	3, 3', 5, 5'-tetramethylbenzidine
TCO	Transparent conductive oxide
XDH	Xanthine dehydrogenase
XDHwt	Xanthine dehydrogenase wild type
XOD	Xanthine oxidase

Abstract

In this thesis, different aspects within the research field of protein spectro- and electro-chemistry on nanostructured materials are addressed. On the one hand, this work is related to the investigation of nanostructured transparent and conductive metal oxides as platform for the immobilization of electroactive enzymes. On the other hand the second part of this work is related to the immobilization of sulfite oxidase on gold nanoparticles modified electrode. Finally direct and mediated spectroelectrochemistry protein with high structure complexity such as the xanthine dehydrogenase from *Rhodobacter capsulatus* and its high homologues the mouse aldehyde oxidase homolog 1.

Stable immobilization and reversible electrochemistry of cytochrome *c* in a transparent and conductive tin-doped and *tin-rich* indium oxide film with a well-defined mesoporosity is reported. The transparency and good conductivity, in combination with the large surface area of these materials, allow the incorporation of a high amount of electroactive biomolecules (between 250 and 2500 pmol cm⁻²) and their electrochemical and spectroscopic investigation. Both, the electrochemical behavior and the immobilization of proteins are influenced by the geometric parameters of the porous material, such as the structure and pore shape, the surface chemistry, as well as the protein size and charge. UV-Vis and resonance Raman spectroscopy, in combination with direct protein voltammetry, are employed for the characterization of cytochrome *c* immobilized in the mesoporous indium tin oxide and reveal no perturbation of the structural integrity of the redox protein. A long term protein immobilization is reached using these unmodified mesoporous indium oxide based materials, i.e. more than two weeks even at high ionic strength.

The potential of this modified material as an amperometric biosensor for the detection of superoxide anions is demonstrated. A sensitivity of about 100 A M⁻¹ m⁻², in a linear measuring range of the superoxide concentration between 0.13 and 0.67 μM, is estimated.

In addition an electrochemical switchable protein-based optical device is designed with the core part composed of cytochrome *c* immobilized on a mesoporous indium tin oxide film. A color developing redox sensitive dye is used as switchable component of the system. The cytochrome *c*-catalyzed oxidation of the dye by

hydrogen peroxide is spectroscopically investigated. When the dye is co-immobilized with the protein, its redox state is easily controlled by application of an electrical potential at the supporting material. This enables to electrochemically reset the system to the initial state and repetitive signal generation.

The case of negative charged proteins, which does not have a good interaction with the negative charged indium oxide based films, is also explored. The modification of an indium tin oxide film with a positive charged polymer and the employment of an antimony doped tin oxide film were investigated in this work in order to overcome the repulsion induced by similar charges of the protein and electrode. *Human* sulfite oxidase and its separated heme-containing domain are able to directly exchange electrons with the supporting material.

A study of a new approach for sulfite biosensing, based on enhanced direct electron transfer of a *human* sulfite oxidase immobilized on a gold nanoparticles modified electrode is reported. The spherical gold nanoparticles were prepared via a novel method by reduction of HAuCl_4 with branched poly(ethyleneimine) in an ionic liquid resulting in particles of about 10 nm in hydrodynamic diameter.

These nanoparticles were covalently attached to a mercaptoundecanoic acid modified Au-electrode and act as platform where *human* sulfite oxidase is adsorbed. An enhanced interfacial electron transfer and electrocatalysis is therefore achieved. UV-Vis and resonance Raman spectroscopy, in combination with direct protein voltammetry, were employed for the characterization of the system and reveal no perturbation of the structural integrity of the redox protein. The proposed biosensor exhibited a quick steady-state current response, within 2 s and a linear detection range between 0.5 and 5.4 μM with high sensitivity ($1.85 \text{ nA } \mu\text{M}^{-1}$). The investigated system provides remarkable advantages, since it works at low applied potential and at very high ionic strength. Therefore these properties could make the proposed system useful in the development of bioelectronic devices and its application in real samples.

Finally protein with high structure complexity such as the xanthine dehydrogenase from *Rhodobacter capsulatus* and the *mouse* aldehyde oxidase homolog 1 were spectroelectrochemically studied. It could be demonstrated that different cofactors present in the protein structure, like the FAD and the molybdenum cofactor, are able

to directly exchange electrons with an electrode and are displayed as a single peak in a square wave voltammogram. Protein mutants bearing a serine substituted to the cysteines, bounding to the most exposed iron sulfur cluster additionally showed direct electron transfer which can be attributable to this cluster. On the other hand a mediated spectroelectrochemical titration of the protein bound FAD cofactor was performed in presence of transparent iron and cobalt complex mediators. The results showed the formation of the stable semiquinone and the fully reduced flavin. Two formal potentials for each single electron exchange step were then determined.

Zusammenfassung

In dieser Arbeit werden verschiedenen Aspekte im Forschungsfeld der Protein-Spekro- und Elektro-Chemie an nanostrukturierte Materialien behandelt. Zum einen werden in dieser Arbeit nanostrukturierte, transparente und leitfähige Metalloxide als Basis für die Immobilisierung von elektroaktiven Enzym untersucht.

Des Weiteren behandelt diese Arbeit die Immobilisierung von *humaner* Sulfitoxidase auf einer Gold-Nanopartikel-modifizierten Elektrode. Schließlich wird die direkte und die vermittelte Elektrochemie von Xanthindehydrogenase aus *Rhodobacter capsulatus* und Aldehydoxidase Homolog 1, aus *Mause*, vorgestellt.

Im ersten Teil der Arbeit wird über die stabile Immobilisierung und reversible Elektrochemie von Cytochrom *c* in einem transparenten und leitfähigen Zinn-dotierten und Zinn-reichen Indiumoxid Film mit einer gut definierten Mesoporosität berichtet. Die Transparenz und gute Leitfähigkeit in Kombination mit der großen Oberfläche dieser Materialien erlauben die Inkorporation einer große Menge elektroaktiver Biomoleküle (zwischen 250 und 2500 pmol cm⁻²) und deren elektrochemische und spektroskopische Untersuchung. Das elektrochemische Verhalten und die Proteinimmobilisierung sind durch die geometrischen Parameter des porösen Materials, wie die Struktur und Porenform, die Oberflächenchemie, sowie die Größe und Ladung des Proteins beeinflusst. UV-Vis und Resonanz-Raman-Spektroskopie in Kombination mit direkter Protein-Voltammetrie werden für die Charakterisierung von Cytochrom *c* eingesetzt und zeigen keine Störung der strukturellen Integrität des Redox-Proteins durch die Immobilisierung. Eine langfristige Immobilisierung des Proteins von mehr als zwei Wochen auch bei hoher Ionenstärke wurde unter Verwendung dieser unmodifizierten mesoporösen Indiumoxid-basierten Materialien erreicht.

Das Potential dieses modifizierten Materials für die Verwendung in einem amperometrischen Biosensor zum Nachweis von Superoxid-Anionen wurde aufgezeigt. Es wurde eine Empfindlichkeit von etwa 100 A M⁻¹ m⁻², in einem linearen Messbereich der Superoxidkonzentration zwischen 0,13 und 0,67 µM, erreicht.

Außerdem wurde ein elektrochemisch umschaltbares Protein-basiertes optisches Gerät konzipiert mit Cytochrom *c* und der mesoporösen Indiumzinnoxidschicht. Ein redox-sensitiver Farbstoff wurde als schaltbare Komponente des Systems

verwendet. Die Cytochrom c Oxidation des Farbstoffs durch Wasserstoffperoxid wurde spektroskopisch untersucht. Der Redox-Zustand des Farbstoffs, co-immobilisiert mit dem Protein, ist leicht durch das Anlegen eines elektrischen Potentials an das Trägermaterial kontrollierbar. Dadurch wird die elektrochemische Zurücksetzung des Systems auf den Anfangszustand und eine repetitive Signalerzeugung ermöglicht.

Für negativ geladene Proteine, die keine gute Interaktion mit dem negativ geladenen Indiumoxid-basierten Film zeigen wurden die Modifikation der Indiumzinnoxidschicht mit einem positiv geladenen Polymer sowie die Verwendung eines Antimon-dotierten Zinnoxid Films vorgeschlagen. Dadurch konnte die Abstoßung induziert durch die ähnliche Ladung des Proteins und der Elektrode überwunden werden. Es gelang für die *humane* Sulfite-Oxidase und die separate Häm-haltige Domäne der Austausch von Elektronen mit dem Trägermaterial.

Im zweiten Teil der Arbeit wird über eine neue Methode für die Biosensorik von Sulfite berichtet, bei der direkte Elektronentransfer von *humaner* Sulfiteoxidase immobilisierten auf einer mit Gold-Nanopartikeln modifizierten Elektrode verstärkt wurde. Die sphärischen Gold-Nanopartikeln, von etwa 10 nm im Durchmesser, wurden über eine neue Methode durch Reduktion von HAuCl_4 mit verzweigtem Polyethylenimin in einer ionischen Flüssigkeit synthetisiert.

Diese Nanopartikel wurden kovalent an eine mit Mercaptoundecansäure modifizierten Gold-Elektrode immobilisiert und dienen als Basis für die Adsorption von Sulfiteoxidase adsorbiert wurde. Dadurch wurde ein schneller heterogener Elektronen-Transfer und verbesserte Elektrokatalyse erreicht. Für die Charakterisierung des verwendeten Systems eingesetzt wurden UV-Vis und Resonanz-Raman-Spektroskopie in Kombination mit direkter Protein-Voltammetrie. Es wurde keine Störung der strukturellen Integrität des Redox-Proteins beobachtet. Der vorgeschlagene Biosensor zeigte eine schnelle steady-state Stromantwort innerhalb von 2 s, eine lineare Detektion im Bereich zwischen 0,5 und 5,4 μM Sulfite mit einer hohen Empfindlichkeit ($1,85 \text{ nA } \mu\text{M}^{-1}$). Das untersuchte System bietet bemerkenswerte Vorteile da es ermöglicht bei niedriger angelegter Spannung und bei sehr hoher Ionenstärke zu arbeiten. Aufgrund dieser Eigenschaften hat das vorgeschlagene System großes Potential für die Entwicklung von bioelektronischen Geräten und der Anwendung in realen Proben.

Schließlich werden im letzten Teil der Arbeit die komplexeren Enzymen Xanthindehydrogenase aus *Rhodobacter capsulatus* und Maus Aldehydoxidase Homolog 1 spektro- und elektrochemisch untersucht. Es konnte gezeigt werden, dass verschiedene Kofaktoren in der Proteinstruktur, wie FAD und der Molybdän-Kofaktor direkt Elektronen mit einer Elektrode austauschen können, was durch einzelne Peaks im Square Wave Voltammogramm angezeigt wird. Es konnte eine zusätzliche redoxaktive Gruppe mit direktem Elektronen-Transfer nach Austausch eines Cysteins durch Serin am exponierten Eisen-Schwefel-Cluster gezeigt werden. Außerdem wurde eine vermittelte spektroelektrochemische Titration des FAD-Kofaktors in Anwesenheit von Mediatoren der Klasse der Eisen und Kobalt-Komplexe durchgeführt. Die Ergebnisse zeigen, dass FAD in *R. capsulatus* XDH zu einem stabilen Semichinone reduziert werden kann. Es gelang die formalen Potentiale für die zwei einzigen Elektrontransferprozesse zu bestimmen.

Riassunto

In questa tesi sono affrontati diversi aspetti nello studio spettro- ed elettro-chimico di proteine su materiali nanostrutturati. Nel presente lavoro è inizialmente discussa la ricerca svolta su ossidi metallici nanostrutturati, trasparenti ed elettricamente conduttivi usati da piattaforma per l'immobilizzazione di proteine elettroattive. La seconda parte riguarda l'immobilizzazione della solfito ossidasi su elettrodi modificati con nanoparticelle di oro. Infine viene presentata l'analisi spettroelettrochimica diretta e mediata della xantina deidrogenasi del *Rhodobacter capsulatus* e del suo omologo l'aldeide ossidasi omologo 1, del *topo*.

In questa tesi vengono inizialmente discusse la reversibile elettrochimica e la stabile immobilizzazione del citocromo *c* su pellicole trasparenti e conduttive, quali l'ossido d'indio drogato allo stagno e l'ossido d'indio ricco di stagno, dotate di una ben definita mesoporosità. La loro trasparenza unita alla buona conduttività, in combinazione con l'estesa superficie di questi materiali, permette l'intrappolamento di un'elevata quantità di biomolecole elettroattive (tra 250 e 2500 pmol cm⁻²) e il loro studio sia elettrochimico che spettroscopico. Il comportamento elettrochimico così come l'immobilizzazione proteica sono influenzati dai parametri geometrici del materiale poroso, come ad esempio la struttura e la forma dei pori, dalla chimica di superficie, così come dalle dimensioni e la carica della proteina in esame. La spettroscopia UV-Vis e risonanza Raman, in combinazione con la voltammetria diretta, sono impiegati per la caratterizzazione del citocromo *c* immobilizzato nella porosità dei materiali. Nessuna perturbazione nell'integrità strutturale della proteina è stata rilevata. Un'immobilizzazione della proteina a lungo termine è stata ottenuta utilizzando questi materiali mesoporosi a base di ossido di indio senza alcuna modificazione. Nello specifico il sistema risulta stabile per più di due settimane anche ad elevata forza ionica.

Il potenziale di del sistema proposto come biosensore amperometrico viene mostrato per la rilevazione di anioni superossido. La sensibilità risulta essere di circa 100 A M⁻¹ m⁻², in un intervallo lineare di misura per la concentrazione del superossido compreso tra 0,13 e 0,67 μM.

Inoltre, un dispositivo ottico commutabile elettrochimicamente e basato su citocromo *c* immobilizzato su una pellicola mesoporosa di ossido d'indio e stagno è

stato progettato e sviluppato. Un visibile colorante redox è stato utilizzato come elemento commutabile nel sistema. Spettroscopicamente si è indagata l'ossidazione del colorante da parte di perossido d'idrogeno e catalizzata dal citocromo. Quando il colorante viene *co*-immobilizzato con la proteina, il suo stato redox è facilmente controllabile mediante l'applicazione di un potenziale elettrico al materiale di supporto. Ciò consente di ripristinare il sistema elettrochimico nello stato iniziale e la generazione ripetitiva di nuovi segnali.

Il caso di proteine cariche negativamente, le quali non presentano una buona interazione con pellicole basate sull'ossido d'indio, anch'esse cariche negativamente, è stato anche esplorato. La modifica di una pellicola di ossido d'indio e stagno con un polimero carico positivamente e l'impiego di una pellicola di ossido di stagno drogato con antimonio sono stati studiati in questo lavoro al fine di superare la repulsione indotta dall'analogia di carica tra proteina ed elettrodo. Solfito ossidasi *umana* e il suo isolato dominio contenente l'eme sono in grado di scambiare elettroni direttamente con il materiale di supporto.

Si riporta inoltre lo studio di un nuovo approccio per la biopercezione di solfito, basato su un migliorato trasferimento elettronico diretto della solfito ossidasi *umana* mediante immobilizzazione su un elettrodo modificato con nanoparticelle di oro. Le nanoparticelle di oro sferiche sono state sintetizzate attraverso un inedito metodo consistente nella riduzione di HAuCl_4 in uno ione liquido per mezzo di polietilenimina ramificata. Il diametro idrodinamico risultante è stato rilevato di circa 10 nm.

Tali nanoparticelle sono state fissate covalentemente su un elettrodo di oro modificato con acido mercaptoundecanoico e fungono da piattaforma per l'assorbimento della solfito ossidasi. Elettrocatalisi, in presenza di substrato, e un trasferimento di elettroni all'interfaccia migliorati rispetto ad uno stesso elettrodo senza nanoparticelle è stato così ottenuto. UV-Vis e spettroscopia Raman amplificata da superfici, in combinazione con la voltammetria diretta, sono stati impiegati per la caratterizzazione del sistema e non rivelano perturbazione nell'integrità strutturale dell'enzima. Il biosensore proposto mostra un rapido raggiungimento di una stabile risposta, in circa 2 s, un intervallo di rilevamento lineare compreso tra 0,5 e 5,4 mM e una elevata sensibilità ($1,85 \text{ mM}^{-1} \text{ nA}$). Il sistema studiato fornisce notevoli vantaggi come la possibilità di lavorare a un'alta forza ionica e applicando un basso

potenziale. Queste proprietà potrebbero pertanto rendere il sistema proposto utile nello sviluppo di dispositivi bioelettronici e il loro utilizzo per campioni reali.

Infine proteine molto complesse come la xantina deidrogenasi del *Rhodobacter capsulatus* e l'aldeide ossidasi, omologo 1, del *topo*, sono state studiate spettroelettrochimicamente. In questo lavoro viene dimostrato che cofattori diversi presenti nella struttura delle proteine, come la FAD e il cofattore molibdeno, sono in grado di scambiare direttamente elettroni con un elettrodo e vengono visualizzati come un unico picco in voltammetria ad onda quadra. Proteine mutanti, recanti una serina sostituita a una delle cisteine leganti il più esposto dei centri ferro-zolfo, mostrano inoltre trasferimento diretto di elettroni attribuibile a tale centro. Un ulteriore studio del cofattore FAD è stata eseguita per mezzo di titolazione spettroelettrochimica mediata. Complessi trasparenti di ferro e cobalto sono stati usati come mediatori. I risultati dimostrano la formazione di un semichinone stabile del FAD all'interno della struttura proteica possedente due singoli potenziali formali per ogni scambio di elettroni.

1 Introduction

1.1 Protein electrochemistry

The field of protein electrochemistry deals with redox proteins which are able to exchange electrons with an electrode either with the protein free in solution or confined on an electrode surface. It can be usually divided into two groups (Figure 1).

In one case an external shuttle molecule is employed as mediator to facilitate the electron transfer (ET) and it is referred as mediated electron transfer (MET). In any mediated enzyme catalytic reaction, the mediator must exchange electrons rapidly with the electrode, since a sustained flow of electrons is required. The electrons are provided by the electrode via the mediator.

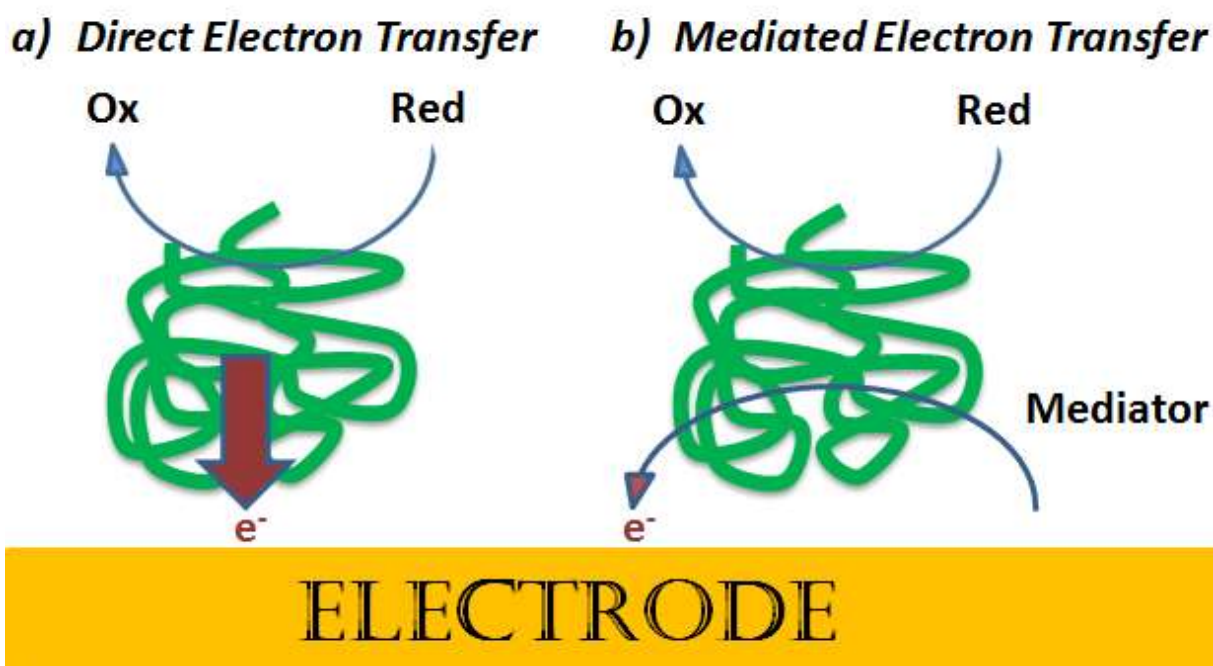


Figure 1. Scheme of electron transfer processes on an electrode surface. (a) Direct Electron Transfer (DET) and (b) Mediated Electron Transfer (MET) between electrode and protein.

In the other case the electron transfer occurs directly between the protein and the electrode and is called direct electron transfer (DET). It was thought for a long time to be virtually impossible. However, from the first publications in the '70s (Eddowes *et al.*, 1977; Yeh *et al.*, 1977) investigations in this field boomed. DET provides rapid and direct measurements of redox properties and a wide range of electrode potentials can be applied. Together with the precise redox control afforded by the

electrode potential it offers an excellent temporal resolution of the activity assay. Therefore a precise characterization how activity quickly evolves with time following an instant change in experimental conditions is possible. Furthermore unspecific side reactions of the mediator, that may cause erroneous results, are prevented.

1.1.1 Direct protein electrochemistry

Direct protein electrochemistry where a protein is confined on an electrode surface is a powerful tool for investigating the catalytic properties of redox enzymes. From an operational perspective, direct protein electrochemistry of surface immobilized molecules also has a number of other advantages, not at least the very small amounts of the often “priceless” biological material required, down to pmol cm^{-2} , in comparison with other more classical techniques (Armstrong *et al.*, 1988; Armstrong, 2002; Léger *et al.*, 2008). After immobilization, the same sample can be reused for the further studies. Precondition for the application of this technique, it is the ability to connect the active site of the enzyme to the electrode. Basically, two different strategies can be employed, either protein modification with genetic or chemical engineering techniques (Campàs *et al.*, 2009; Caruana *et al.*, 2010) or novel interfacial technologies (Hill *et al.*, 1989; Fedurco, 2000).

The ET is a radiation less electronic rearrangement where an electron moves from an initial state on an electrode or reductant to a receiving state on another solvated species or on an electrode of the same energy. The rate is strongly dependent from the potential difference and the spatial distance between the two redox sites (Marcus *et al.*, 1985; Marcus, 1993). Direct protein electrochemistry enables to exploit the naturally high efficiency of biological systems for developing selective biosensors, energy storage and production systems like biofuel cells, heterogeneous catalysts, and biomolecular electronic components (Léger *et al.*, 2008).

The most successful electrodes for proteins so far have been noble metals and carbon due to their elevated conductivity and easy handling. However they often lead to an irreversible adsorption and denaturation of the proteins onto the electrode surface and therefore to the impossibility to establish fast ET. A wide used method to solve this problem is the modification of the electrode by a promoter, which can prevent the protein denaturation and can lead also to a specific protein-electrode orientation (Armstrong, 2002). The promoter can reduce the distance between the active site of the protein and the electrode (Armstrong, 1990). It is not electroactive

itself and can interact with the enzyme by different kind of forces (electrostatic, hydrophobic, hydrogen bounds, etc.). By this approach, a DET reaction can be obtained or in alternative the usage of mediators can solve possible distance problems and permits the electron shuttling (Figure 1). General promoters are self-assembly monolayers of amphiphiles or polyelectrolytes (Scheller *et al.*, 2002; Allen *et al.*, 1984; Fedurco, 2000; Rusling *et al.*, 2008) with several possible functionalities. A drawback of this approach, however, is that the amount of immobilized protein is limited to monolayer coverage. Larger amounts of protein, can be obtained by alternate deposition of proteins and polyelectrolytes (“layer-by-layer” technique) (Beissenhirtz *et al.*, 2004; Grochol *et al.*, 2007; Spricigo *et al.*, 2009; Dronov *et al.*, 2007; Ram *et al.*, 2001; Calvo *et al.*, 2004). However this advantage is counterbalanced by the limited accessibility of the active sites of the proteins in the inner layers and the low stability.

The advent of nanoscaled materials such as nanotubes, nanoparticles, conductive and non-conductive metal oxides opens new horizons for the field of bioelectronics due to the likely deep interactions between the nanomaterials and the proteins (Armstrong, 2002; Bernhardt, 2006; Chen *et al.*, 2007; Wollenberger *et al.*, 2008).

1.1.2 Protein spectroelectrochemistry

The coupling of electrochemical and optical methods has been used for decades to study a large range of organic, inorganic and biological redox systems (Kuwana *et al.*, 1976; Heineman *et al.*, 1984). Although a large variety of electrochemical methods are available, they do not render any structural information of the electrode system besides the detailed knowledge of charge transfer, transport and distribution. The combination of electrochemical and optical methods to monitor the spectroscopic variations associated to the potential changes allows a qualified picture of the chemical structures in electrochemical reactions. The potential of the analyzed solution may be easily changed by addition of reductants or oxidants. On the other hand it can be electronically changed by potential imposition at an electrode. A classical set for such an experiment consist in an optical transparent thin-layer electrochemical (OTTLE) cell, with a metallic paint ensuring electrical conductivity and preserving some degree of transparency (Pinkerton *et al.*, 1980; Bowden, *et al.*, 1982; Heineman *et al.*, 1984; Dai *et al.*, 2011).

A large variety of spectroscopic methods may be coupled, from UV-Vis, infra-red (IR) (Arion *et al.*, 2011), resonance Raman (RR) (Kavan *et al.*, 2009) and surface enhanced resonance Raman (SERR) (Murgida *et al.*, 2006) to electron paramagnetic resonance (EPR) (Paulsen *et al.*, 1992) and nuclear magnetic resonance (NMR) (Klod *et al.*, 2009). Nevertheless, there are some spectroscopic methods which are preferred in spectroelectrochemistry. The choice of the method is often dominated by not the importance of a spectroscopic method which offers the access of important structural data of an electron-transfer reaction in experimental studies, but in most cases, the ease of application. UV-Vis spectroscopy is the most applied method in spectroelectrochemistry irrespective of the fact that other methods would result in more detailed structural informations (Dunsch, 2011).

Spectroelectrochemical studies were usually restricted to solution samples, where a relative concentrated sample is required, attenuated total internal reflection mode or with reflection cells (Bernad *et al.*, 2006). Only with a signal enhancement, like with Raman spectroscopy through surface plasmon resonance, the noteworthy reduction of sample volume and concentration can be obtained.

Absorption UV-Vis spectroelectrochemical investigation of protein boosted in the last time by the improvements in the field of nanostructured transparent conductive oxide. The possibility to entrap a large amount of protein in the porous structure of such materials overcomes the lack of sensitivity (Szamocki *et al.*, 2007). In addition these materials offer a high transparency in the UV-Vis region and elevated conductivity over the whole potential range commonly used for proteins investigation (Topoglidis *et al.*, 2001; Panicco *et al.*, 2008; Renault *et al.*, 2011).

1.1.3 Biosensors

A biosensor is defined as a specific type of chemical sensor comprising a biological or biologically derived recognition element either integrated within or intimately associated with a physicochemical transducer. The biological element is capable of recognizing the presence, activity or concentration of a specific analyte in solution (Thévenot *et al.*, 1999; Thévenot *et al.*, 2001; Hall, 2002). An analyte is the compound whose concentration has to be measured. Biosensors basically involve the quantitative analysis of various substances by converting their biological actions into measurable signals. Generally the performance of the biosensors is mostly

dependent on the specificity and sensitivity of the biological reaction, besides the stability of the biological element.

In general a biosensor comprises three parts: a biological recognition element, a suitable transducer and an amplification element (Figure 2).

The transducer is an important component of a biosensor through which the measurement of the target analyte(s) is achieved by selective transformation of a biomolecule-analyte interaction into a quantifiable output signal. The mode of transduction may be one of several approaches, including electrochemical, optical, piezoelectric, magnetic or thermometric transducers.

Every biomolecule from enzyme to an antibody, a nucleic acid, a hormone, an organelle or whole cell which can selectively interact with other substances, can be theoretically qualified for biosensor development. Usually, sensors are distinguished (Thévenot *et al.*, 1999) in sensors using *catalytic* biorecognition elements (enzymes, cells, microorganisms) (Gu *et al.*, 2004) and *affinity*-based recognition elements (antibodies, antigens, protein receptors, synthetic receptors, nucleic acids) (Paleček, 2005) (Ge *et al.*, 2008). Catalytic sensors own the concomitant ability to amplify the signal and regenerate the active site of the biorecognition element (Dryhurst *et al.*, 1982).

A wide range of enzymes, owing a combination of specificity and amplification properties, has been successfully used as a recognition element. Since enzymes allow a wide range of transduction technologies, they have found very wide applications in the field of biosensors (Schuhmann *et al.*, 2003).

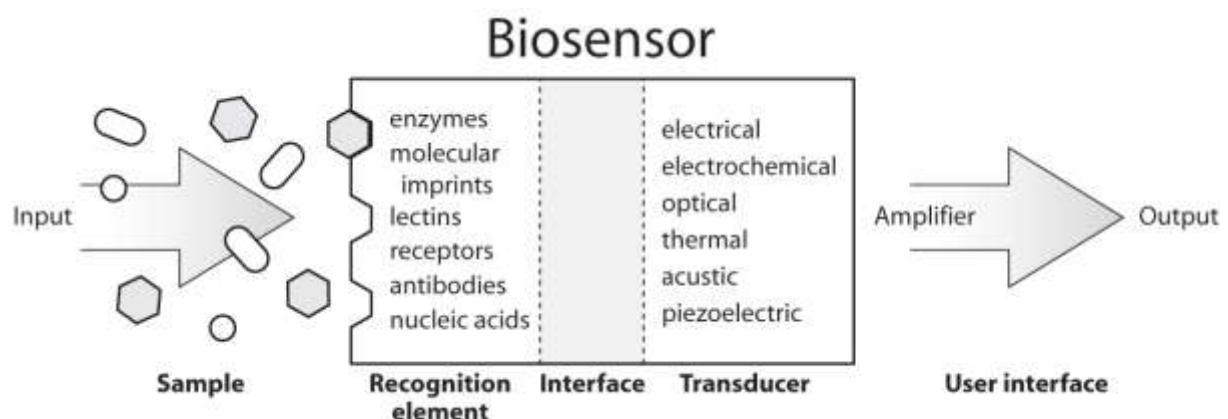


Figure 2. Configuration of a biosensor showing biorecognition, interface, and transduction elements (Chambers *et al.*, 2008).

Other kinds of proteins used are for example membrane bound receptors that change their structural conformation binding specific ligands. This modification triggers an amplified physiological response, such as ion channel opening or secreting an enzyme. High affinity and specificity towards the natural targets are the advantages of such recognition system.

Although the biosensors suffer general problem of stability and complexity connected to the biological recognition element, they offer many advantage in respect to classical analytical methods. Biosensors show a very broad range of detectable analytes, depending on the nature of the recognition element, and high analyte selectivity with the limitation of interferences in complex samples. Furthermore, the current tendency in biosensor development is the miniaturization. This enables and will further expand the integration and parallelization of biosensors in sophisticated systems.

1.1.3.1 Electrochemical enzyme based biosensors

Biosensors that utilize enzymes as recognition elements represent a wide extensively studied area, with glucose biosensors dominating the market (Frost & Sullivan, 2006). Enzymes are favored as recognition elements in biosensors because they provide a broad range of changes of physical and chemical parameters during the enzymatic reaction, such as electrons, protons, ions, mass, light and heat. These changes can be detected using suitable transducer elements. Different electrochemical methods as potentiometry, voltammetry and amperometry exist, where either the potential or the current change depending on the concentration of the analyte can be measured. Selective and sensitive catalysis of a substrate at relative low potentials are the great power of enzymes.

Electrochemical enzyme-based sensors are often separated in three different types or generations. *First generation* sensors measure the signal via the natural secondary substrates and products of the enzyme catalyzed reaction. In the *second generation* sensors an artificial electron mediator is used instead of the natural *co*-substrates. Indeed enzymes in direct electronic contact, based on direct protein electrochemistry are considered as *third generation* sensors. Their direct electron transfer (DET) between the electrode and the protein (Figure 1) may avoid most of the interferences (Wollenberger, 2005).

1.2 Electrodes

1.2.1 Nanostructured electrode materials

Nanomaterials have number of features that make them ideally suited for sensor applications, such as its high surface area, high reactivity, controlled electrode modification and defined interaction with other partner, e.g. biomolecules. They find large employ in different fields ranging from biosensors to biofuel cells or more complex bioelectronic systems. Nanostructured materials include dendrimers, nanoparticles, nanotubes, nanopores etc (Umasankar *et al.*, 2009).

1.2.1.1 Indium Tin Oxide

Using film of intrinsic stoichiometric materials like metals partial transparency, with moderate reduction in conductivity, can be obtained. However such materials may not achieve high transparency and coincidentally elevated conductivity.

A solution is to create electron degeneracy in a material with a wide energy bandgap ($E_g > 3\text{eV}$ or more for visible radiation) by introduction of non-stoichiometry and/or appropriate dopants. A large number of non-stoichiometric and doped oxide films (indium, tin, antimony, cadmium, zinc etc.) meet these conditions and exhibit high transmittance and nearly metallic conductivity (Chopra *et al.*, 1983).

Tin doped indium oxide or indium tin oxide (ITO), with a mean transmittance of 95% and conductivity as high as $10^4 \text{ S}^{-1}\text{cm}^{-1}$, is among the most popular of these thin films (Granqvist *et al.*, 2002).

ITO is essentially formed by substitutional doping of In_2O_3 with Sn which replaces the In^{3+} atoms from the cubic bixbyte structure of indium oxide (Fan *et al.*, 1977). Tin, which exists either as SnO or SnO_2 , forms an interstitial bond with oxygen. These two valency states have a direct influence on the ultimate conductivity of ITO. The lower valence state (+2) results in a net reduction in carrier concentration since the hole created acts as a trap and reduces the conductivity. On the other hand, predominance of the SnO_2 state (+4) acts as a *n*-type donor releasing electrons to the conduction band. The high conductivity of ITO films is due to high carrier concentration and their mobility increases due to enhanced crystallinity of films deposited at high temperatures (Balasubramanian *et al.*, 1989).

The high optical transmittance of this material is a direct consequence of being a semiconductor with a wide bandgap and therefore the absorption region generally lies in the ultraviolet part of the electromagnetic spectrum and shifts to shorter wavelengths with increasing carrier concentration (Gupta *et al.*, 1989). The transmittance of ITO films is also influenced by a number of minor defects which include surface roughness and optical inhomogeneity. Opaqueness has been attributed also to unoxidised tin metal grains on the ITO surface as a result of instability due to the absence of sufficient oxygen during the deposition (Fan *et al.*, 1977) or external induction by an applied potential (Kraft *et al.*, 1994; Senthilkumar *et al.*, 2008).

X-ray photoelectron spectroscopy studies of ITO surfaces showed high concentrations of $\text{In}(\text{OH})_3$ -like and InOOH -like surface species, indicating an excess of negative surface charge (Milliron *et al.*, 2000).

ITO has found an employment in electronic, opto-electronic and mechanical applications. Uses of ITO have traditionally ranged from transparent heating elements of aircraft and car windows, heat reflecting mirrors, antireflection and antistatic coatings, over electronic instrument display panels and even in high temperature gas sensors. Early electro-optic devices using ITO include charge-coupled devices, liquid crystal displays and as transparent electrodes for various display devices like touchscreens. More recently, ITO has been used as a transparent contact in advanced optoelectronic devices such as solar cells, light emitting and photo diodes, photo transistors and lasers.

In parallel to the planar films, ITO with a well-defined mesoporous framework (mpITO) is of considerable interest. With its unique combination of transparency, high conductivity, well-defined 3D mesoporosity and high surface area, mpITO allows the incorporation of a high amount of optoelectroactive species, facilitates electron transport to these centers, and efficiently harvests the electron-induced optical response or, vice versa, the photon-induced electron flow.

This material thus could open new pathways to novel, highly efficient solar cells and optoelectronic systems based on transparent electrodes and sensors.

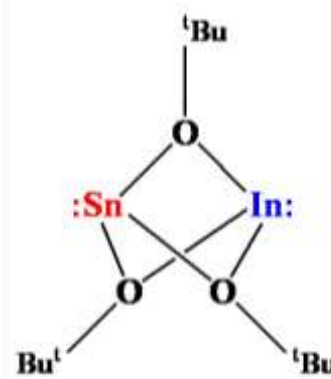
1.2.1.2 Tin rich indium tin oxide

A general problem in the production of ITO is the limited amount of tin, which, although the cheaper component, is only slightly soluble in the In_2O_3 phase, typically

around 1–10 wt %. In case of organized mesostructured ITO, a second problem appears from the compromise between the conductivity and regular porosity.

To avoid phase segregation of *tin-rich* ITO, a low-temperature approach with high control over the In/Sn molar ratio was reported recently, based on the molecular single-source precursor indium tin tris-*tert*-butoxide (ITBO; Scheme 1) containing indium and tin in the molar ratio of 1:1, which facilitates the formation of *tin-rich* ITO with an identical stoichiometry in the final product (Aksu *et al.*, 2009).

Most importantly, the resulting *tin-rich* ITO shows high conductivity and transparency even in an amorphous state. Using such approach it was possible to overcome all of the problems connected with the pore collapse during the crystallization typical for the template-assisted approach toward mesoporous ITO (Fattakhova-Rohlfing *et al.*, 2006). As the ITBO precursor enables the formation of transparent conducting films without any crystallization step, the main cause of pore collapse of mesoporous metal oxides is excluded in these materials. Thus, ITBO appeared as highly suitable for the preparation of mesoporous, *tin-rich* ITO films with reliable high electrical conductivity and transparency using different templates (Aksu *et al.*, 2011).



Scheme 1 Structure of indium tin tris-*tert*-butoxide (ITBO).

1.2.1.3 Antimony doped tin oxide

The research toward the replacing of the rare and expensive indium in transparent conducting films is of great interest and may in addition provide a different surface chemistry and energy-level properties.

The most promising materials are the extrinsically doped tin oxides, such as fluorine- or antimony-doped tin oxide (ATO) (Batzill *et al.*, 2005). Sb is a common *n*-type dopant in SnO₂. Stjerna (Stjerna *et al.*, 1994) reported a strong increase in the free electron concentration in the SnO₂ band gap when doped with Sb. Therefore it was concluded that this band could be a half-filled metallic band and that additional thermal excitation into the Sn-like bands could increase the conductivity. In recent years, some communications have been published reporting macro and mesoporous ATO electrodes (Hou *et al.*, 2009; Wang *et al.*, 2009; Urbanová *et al.*, 2010).

1.2.1.4 Gold nanoparticles

An interesting way to build up conductive three dimensional structures on electrode is offered by metal nanoparticles (NPs). The chemical functionalities associated with nanoparticles enable the assembly of 2D and 3D NP architectures on surfaces (Shipway *et al.*, 2000). On the basis of the tremendous success in supramolecular chemistry, NPs functionalized with various molecular and biomolecular units were assembled into complex hybrid systems. The electronic triggering of redox proteins by the incorporation of nanoparticles represents a novel strategy for the electrical contacting of redox enzymes with their macroscopic environment.

Colloidal gold nanoparticles (AuNPs) have been around for centuries predominantly in the work of artists and craftsman because of their intensive visible colors. However, through research on size, shape, surface chemistry, and optical properties of gold nanoparticles a door to some very unique and exciting capabilities has been opened. Gold nanoparticle chemistry and physics has emerged as a broad new subdiscipline in the domain of colloids and surfaces. NPs with fewer than 300 gold atoms can display distinct optical and electronic properties compared to the bulk metal. These unusual optical properties of small gold particles, their size-dependent electrochemistry, and their high chemical stability have made them the model system of choice for exploring a wide range of phenomena including self-assembly, biolabeling, catalysis, electron-transfer theories, phase transfer, DNA melting, DNA assays and crystal growth. They found a large application range from photonic device fabrications, to sensing of organic and biomolecules, to charge storage systems (Jennings *et al.*, 2007; Sardar *et al.*, 2009).

The convergence of biotechnology and nanotechnology has led to the development of hybrid nanomaterials that incorporate the highly selective catalytic and recognition properties of biomaterials with the unique electronic, photonic, and catalytic features of nanoparticles. A very interesting property of gold nanoparticles is to provide a suitable microenvironment for biomolecules immobilization retaining their biological activity. Their ability to facilitate ET between the immobilized proteins and electrode surfaces, in addition to the light-scattering properties and extremely large enhancement ability of the local electromagnetic field led to an intensive use of this nanomaterial for the construction of biosensors (Li *et al.*, 2010) and electrochemical biosensors (Pingarrón *et al.*, 2008; Bon Saint Côme *et al.*, 2011).

Their high surface-to-volume ratio, high surface energy, ability to decrease proteins–metal particles distance, and the functioning as electron-conducting pathways between prosthetic groups and the electrode surface, are regarded to be the general characteristics of gold nanoparticles responsible to facilitate electron transfer between redox proteins and electrode surfaces (Liu *et al.*, 2003).

Gold nanoparticles are prepared with a wide variety of preparative methods. These methods are mostly based on precursors containing gold complexes with tetrachloroauric acid (HAuCl₄), being the precursor most commonly used. Various in situ reactions, such as chemical, photo-induced, thermal decompositions or controlled solvent evaporation are used for the reduction process (Rao *et al.*, 2000).

Nanoparticles show a relative stabilization in solution towards aggregation and other modes of decay due to the acquisition of charges either from surface charged groups or by specific ion adsorption from the bulk solution. Such charges lead to a repulsive double-layer force between particles. On the other hand nanoparticle systems adsorbing a polymeric layer can be sterically stabilized due to a steric barrier which prevents the particles against collision. A much better stabilization is provided when the adsorbed polymer is a polyelectrolyte. In this case both types of stabilization can be combined giving rise to electrosterically stabilized systems (Koetz *et al.*, 2007).

1.3 Proteins

1.3.1 Cytochrome c

Cytochrome c (cyt c) is a small globular redox protein with a molecular weight of about 12 kDa. Cyt c is highly soluble, in contrast to other cytochromes, with an aqueous solubility of about 100 g L^{-1} . It contains a single polypeptide chain of about 100 residues and a mono c-type heme as prosthetic group (protoporphyrin IX, see Figure 3 left), covalently bound to two cysteine residues and responsible for its characteristic red color. About 40% of the polypeptide is in α -helical segments while the rest consist in turns, irregularly coiled and extended segments (Figure 3 right) (De Biase *et al.*, 2009). The 18 positively charged lysine residues contribute largely to the basic isoelectric point in the range of 10.0 – 10.5 (van Gelder *et al.*, 1962).

The real electron carrier of cyt c is the iron coordinated at the center of the porphyrin ring and to a histidine and a methionine. It can exist in the oxidized (ferric, Fe^{3+}) or the reduced (ferrous, Fe^{2+}) form and shows a redox potential of around 250 mV vs NHE at pH 7 and 25 °C.

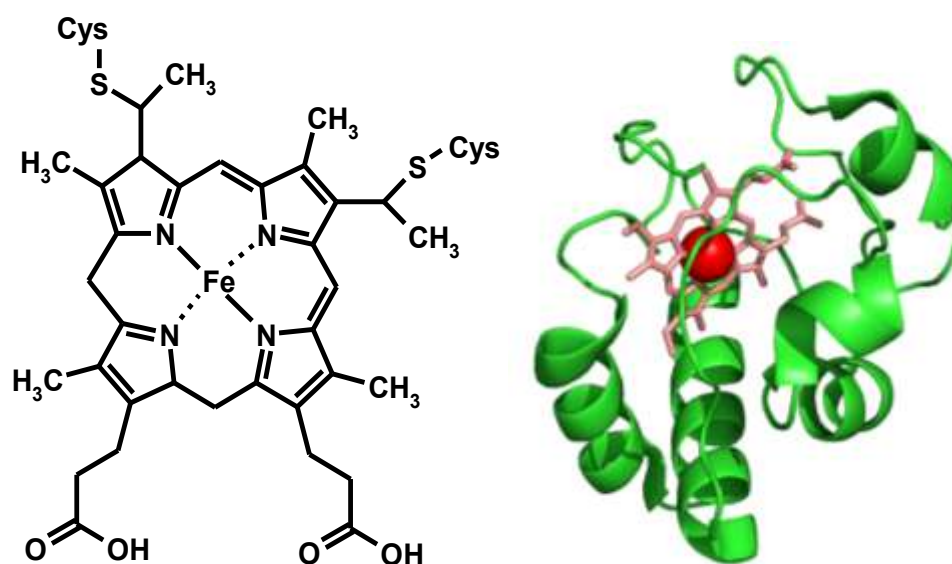


Figure 3. Structure of the heme group of c-type cytochromes (left) and structure of the horse heart cytochrome c (right). Picture made with Pymol using the PDB-file 1HRC (Bushnell *et al.*, 1990).

Cyt c is found in many species ranging from eukaryotes to bacteria and Archaea (Bertini *et al.*, 2006). In eukaryotes cyt c is a freely diffusing protein of the mitochondrial intermembrane. Cyt c in the mitochondria is involved in the electron shuttle between cyt c reductase and cyt c oxidase during oxidative phosphorylation in

the respiratory chain. In chloroplasts, cyt *c* transfers electrons from the cytochrome *bf* complex to photosystem I. In prokaryotes, cyt *c* is involved in both aerobic and anaerobic respiration.

In general it is also involved in early events of apoptosis when released to the cytoplasm (Ow *et al.*, 2008; Caroppi *et al.*, 2009).

Scavenging superoxide and hydrogen peroxide in mitochondria (Min *et al.*, 2007) may also be connected to the apoptosis, since these reactive oxygen species are shown to act as redox signal molecules. However the effort to discover new functions of cyt *c* beyond that of an electron carrier in respiration seem still not to be finished and contribute to the ongoing high interest for this protein.

A quasi-reversible exchange of horse heart cytochrome *c* was first reported in the 1977 on tin-doped indium oxide electrode (Yeh *et al.*, 1977) and 4, 4'-bipyridine modified gold electrode (Eddowes *et al.*, 1977) (Figure 4).

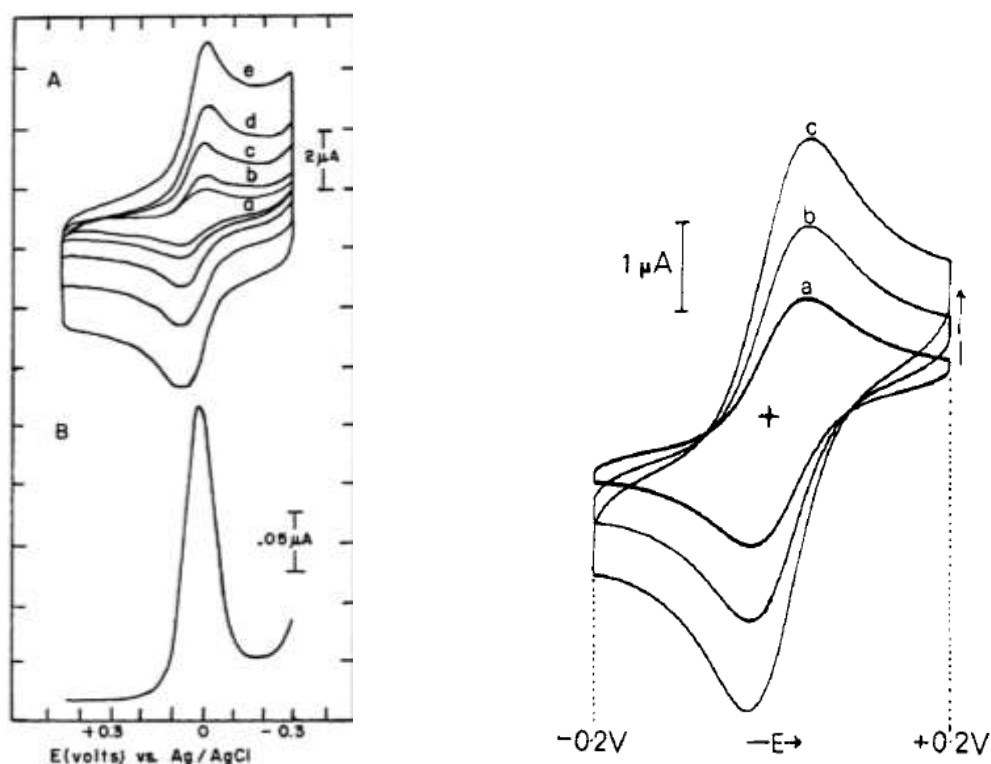


Figure 4. (Left) Cyclic voltammetry (a) (scan rate 10, 20, 50, 100, and 200 mV s^{-1}) and differential pulse voltammetry (b) (scan rate 2 mV s^{-1} , pulse height 50 mV, and pulse width 0.5 s) in phosphate buffer (ionic strength=0.15 M, pH=7.0) at ITO (Yeh *et al.*, 1977) and (right) cyclic voltammetry in NaClO_4 (0.1 M), phosphate buffer (0.02 M) at pH 7 in the presence of 4,4'-bipyridyl (10^{-2} M) (scan rate 20, 50 and 100 mV s^{-1} , reference SCE) at bare gold electrode (Eddowes *et al.*, 1979) of a cyt *c* solution.

The extensive studies on cytochrome *c* suggest that adsorption at the electrode-solution interface plays a prominent role in the electrode process. It has been demonstrated that the adsorption of cytochrome *c* can be accompanied by noticeable changes in the protein conformation and even the coordination shell of the heme iron. Non-electrochemical studies such by spectroreflectance (Hinnen *et al.*, 1983; Niki *et al.*, 1987) and surface-enhanced resonance Raman spectroscopy (Adelhelm *et al.*, 1989) coupled to electrochemistry confirmed the irreversible adsorption of cytochrome *c* at bare gold and silver electrodes.

On the other hand *cyt c* adsorbs strongly on indium oxide, but not completely irreversibly, while retaining its native redox potential (El Kasmi *et al.*, 2002). Several other metal oxide electrodes were used successfully (Bowden *et al.*, 1984; Topoglidis *et al.*, 2003; Li *et al.*, 2001; Xu *et al.*, 2004; Deng *et al.*, 2009), but the electrode responses have been found to be very sensitive to the experimental conditions, especially pretreatment procedures.

In case of self-assembly monolayer (SAM), like with 4,4'-bipyridine, the modifier acts by adsorbing to the gold surface, thereby providing a suitable interface for interaction with cytochrome *c*. Most recently investigations on the electrochemistry of *cyt c* were carried out using a large variety of different modifiers (Scheller *et al.*, 1999; Fedurco, 2000; Wang *et al.*, 2011; Matsui *et al.*, 2011; Hoffmann *et al.*, 2011).

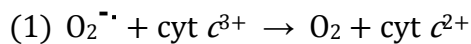
The formal potential (E^0) of the absorbed protein is negative shifted when compared to the respective solution values. Shifts of this type have been well documented (Jin *et al.*, 1997; Ge *et al.*, 2002) and are still in discussion whether it should be attributed to the greater relative binding affinity of the ferric form of the protein (Willit *et al.*, 1990) or to the conversion of a portion of the immobilized *cyt c* to a conformational state lacking the axial Met-80 ligand of the heme induced by the electric field at the binding site (Murgida *et al.*, 2001).

Metal oxides or modified gold surfaces are not the only way for obtaining rapid electron exchanges between cytochrome *c* and the electrode. Direct electron transfer has been observed at a bare glassy carbon electrode (Hagen, 1989) at single-wall carbon nanotubes (Wang *et al.*, 2002), bio sol-gel matrix (Deriu *et al.*, 2007) and boron-doped diamond electrodes (Marken *et al.*, 2002).

Another promising way is the use of modified-electrode interfaces obtained through deposited lipids. These films appear to yield novel opportunities to fashion "tailor-made" surfaces which can integrate cytochromes and ultimately mimic the

operating environment of membrane-bound electron-transfer systems (Guerrieri *et al.*, 1991; Salamona *et al.*, 1991).

The cyt *c* reduction assay for superoxide-generating enzyme is widely used since decades, and was for the first time reported in the 1968 (McCord *et al.*, 1968). Cyt *c* oxidizes superoxide to molecular oxygen:



High interest is placed in the development of superoxide biosensors employing the possibility to reoxidize the reduced cyt c^{2+} to generate current which is correlated to the superoxide concentration (McNeil *et al.*, 1989; Campanella *et al.*, 1997; Scheller *et al.*, 1999; Ge *et al.*, 2002; Wegerich *et al.*, 2009).

1.3.2 Mononuclear Molybdoenzymes

Molybdenum is an integral component of diverse groups of enzymes and is necessary for most living organisms. Molybdenum is widely available to biological systems due to the solubility of its high-valent oxides in water, being the only second row transition metal in nature with biological importance.

So far, over 50 molybdoenzymes were discovered to be involved in the catalysis of reactions at carbon, sulfur and nitrogen cycles and it is found in two basic forms. A multinuclear MoFe₇ cluster is found in nitrogenases (Burgess *et al.*, 1996; Howard *et al.*, 1996) whereas mononuclear active sites in general catalyze oxygen atom transfer either to or from a physiological acceptor/donor molecule.

According of the classification proposed by Hille based on a different active site structure and type of reaction catalyzed (Hille, 1996; Hille, 2002), the mononuclear molybdenum enzymes were subdivided in three families (Figure 5).

In all known cases the enzymes possess a pterin (Figure 5a) and the cofactor is referred in the literature as molybdopterin or Moco from *molybdenum cofactor* (Truglio *et al.*, 2002; Romão, 2009) since it was originally believed to be present only in molybdenum enzymes. Nevertheless the same form was found later in some tungsten enzymes (Johnson *et al.*, 1996).

The first family, with the xanthine oxidase from cow's milk as progenitor, possesses a Mo^{VI}OS(OH) nucleus and one pyranopterin but no covalent bonding of the metal to the polypeptide chain. These enzymes typically have been found to be

remarkably similar in their overall size and composition of redox centers, as well as their ability to oxidize a large variety of purine, pyrimidine, pterin, and aldehyde substrates (Hille, 1996; Hille *et al.*, 1995).

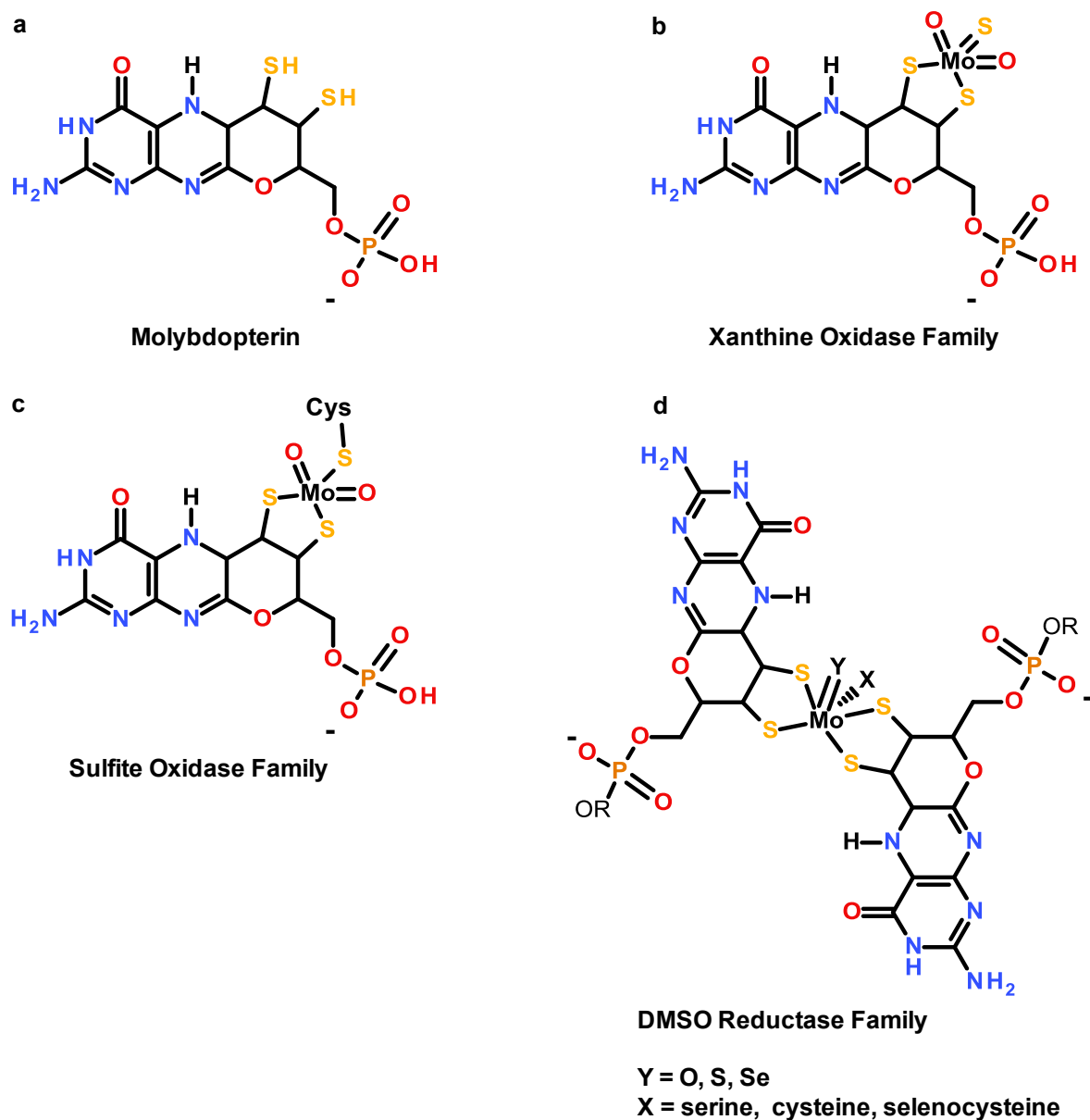


Figure 5. (a) Chemical structure of the MPT and the MoCo belonging to three different protein families. (b) Members of the xanthine oxidase family have Mo centers consisting of a single MPT dithiolene ligand (L) coordinated to MoOS-OH. (c) Members of the sulfite oxidase family possess a single MPT dithiolene coordinated to a MoO₂ (additional coordination may be taken by water and/or a cysteine residue that is conserved within the family) (d) Enzymes belonging to the third family are distinguished by bisdithiolene coordination of the Mo.

The second family includes sulfite oxidase and nitrate reductase (from plants that assimilate nitrate from the soil). The (oxidized) metal center has a single equivalent of the MPT with the polypeptide chain coordinates directly to the molybdenum site by a

cysteinylyl residue ($\text{LMo}^{\text{VI}}\text{O}_2(\text{S-Cys})$). Members of this second family catalyze the oxygen atom transfer reactions either to or from an available ion pair of electrons on the substrate.

The third family differs either in structure and function, with all members having two equivalents of the MPT bound to the metal. The Mo coordination sphere is usually completed by a single Mo=O group and a sixth ligand in an $\text{L}_2\text{Mo}^{\text{VI}}\text{O}(\text{X})$ core. The reactions catalyzed by members of this last family frequently involve oxygen atom transfer, but dehydrogenation reactions also occur (Kniemeyer *et al.*, 2001).

In eukaryotes the pyranopterin has a terminal phosphate group on the pyranopterin side chain. In prokaryotes it is conjugated to nucleosides, usually cytosine (molybdopterin cytosine dinucleotide e.g. quinoline oxidoreductase from *Pseudomonas putida*) or guanosine (molybdopterin guanosine dinucleotide e.g. DMSO reductase and nitrate reductase from *R. sphaeroides*, formate dehydrogenase from *Escherichia coli*), and occasionally adenosine (e.g. formylmethanofuran dehydrogenase from *Methanococcus thermoautotrophicum*) or inosine (Rajagopalan *et al.*, 1992). The primary role of the pterin cofactor is to position the catalytic metal in the active site. In addition, it modulates the redox potential at the Mo centre and is involved, via the pterin ring system, in the transfer of electrons to or from other prosthetic groups. The pathway by which the pyranopterin core of the cofactor is synthesized involves a large number of proteins in bacteria and appears to be universally conserved in biology (Joshi *et al.*, 1996; Schwarz, 2005; Fischer *et al.*, 2010; Leimkühler *et al.*, 2011).

The mononuclear Mo-enzymes show a large diversity of substrates that they are capable of oxidizing or reducing and since electron transfer is involved in the catalytic mechanisms, a large investigation is focused on their application in biosensor and bioelectronic (Bernhardt, 2009).

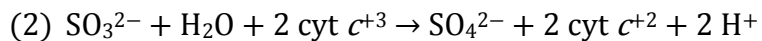
1.3.2.1 Sulfite oxidizing enzymes

The group of the sulfite oxidizing enzymes is composed of two subclasses based on their ability to transfer electrons to molecular oxygen (Hille, 2002): the sulfite oxidases (SO, found in animals and plants), and the sulfite dehydrogenases (SDH, found in bacteria).

In animals SO is a dimer and each monomer has three domains. A first domain (9 kDa) binding a *b*-type heme (Heme domain, HD), a second containing the Moco

domain (Moco domain, MD) and a third domain involved in the dimerization between the two monomers. The HD and the MD are linked by a 10 amino acid flexible loop (Pacheco *et al.*, 1999).

It catalyzes the oxidation of sulfite to sulfate, with the oxidized cyt *c* as the physiological electron acceptor (Hille, 1996; Temple *et al.*, 2000):



The bacterial SDH is a $\alpha\beta$ heterodimer, consisting of a subunit containing a Moco and a cytochrome *c552* subunit. The natural electron acceptor for SDH from *Thiobacillus novellus* seems to be the cytochrome *c550* (Kappler *et al.*, 2000; Kappler *et al.*, 2005).

Plant sulfite oxidizing enzymes, like the *Arabidopsis thaliana* SO, consist in a simple Moco binding domain and lack a heme containing domain (Eilers *et al.*, 2001; Schrader *et al.*, 2003). It has been shown that oxygen acts as the terminal electron acceptor for plant SO (Hänsch *et al.*, 2006; Byrne *et al.*, 2009).

1.3.2.1.1 Animal sulfite oxidase structure

The structure of the human SO has not been solved so far, although the structure of the human SO heme domain is already available (Rudolph *et al.*, 2003). Nevertheless, the X-ray structure of its high homologues (chicken SO) was reported (Kisker *et al.*, 1997) (Figure 6). CSO is a homodimeric sulfite oxidase contains two identical subunits formed from a small N-terminal *b5*-type cytochrome domain (HD), a large central Mo-binding domain (MD), and a large C-terminal interface domain.

In each subunit the MD and the HD are linked by a flexible peptide loop of 10 amino acids. It was also observed that the dispositions of the HDs within the dimeric protein of the unit cell are not in an equivalent position relative to their respective MDs. This variation in HDs orientation has been interpreted as evidence of domain-domain flexibility, and supports the hypothesis that conformational change is involved in the electron transfer between the Moco and heme centers. In the X-ray SO structure the Mo and Fe centers are ~32 Å apart in a not optimal position and orientation of the respective redox partners for an IET (Pacheco *et al.*, 1999). Rearrangement to a more “productive” orientation may occur before IET, which suggests that fast ET between Mo and Fe centers requires delicate and precise positioning, orientation, and docking of the two redox partners. The flexible loop

could provide to the heme domain the necessary mobility to allow its negative charged exposed edge to interact electrostatically with the positively charged MD.

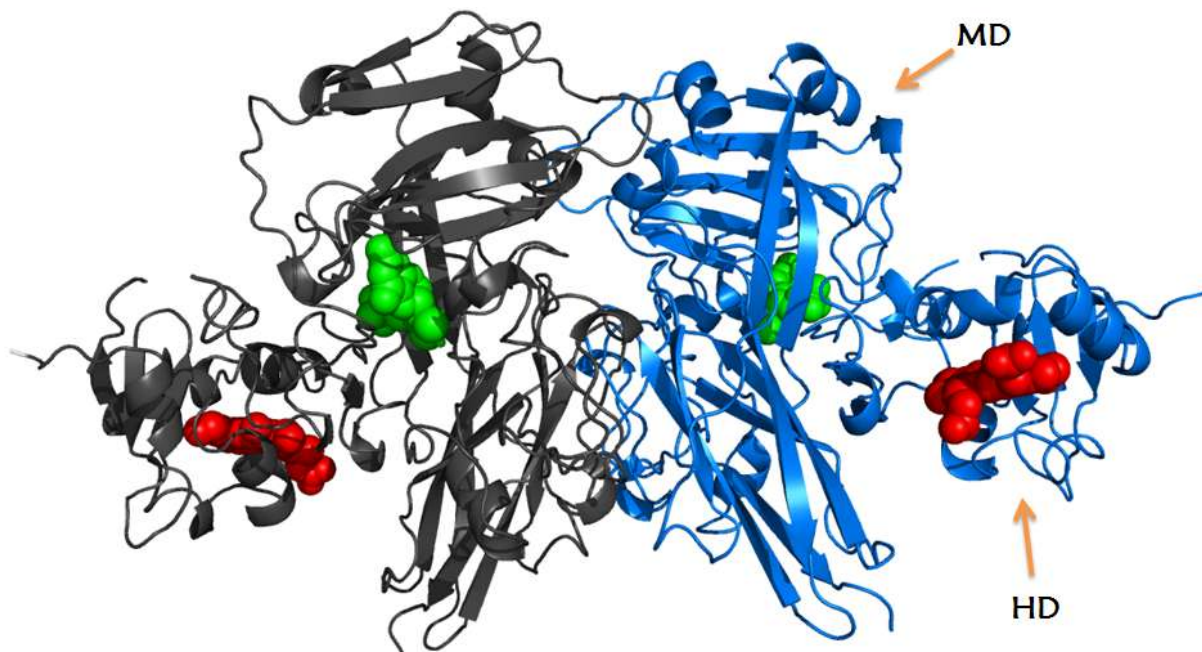


Figure 6. Crystal structure of chicken liver SO. The dimeric structure is underlined by differently colored monomers. The MD and HD positions are highlighted only for one subunit for simplicity. The heme *b5* group is indicated in red, whereas the Moco is depicted in green. Picture made with Pymol using the PDB-file 1SO (Kisker *et al.*, 1997).

Once the IET takes place then the HD moves away from the MD to interact with the positively charged cyt *c*, the physiological electron acceptor. This flexibility seems to guarantee both intra and inter electron transfer reaction. Unlike, in the bacterial SDH, the heterodimer comprising molybdenum and heme *c* binding subunits occupy fixed positions relative to one another during catalysis (Kappler *et al.*, 2000).

In SO the IET reaction rates were found to be affected by various parameters such as pH, anion concentration and even the nature of the anion; thus, Cl^- , SO_4^{2-} , and PO_4^{3-} all have different inhibitory effects (Sullivan Jr. *et al.*, 1993; Pacheco *et al.*, 1999). An appreciable decrease in the IET rate constant value was observed as well with an increase in the solvent viscosity (Feng *et al.*, 2002). These results are consistent with the role of conformational changes electrostatically driven on IET between Mo and Fe centers. The active site of sulfite oxidase is deeply buried in the protein and as expected for binding an anionic substrate, the sulfite-binding site is highly positively charged, and consists of three arginines (R138, R190 and R450)

and two other residues (W204 and Y322). Wilson and Rajagopalan reported a comparative study of the reductive half reaction in the truncated MD and the full-length *human* SO by stopped flow, which suggested the IET reaction as limiting reaction step. This study gives rates for the discrete step of SO reduction by sulfite and the overall reactions (which include the sulfite reduction step followed by IET between Mo^{IV} and Fe^{III}), and thus provides evidence that reduction of the Mo center is quite fast ($\sim 1000 \text{ s}^{-1}$), indicating that this is not the rate-limiting step in the overall catalytic cycle ($\sim 30 \text{ s}^{-1}$) (Wilson *et al.*, 2004).

1.3.2.1.2 Catalytic mechanism of sulfite oxidase

In animals SO catalyzes the physiologically vital oxidation of sulfite to sulfate, the final step in the oxidative degradation of the sulfur-containing amino acids cysteine and methionine. The reaction is critical in detoxifying excess of sulfite. SO deficiency is a fatal genetic disorder that leads to early death, and impaired SO activity is implicated in sulfite neurotoxicity (Johnson, 2003). The overall mechanism of animal SO, originally proposed by Hille, has now become generally accepted.

Sulfite is oxidized to sulfate at the Moco center, and the reducing equivalents are transferred to the heme *b5*, where the terminal electron carrier cyt *c* is reduced (Figure 7) (Brody *et al.*, 1995; Brody *et al.*, 1999; Hille, 1996). The reductive half reaction of the catalytic sequence involves the reaction of the oxidized enzyme with sulfite to yield the reduced enzyme and sulfate, whereas the oxidative half reaction involves the reaction of the SO with cyt *c* to yield oxidized enzyme and reduced cyt *c*. The reductive half reaction starts with the reaction of the Mo^{VI} center in the fully oxidized SO with sulfite to produce sulfate. The transient form of $\text{Mo}^{\text{IV}}/\text{Fe}^{\text{III}}$ undergoes intramolecular electron transfer (IET) to generate the $\text{Mo}^{\text{V}}/\text{Fe}^{\text{II}}$ form (Astashkin *et al.*, 2002). In the oxidative half reaction a one electron reduced form ($\text{Mo}^{\text{V}}/\text{Fe}^{\text{III}}$) of the enzyme is formed. A one-electron transfer to exogenous cyt *c* accomplishes reoxidation of the Fe^{II} . A second IET step, forming $\text{Mo}^{\text{VI}}/\text{Fe}^{\text{II}}$ followed by reduction of a second equivalent of cyt *c*, regenerates the fully oxidized enzyme in the state of $\text{Mo}^{\text{VI}}/\text{Fe}^{\text{III}}$ (Figure 7).

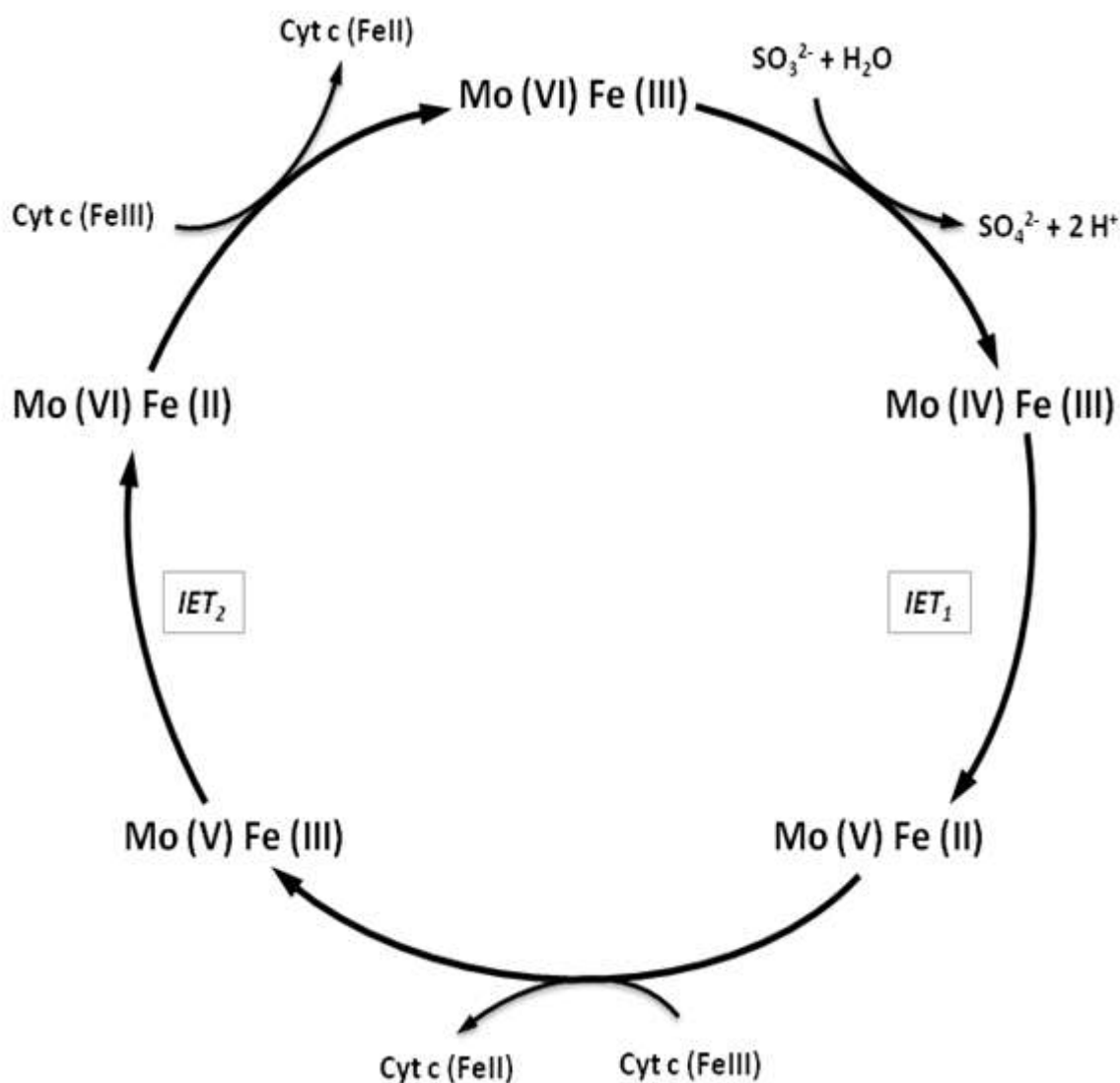


Figure 7. Proposed reaction mechanism for animal SO. Postulated oxidation state changes occurring at the Mo and Fe centers of SO during the catalytic oxidation of sulfite and concomitant reduction of cyt c. IET shows the intramolecular electron transfer between the molybdenum center and the heme.

1.3.2.1.3 Sulfite oxidase electrochemistry

So far, the electrochemistry of sulfite oxidizing enzymes through the direct and mediated communication of heme *b5* has been investigated. The electrochemical behavior of SO was also reported using different synthetic mediators and cyt *c* (Coury Jr. *et al.*, 1991). All employed mediators were able to communicate only via the heme *b5*. The IET reaction of SO was indicated as the limiting step (10 s^{-1}) of the overall ET (Coury Jr. *et al.*, 1991).

Direct electrochemical communication of *gallus gallus* SO with electrodes has been demonstrated (Elliott *et al.*, 2002; Ferapontova *et al.*, 2003).

After immobilization on pyrolytic graphite or gold electrode modified with mercapto-6-hexanol self-assembled monolayer the enzyme can partially retain its activity and a single pair of peaks were observed with a formal potential of + 90 mV (vs. standard hydrogen electrode, SHE). Upon addition of sulfite to the cell solution, the voltammogram changed to an oxidative catalytic wave. However, the immobilized SO showed a decreased catalytic turnover rate ($2\text{-}4\text{ s}^{-1}$) in comparison to SO in solution with cyt *c* (100 s^{-1}) (Elliott *et al.*, 2002). This behavior was attributed to the small fraction of cSO molecules in with an appropriate conformation electrons exchange of the HD with the electrode surface.

A faster heterogeneous electron transfer of cSO immobilized was reached on aminated surface mimicking the natural partner of the enzyme (cyt *c*). Using gold surface modified with 11-mercapto-1-undecanol and 11-mercapto-1-undecanamine the k_{et} was in the order of 15 s^{-1} , whereas the catalytic turnover rate was comparable to the reaction in solution with the natural electron acceptor cyt *c* (Ferafontova *et al.*, 2003). The E^0 was to -120 mV versus Ag/AgCl (KCl_{sat}), correlating fairly well with the reported redox potential for the heme Fe(III/II) couple in SO obtained through optical redox titration (Spence *et al.*, 1991; Ferafontova *et al.*, 2004).

The E^0 for $\text{Mo}^{\text{VI/V}}$ and $\text{Mo}^{\text{V/IV}}$ interpolated at pH 8 were +6 mV and -184 mV (vs. NHE), hence the half reduced state of the active site (Mo^{V}) is stable (Spence *et al.*, 1991). These data are in agreement with the IET rates determined at pH 8 using flash photolysis on the same enzyme (Sullivan Jr. *et al.*, 1993).

CSO has been employed for the constitution of first (Situmorang *et al.*, 1999) and second (Abass, 2000; Svitel *et al.*, 1998) generation of sulfite biosensors.

Only recently the research is addressing the *human* variant of the sulfite oxidase enzyme. Three different approaches for the fabrication of a sulfite biosensing system have been proposed. In one case the natural partner of the *h*SO was employed for the electrochemical mediation with the electrode. Complex protein architectures containing *h*SO and cyt *c* were construct by the layer-by-layer technique (Dronov *et al.*, 2008) as well as alternated by an anionic polyelectrolyte (Spricigo *et al.*, 2008) (Spricigo *et al.*, 2009). It resulted in an enhanced sensitivity towards the sulfite concentration. The system showed appreciable stability only at very low ionic strength.

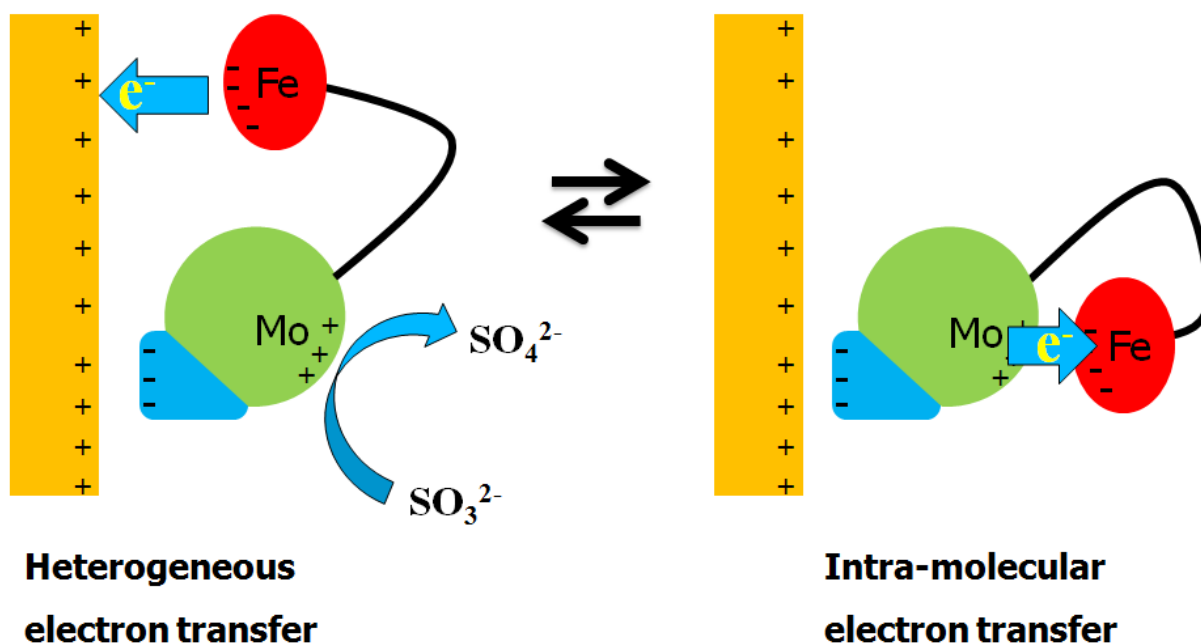


Figure 8. Schematic view of proposed conformational change by electrostatic orientation of immobilized animal SO on a positive charged electrode during the catalytic oxidation of sulfite surface. Only a single subunit schematic representation of SO is portrayed. Modified after Sezer *et al.* 2010.

The direct electrochemical communication of the HD was reported on amino functionalized silver electrode, with the possibility to work at high ionic strength. These investigations were complemented by a spectroelectrochemical study using surface enhanced resonance Raman spectroscopy (SERRS) following the Raman scattering variation of the heme contained in the *h*SO. Finally molecular modeling suggested that a high ionic strength increases the mobility of the HD while the enzyme is immobilized via the dimerization domain to the SAM surface. The flexible loop connecting the HD allows alternating contact with the MD and the electrode surface, thereby promoting the intramolecular and heterogeneous electron transfer (Sezer *et al.*, 2010).

In the third case either the heme center or the molybdenum center were wired by mean of an osmium polymer and a direct electrochemical communication of the isolated MD with electrocatalysis was showed (Spricigo, 2009; Spricigo *et al.*, 2010).

Similarly sulfite dehydrogenase, from *Starkeya novella*, has been also characterized electrochemically. Bacterial SDH is a heterodimer of a Moco containing domain and a heme *c* containing domain and shows some characteristics of eukaryotic SO, such as the inhibition by small anions. The voltammetric response of the Mo center of the bacterial SDH in the presence and absence of substrate was

published (Aguey-Zinsou *et al.*, 2003; Rapson *et al.*, 2008). For this investigation, an edge-plane pyrolytic graphite electrode surface was modified with surfactants (DDAB and polylysine) and signals from the single redox sites were recorded. More recently SDH has been employed, in combination with cyt c in the construction of a second generation sulfite biosensor (Kalimuthu *et al.*, 2010) in analogy to the system reported by Spricigo (Spricigo *et al.*, 2008; Spricigo *et al.*, 2009).

1.3.2.2 Xanthine oxidoreductase enzymes

Enzymes catalyzing the oxidation of hypoxanthine and xanthine, named xanthine oxidoreductases, are widespread in nature and have been isolated from a wide range of organisms, from bacteria to man. In terms of their electron acceptor, they fall into two broad groups by using preferentially molecular oxygen (the oxidases) or NAD^+ (the dehydrogenases) (Hille *et al.*, 1995).

Xanthine oxidoreductase (XOR) was described already in 1902 as the substance in milk which could decolorize methylene blue and it was identified originally as aldehyde oxidase (Scharinger, 1902). The mammalian enzymes, are synthesized as the dehydrogenase form xanthine dehydrogenase and exist mostly as such in the cell but can undergo a dehydrogenase to oxidase conversion ($\text{XDH} \rightarrow \text{XOD}$) by proteolysis or by oxidation of sulfhydryl residues. One of the major difference between XDH and XOD is the large formation of the blue neutral semiquinone observed during reductive titrations of XDH, very little semiquinone is seen during XO reductions (Massey *et al.*, 1979), indicating a large difference in redox potential between the two enzyme forms.

The enzyme is a target of drugs against gout and hyperuricemia (Elion, 1989), and the conversion of XDH to XO is of major medical interest as it has been implicated in diseases characterized by oxygen-radical-induced tissue damage, such as postischemic reperfusion injury (Richard *et al.*, 1990). XO also might be associated with blood pressure regulation (Suzuki *et al.*, 1998; Harrison, 2002).

An interesting prokaryotic XDH with similar activity to the mammalian enzymes was isolated from the phototrophic purple bacterium *Rhodobacter capsulatus* (Leimkühler *et al.*, 1998). Despite the similarities to the mammalian XOR enzymes, the *R. capsulatus* XDH is isolated with high reactivity toward NAD^+ and low reactivity toward oxygen as electron acceptor and does not undergo the conversion to the oxidase form.

1.3.2.2.1 Xanthine dehydrogenas structure

The solved crystal structure of *R. capsulatus* XDH (Truglio *et al.*, 2002) shows that the bacterial and bovine XDH (Enroth *et al.*, 2000) have highly similar folds despite differences in subunit composition. However, the two structures differ in important details, including the regions necessary for XDH to XOD conversion. Because of the high structural similarities of the mammalian XOR and *R. capsulatus* XDH, the bacterial enzyme is a good model system for studying the mechanism of the enzyme and can be used for the generation of site-specific mutants.

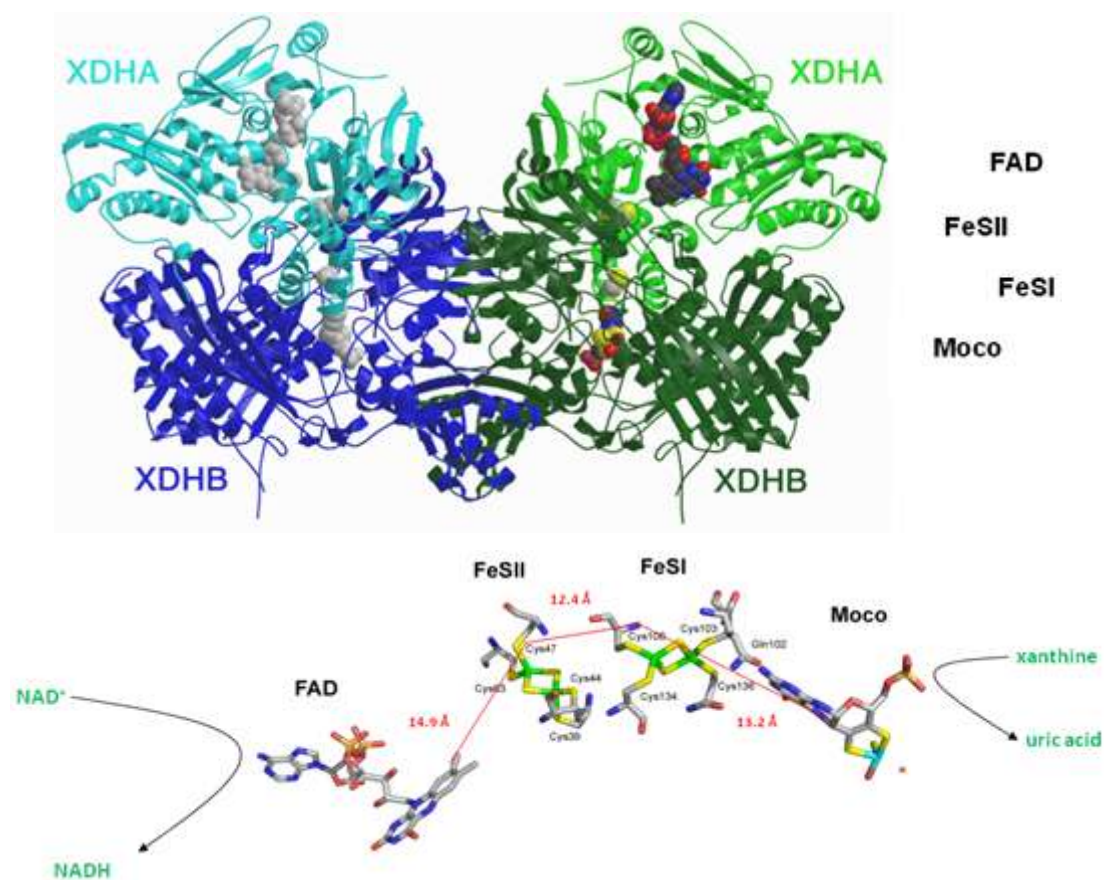


Figure 9. (Upper) Butterfly structure of *R. capsulatus* XDH. The Moco, the two [2Fe-2S] and the FAD cofactor are shown as space-filling models. (down) Alignment of the four cofactors in one single heterodimer, the catalytic reactions in their respective places, the distances between cofactors and the cysteines bound at the iron atom are also depicted (Truglio *et al.*, 2002).

The enzyme is a butterfly-shaped ($\alpha\beta$)₂ heterotetramer of molecular mass around 300 kDa, with each catalytically independent subunit possessing four prosthetic groups. One molybdenum active site is located at the bottom of a 15 Å hydrophobic channel, two spectroscopically different [2Fe-2S] iron-sulfur centers one of which a type I cluster buried ca. 12 Å below the protein surface and the other a type II

[2Fe-2S] cluster solvent exposed, and one FAD. The oxidation of xanthine takes place at the Moco. The two reducing equivalents generated in the course of the reaction are transferred to an external electron acceptor and the electron flow in and out of the molybdenum centre is mediated by the pterin cofactor to the closest FeS1 centre and then via the FeS2 to the FAD. Reoxidation of the reduced enzyme by oxidant substrate occurs through FAD (Olson *et al.*, 1974).

1.3.2.2.2 Electrochemistry of xanthine oxidoreductases

XOR from cow milk is the most electrochemical investigated protein of all mononuclear molybdoenzymes. XOR is widely studied for the detection of xanthine or hypoxanthine, mainly via detection of the products uric acid, hydrogen peroxide and superoxide (Sternson, 1976; Kirgöz *et al.*, 2004; Nakatani *et al.*, 2005; Dronov *et al.*, 2007; Çubukçu *et al.*, 2007; Shan *et al.*, 2009). Only few groups showed a direct electrochemistry of this enzyme, although often with confusing results. The protein was studied upon immobilization on a number of electrode materials. First was adsorbed on glassy carbon (GC) and mercury electrode (Rodrigues *et al.*, 1991), where evidence of protein denaturation was shown. In recent years XOR was immobilized on gold (Wang *et al.*, 2004), glassy carbon electrode modified with single-wall carbon nanotubes (Wu *et al.*, 2007), co-immobilized with nanocrystalline TiO₂ (Zhou *et al.*, 2006) or between two layers of didodecyl-dimethylammonium bromide (DDAB) (Bernhardt *et al.*, 2006) on pyrolytic graphite (PG) electrode, with the help of DNA as matrix to embed xanthine oxidase (Liu *et al.*, 2005) and more recently immobilized on glassy carbon electrode (GCE) by laponite nanoparticles (Shan *et al.*, 2009). In all cases the DET of the FAD was detectable. Rarely the DET of the Molybdenum center was reported and only Wu *et al.* was able to show it for one of the FeS.

In these publications direct catalytic current of the natural substrates was detected at potentials 0.6-0.8 V higher than the more positive cofactor potential. In addition unusual electrocatalytic activity towards nitric oxide and nitrate has been reported.

The discovery of new proteins, belonging to the xanthine oxidase family, led to an increasing interest to develop methods for the determination of the reduction potential of the cofactors and to achieve a direct electrochemical communication with an electrode for a future developing a third generation biosensors exploiting the selectivity of the enzyme. The XDH from *R. capsulatus* was studied on freshly

cleaved PG electrode. It also showed extreme overpotential in the catalytic activity. This rare phenomenon was first explained as due to an inactive opened pyranopterin (Aguey-Zinsou *et al.*, 2003) and later as an autocatalytic process associated to the reaction product uric acid (Kalimuthu *et al.*, 2011). Correia dos Santos published a direct electrochemistry of an aldehyde oxidoreductase from *Desulfovibrio gigas* immobilized on PG and GC electrodes (Correia dos Santos *et al.*, 2004). This member of the xanthine oxidase family is a FAD-independent enzyme and showed DET of the FeS II at carbon electrodes (PG and GC) and DET of the Moco at gold electrode in presence of neomycin.

All the published DET potentials are summarized in the table 2 in the chapter 5.

2 Aim of the work

The aim of this work consists in the electrochemical and optical studies of *heme*- and *molybdenum*-containing enzymes in respect to their interaction with diverse nanostructured materials. Spectro- and electrochemical methods shall be applied in order to implement new materials for electrochemical and catalytic studies and for the development of biosensing systems. With these methods also complex redox enzymes shall be investigated.

For this purpose, high transparent mesoporous metal oxides films and nanoparticles shall be employed as support for the enzyme adsorption. Out of this investigation suitable combinations of different protein and nanostructured materials should be developed to obtain an electrochemical and optical detection systems for several small molecules, like superoxide, hydrogen peroxide and sulfite. Finally the investigation shall be extended to direct and mediated spectroelectrochemical studies of the behavior of proteins with high structure complexity such as xanthine dehydrogenase from *Rhodobacter capsulatus* and its homologous the *mouse* aldehyde oxidase homolog 1.

3 Materials and Methods

3.1 Materials

3.1.1 Chemicals

Horse heart cytochrome c, used without further purification, H₂O₂ (30% solution in water), N-ethyl-N'-(3-dimethylaminopropyl)carbodiimide hydrochloride (EDC), poly-L-lysine, hypoxanthine and 3, 3', 5, 5'-tetramethylbenzidine (TMB) were purchased from Sigma (Steinheim, Germany). 11-mercapto-1-undecanoic acid (MUA), 11-mercapto-1-undecanol (MU) and HAuCl₄ were provided by Aldrich (Taufkirchen, Germany). Acetic acid and toluene (99%) were purchased from Fluka (Schnellendorf, Germany). Potassium dihydrogen phosphate, dipotassium hydrogen phosphate, disodium sulfite, sodium sulfate, ferrocene, sodium chloride, sodium phosphate, phosphoric acid, potassium chloride, 1-butyl-3-methylimidazolium octylsulfate (bmimOctOSO₃) (99%), 1-ethyl-3-methylimidazolium ethylsulfate (emimEtOSO₃) (99%) and ferrocene were purchased from Merck (Darmstadt, Germany). Potassium hexacyanoferrate (III) and 4-(2-hydroxyethyl)-1-piperazineethanesulfonic acid (Hepes) were purchased from Roth (Karlsruhe, Germany). Xanthine oxidase from cow's milk (XOD, 5.87 U ml⁻¹) and superoxide dismutase (SOD, 4890 U mg⁻¹) were provided by ICN Biomedicals Inc. (Aurora, USA). Branched poly(ethyleneimine) with a molecular weight of Mn= 5000 g/mol was obtained from BASF. [Co(*trans*diammac)]ClO₄)₃, [Co(*cis*-diammac)](ClO₄)₃, [Co(AMMEsar)]Cl₃, [Co(sep)]Cl₃, [Co(AMME-N₅S-sar)]Cl₃, [Co(CLME-N₄S₂-sar)]Cl₃, [Co((NMe₃)₂sar)]Cl₅, [Fe(tacn)₂]Br₃ and Fe(NOTA) (Bernhardt *et al.*, 2006) were a kind gift of Prof. Paul V. Bernhardt from Queensland University, Brisbane (Australia). XDH and hSO were expressed and purified in the Prof. Silke Leimkühler's laboratories as described in (Leimkühler *et al.*, 2003) and in (Temple *et al.*, 2000) respectively. Other reagents were of analytical reagent grade and used as received. Goodfellow (Bad Nauheim, Germany) supplied gold and platinum wires with a diameter of 0.5 mm. All the solutions were prepared in 18 MΩ Millipore water (Millipore, Eschborn, Germany).

3.1.2 Instruments

The electrochemical measurements for *h*SO at AuNP and for XDH at EP-GCE were performed in a home-made three-electrode electrochemical cell with a total volume of 1 mL employing a platinum wire as the counter electrode, an Ag/AgCl (1M KCl) reference electrode. The working electrode can be a gold wire or a glassy carbon electrode (GCE). Cyclic voltammetric, square wave and amperometric experiments were performed with PalmSens potentiostat and analyzed with PSLite 1.8 software, or with Gamry Reference 600TM potentiostat (Gamry, USA) and analyzed with Gamry Echem Analyst 5.50 software.

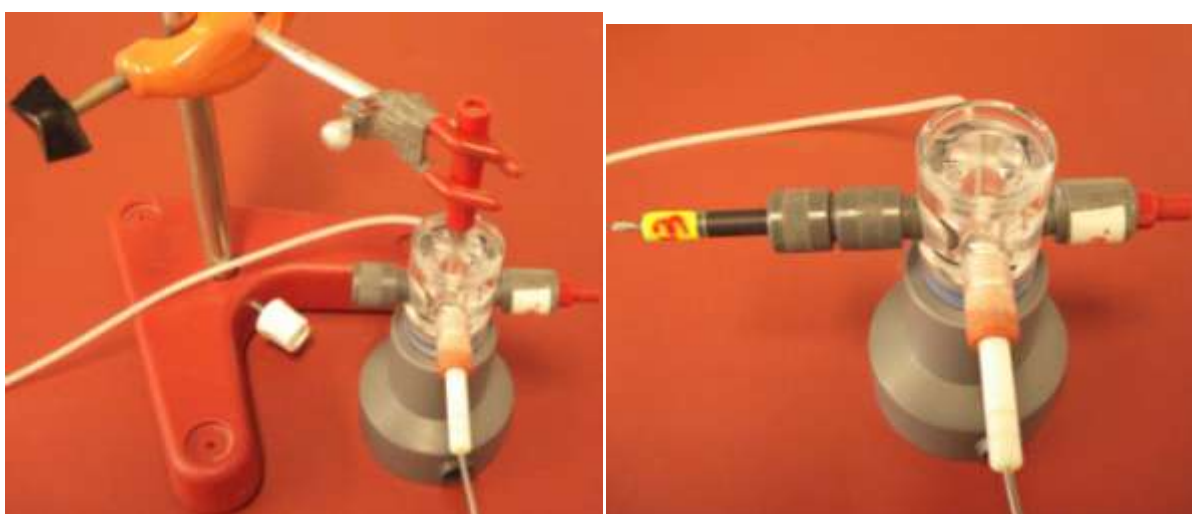


Figure 10. Electrochemical cell 1 in with (bottom left) a gold wire and (bottom right) glassy carbon working electrode.

The electrochemical measurements for the coated glass slide were performed in a home-made three-electrode electrochemical cell with a total volume of 1 mL employing a platinum wire as the counter electrode and an Ag/AgCl (1M KCl) reference electrode. A circular surface area 5.5 mm in diameter of the coated glass slide was the working electrode. Cyclic voltammetry (CV) experiments were carried out with a Gamry Reference 600TM potentiostat (Gamry, USA) and analyzed with Gamry Echem Analyst 5.50 software. All scans were started in the negative potential range. The potentiostat for the amperometrical experiments was a CH Instrument Model 750 A (Austin, USA).

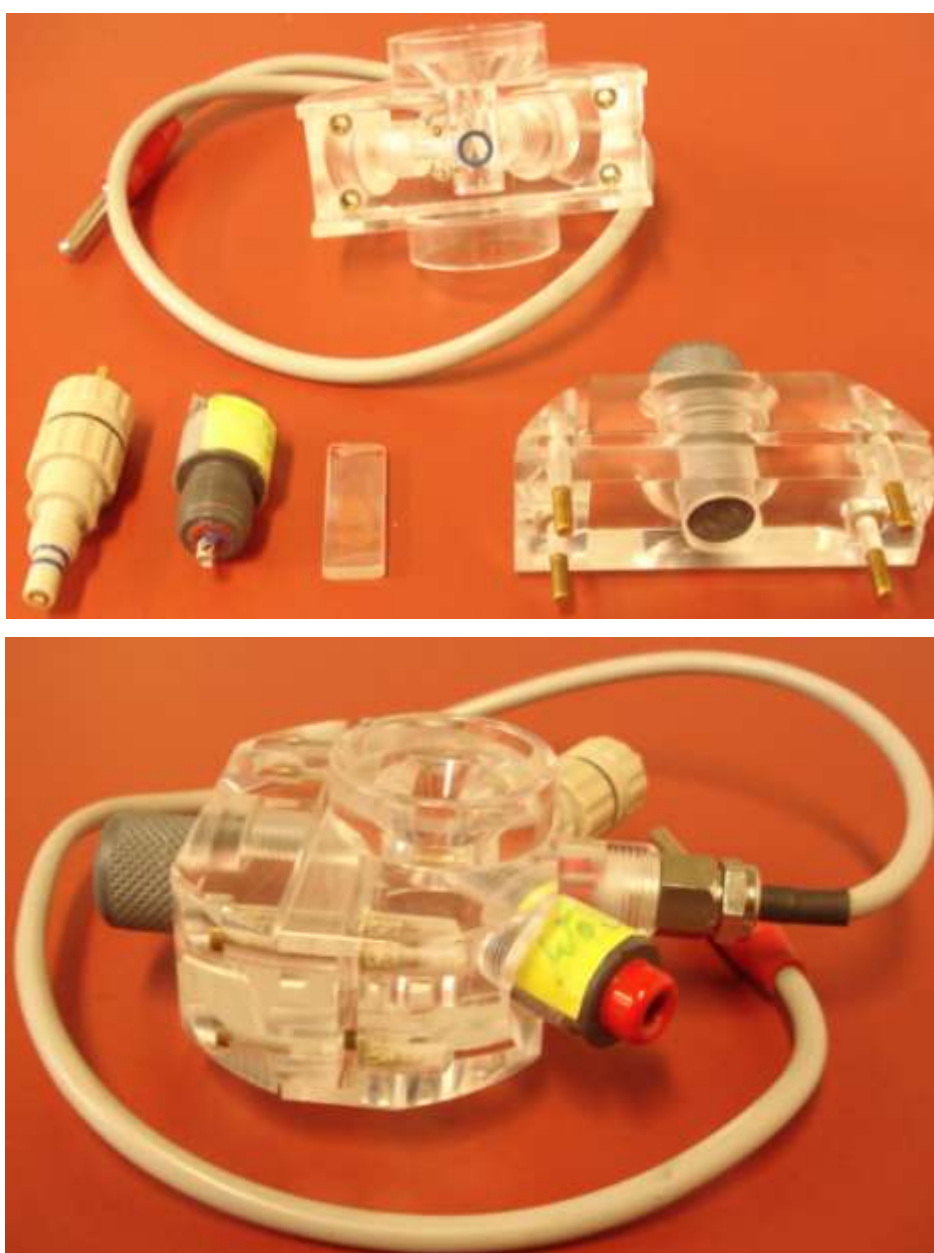


Figure 11. Electrochemical cell 2.

For the stationary spectroelectrochemical experiments a home-made spectroelectrochemical cell with a total volume of 1 mL employing a platinum wire as the counter electrode, an Ag/AgCl (1M KCl) reference electrode, and the coated glass as working electrode with a circular surface area 5.5 mm in diameter were employed. The electrochemical cell equipped with a quartz window was incorporated into the sample compartment of a Beckman DU 640 spectrophotometer whereas the applied potential was controlled by a Gamry Reference 600TM potentiostat (Gamry, USA). The transmission spectra were recorded through the coated glass slide.

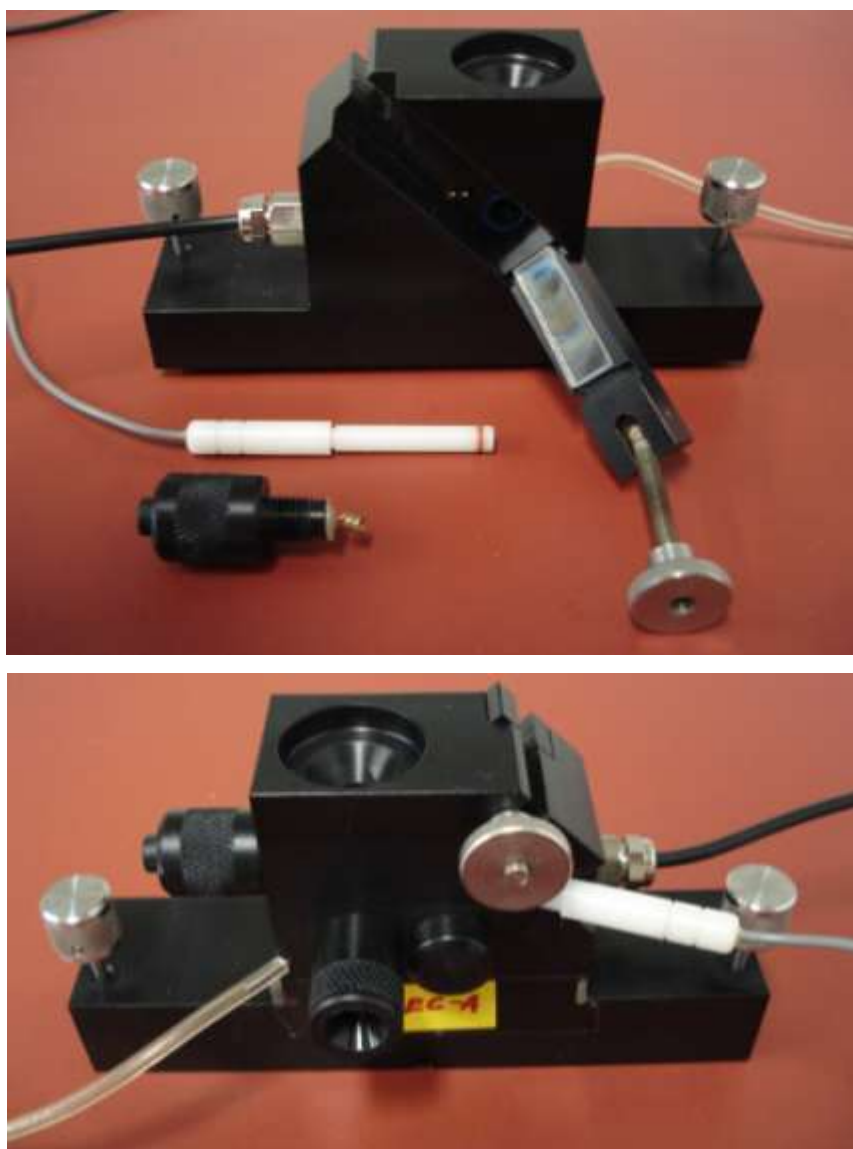


Figure 12. Spectroelectrochemical cell for stationary experiments.

For flow experiments a spectroelectrochemical flow cell has been constructed using an outflow stainless tube as the counter electrode, and an Ag/AgCl (3 M KCl) reference electrode. A coated glass slide was the working electrode. The cell was equipped with SEC-F 1000 μm probe type optical fiber (ALS, Japan) and UV-vis high OH content optical fiber of core diameter 400 μm (Ocean Optics, Germany). The spectra were measured with a SEC2000-Spectrometer (ALS, Japan). The transmission spectra were recorded through the coated glass slide and the quartz glass.

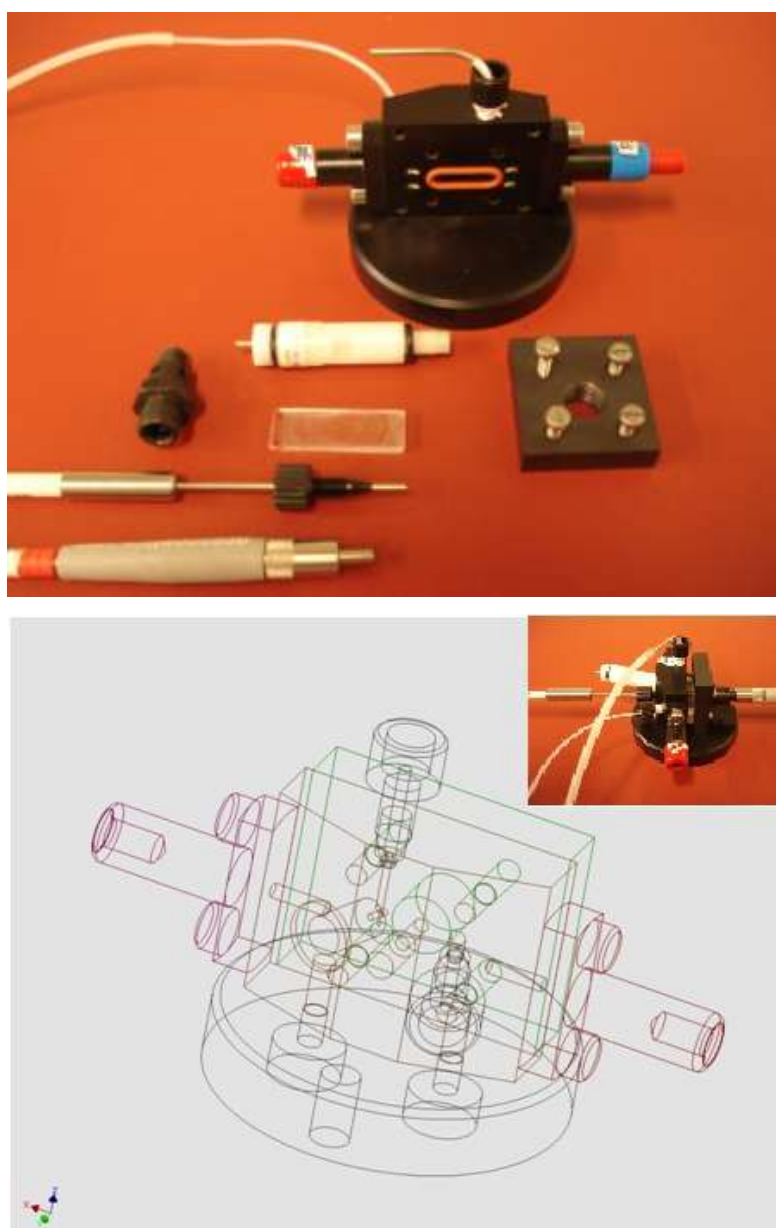


Figure 13. Spectroelectrochemical cell for flow experiments.

The spectroelectrochemical mediated titration was performed under an atmosphere of N_2 at room temperature in a 2 mL cuvette. Potentials were measured using a combination Pt wire and Ag/AgCl reference electrode calibrated against a pH 7 quinhydrone solution ($E^0 = +284$ mV vs NHE at pH7). The redox potential was adjusted by addition of microliter aliquots of Ti^{III} citrate and $K_2S_2O_8$. The solution was constantly stirred. The spectra were measured with a USB4000-UV-VIS Miniature Fiber Optic Spectrometer (Ocean Optics).

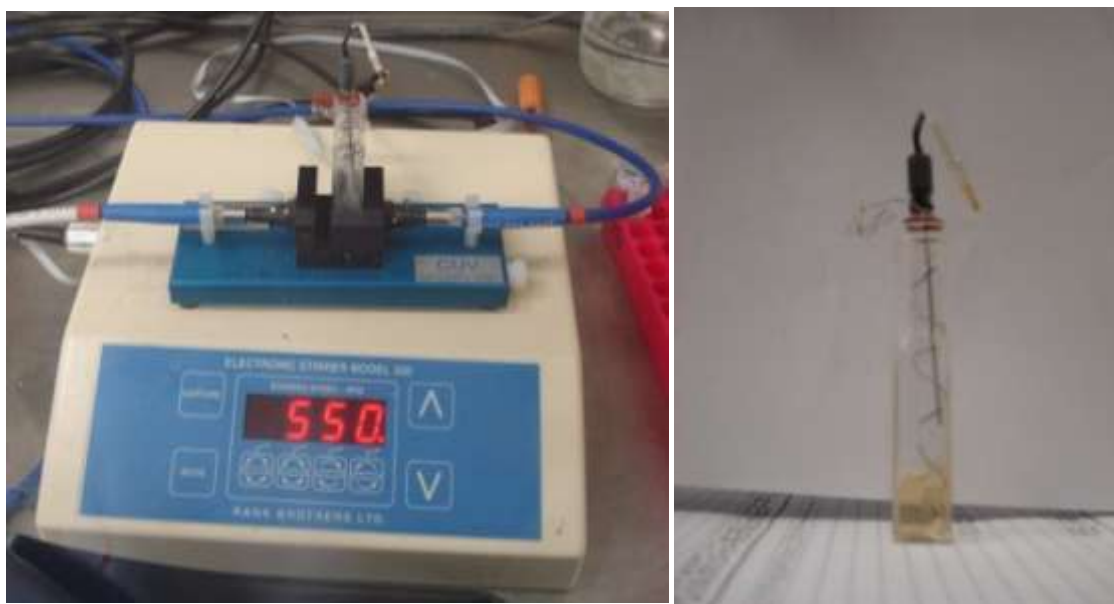


Figure 14. Cuvette arrangement for mediated spectroelectrochemical titration.

3.1.3 Buffers

3.1.3.1 Spectroelectrochemical study of mpITO and mpITBO

5 mM potassium or sodium phosphate pH 7.0 was used for the immobilization and UV-vis and Raman spectroelectrochemical study of cyt *c*, TMB and HD with mpITO and mpITBOs electrodes. 50 mM potassium phosphate pH 7.0 was used for the electrochemical study of $\text{Ru}(\text{NH}_3)_6^{2+/3+}$. 100 mM sodium phosphate pH 7.0, 0.1 M KCl was employed for the spectroelectrochemical study of free TMB in solution with a cyt *c* modified mpITO.

3.1.3.2 Spectroelectrochemical study of XDH and *mAOH1*

50 mM Tris buffer pH 8.0 was employed for the electrochemical study of the immobilized XDH variants and *mAOH1* on GC and for the spectroelectrochemical mediated titration of XDHwt.

3.1.3.3 Electrochemical study of *hSO* using gold nanoparticles

5 mM and 750 mM Tris buffer pH 8.4, with the pH adjustment using acetic acid, were employed for the electrochemical and surface enhanced Raman studies of *hSO* on AuNPs.

3.2 Methods

3.2.1 Molar extinction coefficients

The surface coverage of the mpITO was determined spectroscopically based on the extinction coefficients (ϵ) of $106100\text{M}^{-1}\text{cm}^{-1}$ (410 nm) and $129100\text{M}^{-1}\text{cm}^{-1}$ (416 nm) of ferric and ferrous cyt *c*, respectively (Topoglidis *et al.*, 1998; Collinson *et al.*, 1992).

The concentration of *hSO* and HD were quantified by using the molar extinction coefficient of $113000\text{M}^{-1}\text{cm}^{-1}$ at 413 nm, while for XDH variant the molar extinction coefficient was of $31600\text{M}^{-1}\text{cm}^{-1}$ at 465 nm.

3.2.2 Spectroelectrochemical study of mesoporous materials

3.2.2.1 Preparation of mpITO

The mesoporous indium tin oxide (mpITO) films were prepared in collaboration with Dr. Till von Graberg and, Prof. Bernd M. Smarsly from the Justus Liebig Universität Gießen (Germany).

MpITO-coated borosilicate glass or graphite slides were prepared as reported elsewhere (Fattakhova-Rohlfing *et al.*, 2006; von Graberg *et al.*, 2011). In brief, a thin film of mpITO was obtained by dip-coating the substrate slide in an acetone/methanol solution containing In^{III} acetylacetonate, SnCl_4 , and PIB3000 in a controlled atmosphere (18–20 % relative humidity) and at constant withdrawing rate. Subsequent calcination was performed at low heating rate in air at 300 °C, 450–500 °C and finally in forming gas (mixture of N_2/H_2 90:10) at 300 °C. This procedure generated a film of crystalline indium oxide (cubic bixbyite) with a fine dispersion of Sn ions in the In_2O_3 lattice (Figure 15). The pore sizes were in the range 15–20 nm and pore walls were 5–10 nm in thickness (Figure 15). The total surface area is $410 \text{ m}^2 \text{ cm}^{-3}$, as determined by krypton adsorption (for films with a thickness of 170 nm).

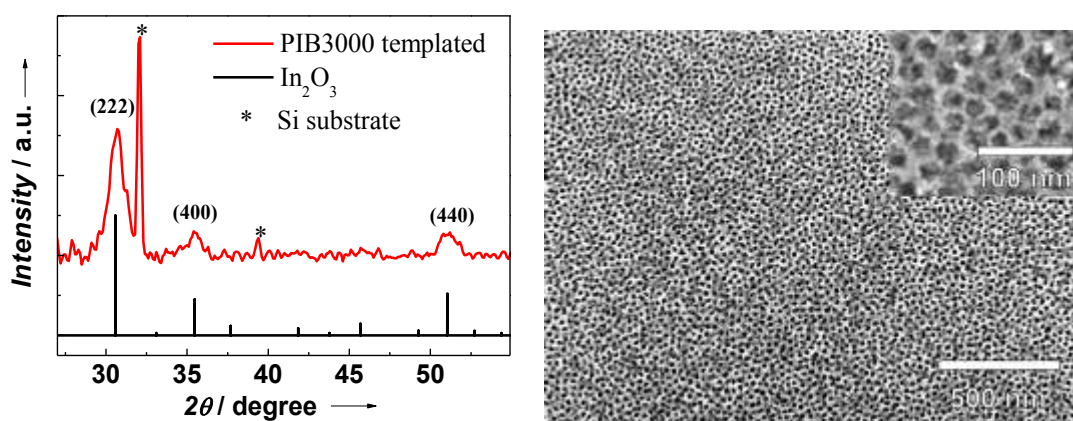


Figure 15. (left) Wide angle X-ray scattering data of ITO film templated with PIB3000 and calcined at 500 °C (red curve); the black columns show reference of indium oxide (cubic bixbyite) according to the Joint Committee for Powder Diffraction Studies (JCPDS). (right) Scanning transmission electron microscopy image of calcined mesoporous ITO film templated with PIB3000. (Frasca *et al.*, 2010)

3.2.2.2 Preparation of mpITBO

The mpITBO was prepared by Dr. Yilmaz Aksu, Prof. Matthias Driess, and Prof. Arne Thomas from the Technische Universität Berlin (Germany).

ITBO was prepared and characterized according to published procedures (Aksu *et al.*, 2009). Blends of ITBO with block-co-polymer, KLE or F127, were prepared by dissolving them in dry tetrahydrofurane (KLE) or dry toluene (F127) at ambient temperature and under nitrogen atmosphere. In a typical procedure, a KLE-ITBO solution was prepared by mixing a KLE (155 mg) solution in tetrahydrofurane (1 mL) with the appropriate amount of ITBO (620 mg) in tetrahydrofurane (1 mL) and stirred for 1 h at room temperature. The glass substrates were cleaned in an ultrasonic cleaner for 10 min with acetone and isopropanol. The substrates were dried in a high-purity nitrogen gas stream just before use. To increase the compatibility of the substrate with the ITBO-polymer mixture and ameliorate the final film quality, the glass substrates were first coated with a solution of pure ITBO in toluene. *Tin-rich* ITO-polymer films were fabricated by spin coating the solutions of the corresponding ITBO-polymer mixtures under nitrogen atmosphere in a glove-box (<1 ppm H₂O and <1 ppm O₂). The coatings were aged for 30 min in nitrogen and then annealed for 2 h in air at different temperatures between 300 and 600 °C (ramp 5 °C min⁻¹). After heat treatment all samples were subsequently annealed at 300 °C in a reductive gas mixture (H₂/N₂:10%/90%, ramp 5 °C min⁻¹) for 90 min.

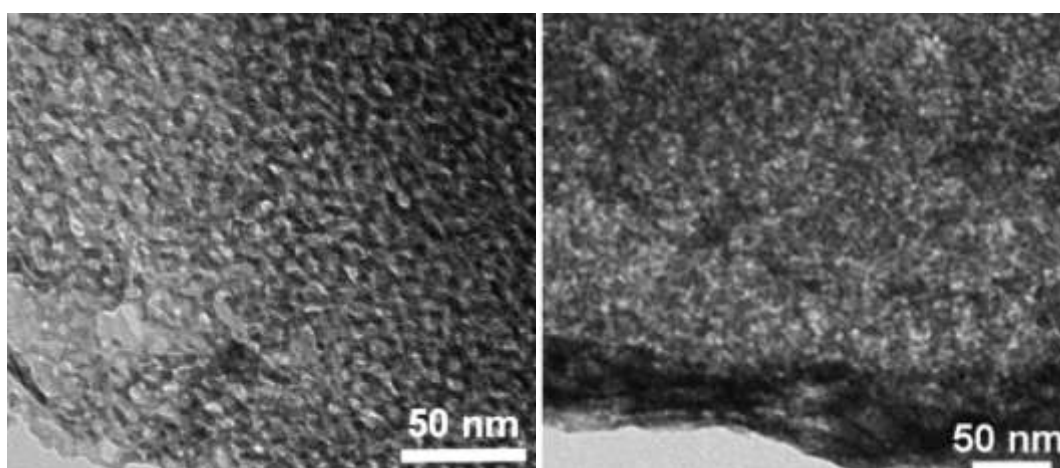


Figure 16. Transmission electron microscopy of mesoporous *tin-rich* ITO (ITBO) films templated with block-co-polymers (left) KLE and (right) F127. (Aksu *et al.*, 2011)

This approach leads to highly conductive, homogeneous, and compact thin films, of amorphous ITBO with different diameter size: F127 with an average pore diameter

of 6.5 nm and KLE with 12.3 nm (Figure 16). The approximate layer thickness, estimated by SEM, was about 750 nm for the ITBO-KLE and 1.5 μm for ITBO-F127 system on average (Figure 17). Assuming that the thickness of the films is uniform the resistivity was calculated in the order of $6.390 \times 10^{-3} \Omega\text{-cm}$ (ITBO-KLE) and $1.725 \times 10^{-2} \Omega\text{-cm}$ (ITBO-F127).

The films show 70–75% optical transmission in the visible range (Figure 18). The durability of the electronic properties of the mesoporous *tin-rich* ITO films is considerably higher in comparison to those prepared from commercially available ITO. No significant change of the conductivity was observed after 3 months in air at room temperature.

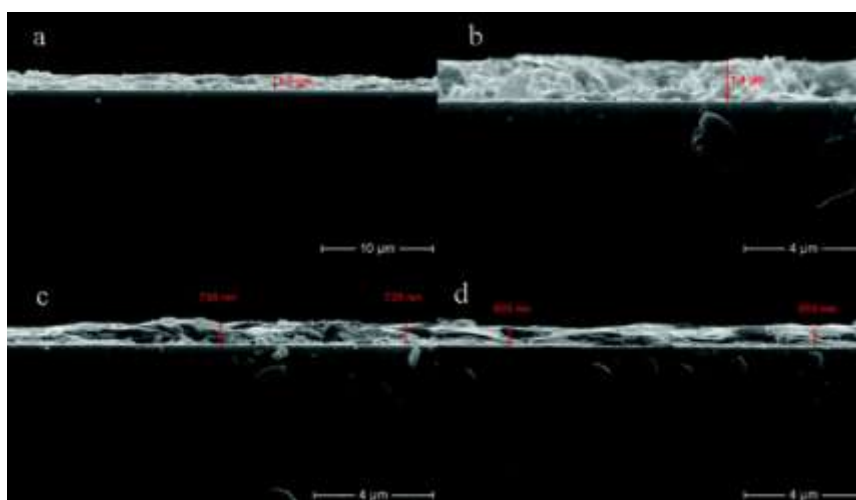


Figure 17. Cross-sectional SEM images of mesoporous, *tin-rich* ITO prepared with the molecular single-source precursor ITBO, using 20 wt % (a, b) F127 and (c, d) KLE as templates, respectively. (Aksu *et al.*, 2011)

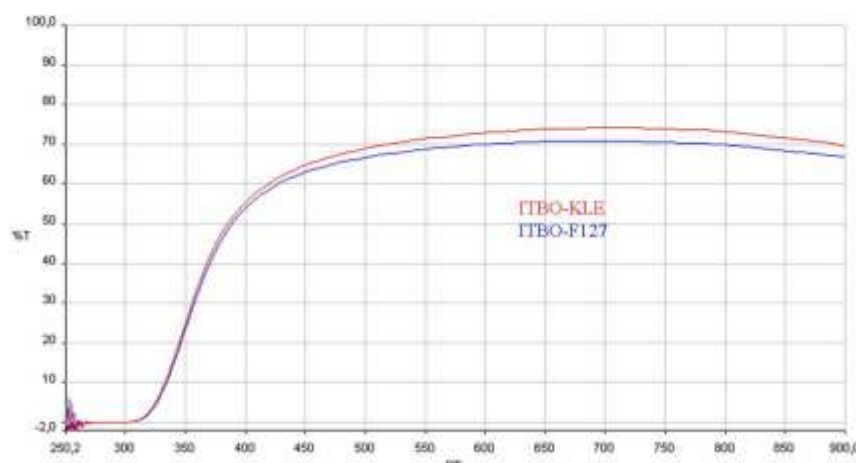


Figure 18. Optical transmission of mesoporous ITBO films in the UV-Vis region. (Aksu *et al.*, 2011)

3.2.2.3 Preparation of pIATO

ATO films were prepared by Dr. Fernando Pérez Caballero and Dr. Anna Fischer from the Technische Universität Berlin (Germany).

The films were prepared by dip-coating a colloidal suspension of ATO nanoparticles on ITO-coated glass. Generally, 160 mg of ATO nanoparticles were dispersed in 2 mL of THF and drops of concentrated HCl solution were added until the solution turn to transparent. When needed, further drops of THF or Ethanol were added in order to reach a full transparency of the solution. The speed of coating was varied between 150 and 300 mm min⁻¹, the relative humidity was set to 25% (± 5%) and the temperature to 25°C (± 2°C). The films were stored at 80 °C for 24 h and then calcined to sinter the ATO particles leading to an increase in conductivity. The films were calcined with an increasing heating (0.6 °C min⁻¹) and finally kept at 450 °C for 30 min.

3.2.2.4 Electrode loading

For mpITO-coated borosilicate glass and mpITO-graphite, the slides were pretreated by immersion for three hours in a stirred solution of 1 % Alconox in water and in ethanol (96 %), and subsequently, three times immersion in Milli-Q water for 30 min. The system was equilibrated over night with 5 mM potassium phosphate buffer solution pH 7.0.

In case of mpITBO, the slide pretreatment was avoided and the material was used as received after 1h equilibration in the measuring buffer.

Immobilization of *cyt c* was achieved dipping the slides into a protein solution (10 µM, unless otherwise reported) 5 mM potassium phosphate buffer solution pH 7.0 for 30 min at 4 °C.

For spectroelectrochemical experiments of the *hSO* heme domain (HD), the protein immobilization was preceded by an equilibrated overnight of a clean mpITO in a poly-lysine solution 2 mg/ml in sodium phosphate buffer (5 mM, pH 8.0). Immobilization of HD was achieved dipping the mpITO slide into a protein solution (3.2 µM) in sodium phosphate buffer solution (5 mM, pH 7.0) for 3 h at 4 °C.

Prior to all the experiments, the supernatant protein-containing solution was removed, the cell was rinsed and stirred for 1 min in a fresh buffer solution. The modified electrode was stored in a low buffer solution at 4 °C until use.

TMB was adsorbed within the porous film by soaking the electrode in 1 mM TMB solution and after 30 minutes equilibration the resulting electrode was washed thoroughly and investigated in a TMB-free phosphate buffer 5mM pH 7.0. The same procedure was used also when the mpITO was already modified with cyt c.

3.2.2.5 Electrochemistry

Electron transfer rate constant, and the heterogeneous electrochemical transfer coefficient α were determined from CV peak separation using Laviron's model (Laviron, 1979) in case of immobilized species and the method of Nicholson in case of species free in solution (Nicholson, 1965).

The electroactive surface coverage was determined from the mean value of the reduction and oxidation peak areas of a background-subtracted cyclic voltammogram.

For superoxide detection a constant potential of +150 mV against the Ag/AgCl (1 M KCl) reference electrode was applied to the working electrode, and the analyte was generated successively by addition of hypoxanthine in a XOD solution.

3.2.2.6 Resonance Raman measurements

The resonance Raman measurements were performed in collaboration with Dr. Jou-Ju Feng, Dr. Inez M. Weidinger and Prof. Peter Hildebrandt from the Technische Universität Berlin (Germany).

Potential-dependent resonance Raman (RR) measurements were carried out with a home-made electrochemical cell using a cylindrical mpITO-covered graphite slide (12 mm diameter) as the working electrode and an Ag/AgCl (3 M KCl) reference electrode. RR spectra were recorded with 413 nm excitation using a confocal Raman microscope (LabRam HR-800, Jobin Yvon). The laser beam was focused onto the surface of the working electrode with a long working distance objective (20× magnification; numerical aperture 0.35). The RR spectra were acquired with a laser power of 3.5 mW, a spectral resolution of 2 cm^{-1} , and an increment per data point of 0.57 cm^{-1} . The accumulation time for each spectrum was 30 s. Further details of the setup are given elsewhere (Wackerbarth *et al.*, 1999; Feng *et al.*, 2008).

3.2.3 Electrochemical study of hSO on AuNPs

3.2.3.1 Synthesis of gold nanoparticles

The gold nanoparticles were prepared in collaboration with Oscar Rojas and Prof. Joachim Koetz from the Potsdam Universität (Germany).

Polyethyleneimine (0.5 wt. %) and the tetrachloroaurate of 2 mM were mixed with 1:1 ratio (wt/wt) at room temperature in an ionic liquid emim EtSO₄ solvent and heated up to 100 °C for 5 min. The change in colour from yellow to dark red indicated the formation of gold nanoparticles. They show an UV-vis absorption maximum at 529 nm, due to the surface plasmon resonance, confirming the formation of gold particles of small dimension (Figure 19). The AuNPs were dissolved in Tris buffer 0.5 mM pH 7.0 and the hydrodynamic diameter was determined by dynamic light scattering (DLS). Measurements were carried out at 25 °C at a fixed angle of 173° (“backscattering detection”) by using a Nano Zetasizer (Malvern) equipped with a He-Ne laser ($\lambda = 633\text{nm}$; 4 mW) and a digital autocorrelator. The refractive indices and viscosities of solvents were adapted to the respective measurements.

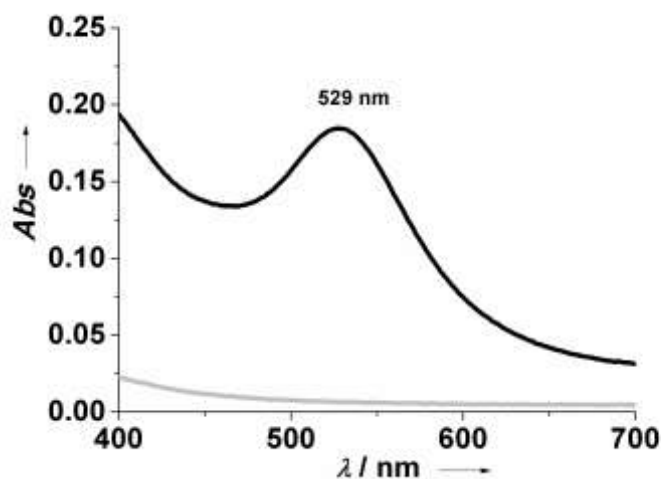


Figure 19. UV-vis spectra indicating the surface plasmon resonance of gold nanoparticles grown in 1-ethyl-3-methylimidazolium ethylsulfate at 100 °C. The grey line indicate the absorption of starting reaction solution, the black line indicate the same solution after 5 min. at 100 °C.

Transmission electron microscopy (TEM) micrographs of the nanoparticles were recorded on an EM 902 microscope from Zeiss. The nanoparticles sample was dissolved in chloroform and prepared by dropping a small amount of the solution, on copper grids, dried and examined in the transmission electron microscope at an

acceleration voltage of 90 kV. The zeta potential was determined by means of the Nano Zetasizer (Malvern) based on the electrophoresis principle which considers the motion of charged particles by applying an electric field.

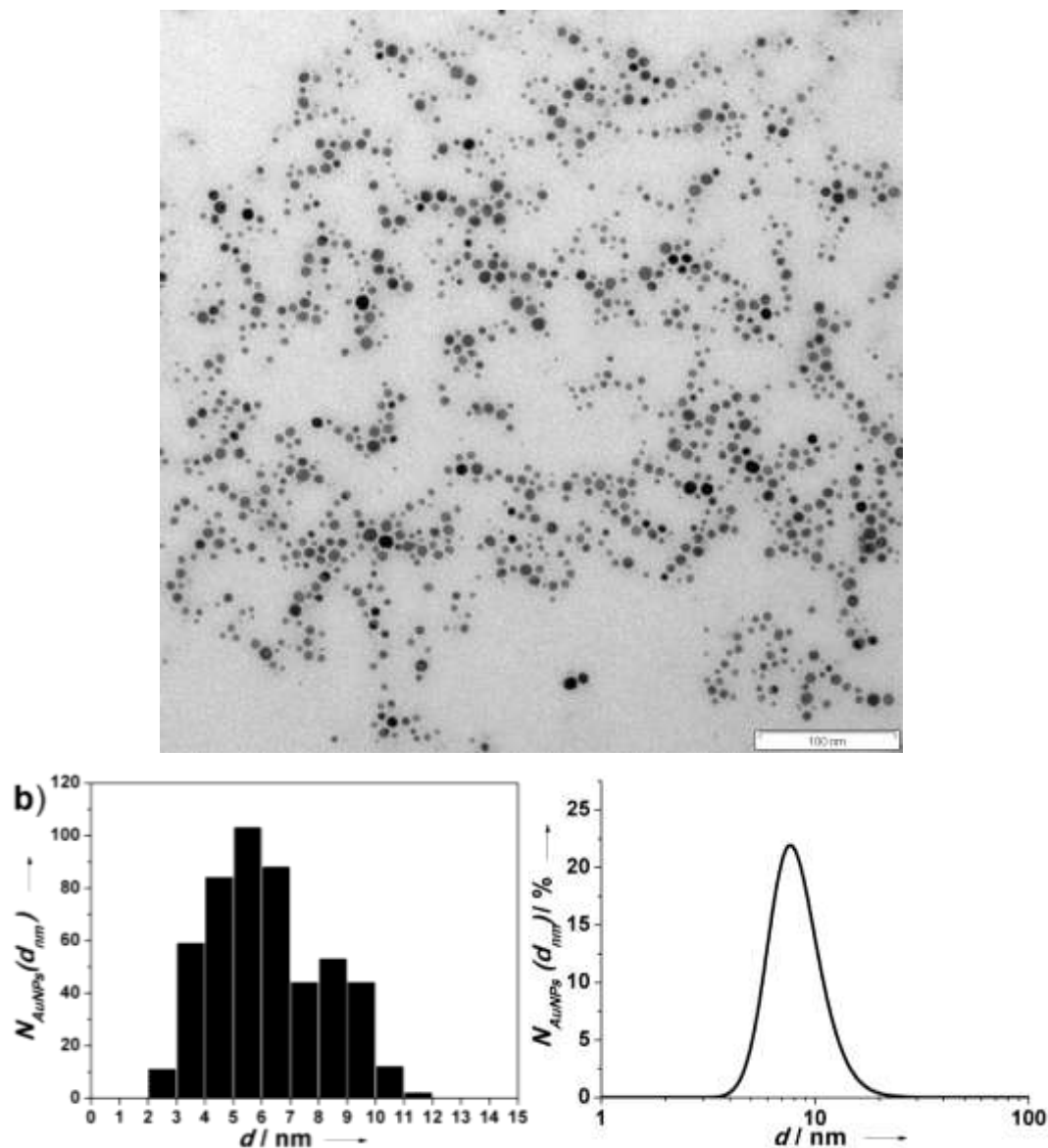


Figure 20. (Top) Electron transmission micrograph of gold nanoparticles synthesized in the ionic liquid 1-ethyl-3-methylimidazolium *n*-ethylsulfate; (bottom left) Histogram showing the particle number density N_{AuNPs} in the size interval Δd of 1 nm as function of the particle diameter d/nm . The mean diameter was 6 ± 2 nm; (bottom right) Number distribution $N_{AuNPs}/\%$, as function of the particle diameter d/nm measured by dynamic light scattering (DLS).

TEM micrograph shows spherical nanoparticles with an average core diameter of about 6 ± 2 nm whereas the hydrodynamic diameter determined by dynamic light scattering (DLS) was 9 ± 1 nm (Figure 20). As TEM images show only the gold core, one can conclude from the hydrodynamic diameter that the gold core is surrounded

by a coating layer of around 2-3 nm. The AuNPs present a positive zeta potential around +20 mV as a result of the cationic polymer coating.

3.2.3.2 Electrode modification

A gold wire (Goodfellow, Bad Nauheim, Germany) with a diameter of 0.5 mm was cleaned by boiling 4 h in 2 M KOH and kept 10 minutes in concentrated HNO₃. A careful rinsing with Millipore water followed every successive step. The electrodes were stored in concentrated H₂SO₄ when not in use. The cleaned electrodes were incubated in an ethanol mixture of 5 mM MUA and 5 mM MU with a volume ratio of 1:3 for at least 24 h at 4 °C. After rinsing with water, the MU/MUA modified electrodes were incubated in a freshly prepared emim EtSO₄ solution of AuNPs for 2 h at room temperature. Further, 5 μL of EDC 0.2 M in H₂O was then added into the solution in order to couple amino functions of the AuNP cap to the carboxylic acid functionalized SAM gold electrode. 20 minutes were used as coupling time. The resulted assembled film {Au/MUA-MU/AuNPs-PEI} was characterized by high resolution scanning electron microscopy (S-4800 microscope, Hitachi, equipped with a field emission gun).

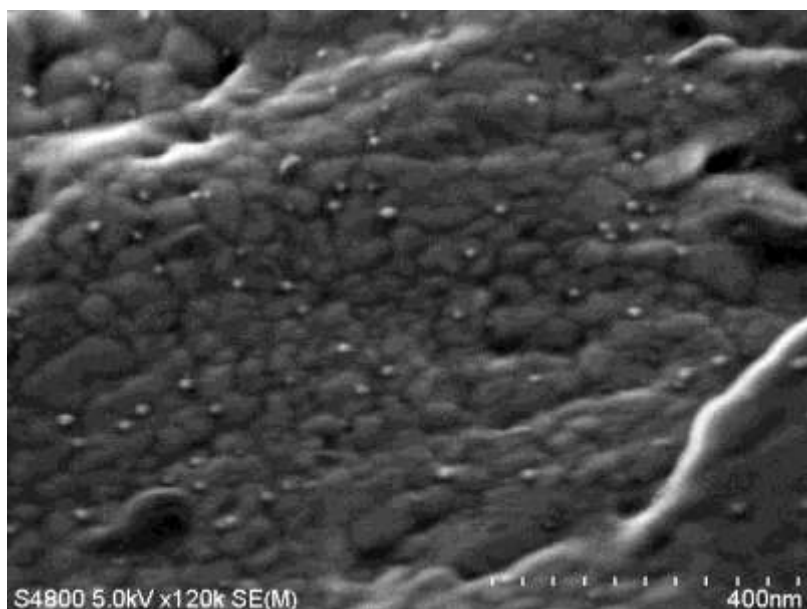


Figure 21. Scanning electron micrograph of the modified gold electrode Au/MUA-MU/AuNPs-PEI.

The employed immobilization method leads finely to disperse single gold particles in the size order between 5 and 10 nm, well resolved in the SEM images (Figure 21). Note that the particles deposited on the electrode surface show no evidence of aggregation after solvent evaporation. The particles are in the same size order

measured by dynamic light scattering and by TEM. The AuNPs are clearly separated from each other forming an accessible surface for protein immobilization.

3.2.3.3 Surface enhanced resonance Raman spectroelectrochemistry

The surface enhanced resonance Raman measurements were performed in collaboration with Johannes Salewski, Dr. Inez M. Weidinger and Prof. Peter Hildebrandt from the Technische Universität Berlin (Germany).

For surface enhanced resonance Raman (SERR) spectroscopic measurements of HD the 413 nm excitation line of a Krypton ion laser and a konfocal Raman spectrometer (Labram, HR-800, Jobin Yvon) were used. Spectro-electrochemistry was performed with a homemade electrochemical cell with a volume of ca. 10 mL. The cell contained an electrochemically roughened and functionalised Ag ring as working electrode, a 3 M KCl Ag/AgCl reference electrode and a platinum counter electrode. The laser power on the sample was 1 mW. SERR spectra were obtained with an accumulation time of 30 s. The working electrode was constantly rotated to avoid laser induced protein degradation. More details about the setup are given elsewhere (Wackerbarth *et al.*, 1999).

3.2.4 XDH spectroelectrochemical study

3.2.4.1 Electrode Pretreatment

Electrochemically pretreated glassy carbon (EP-GC) electrode was prepared as follow. A GC surface was polished to mirror finish using 1 and 0.3 μm alumina slurry for 3 and 5 minutes respectively. The electrode was sonicated in Milli-Q water, after every step for the respective polishing time. After rinsed with Milli-Q H_2O thoroughly, a constant positive potential was applied (1.8 V) under stirring in air saturated potassium phosphate (0.1 M) solution at pH 4. In a fresh solution where then electrochemically cycled between 0.3 and 1.25 V till a steady state was reached and stopped in the oxidation region.

3.2.4.2 Electrode modification

4 μl of protein with a concentration between 40 and 90 μM in its own purification buffer (Tris 50mM pH 8, NaCl 200mM, EDTA 1mM), were dropped onto the freshly

prepared EP-GC electrode. The electrode was covered to ensure the water to evaporate slowly, and equilibrated 30 min. at 4 °C.

The protein immobilization was negligibly affected whether the cyclic scan in the pretreatment was stopped in the oxidation or reduction region.

3.2.4.3 Electrochemical measurement

The electrochemical experiments were carried out in the electrochemical cell 1 (see section 3.1.2), employing a platinum wire as counter electrode, a Ag/AgCl, 1M KCl reference against which all potentials are reported, and a modified glassy carbon disk electrode. All the experiments were performed at room temperature in a oxygen-free 2% H₂ atmosphere with a Gamry Reference 600™ potentiostat (Gamry, USA) and analyzed with GamryEchem Analyst 5.50 software.

The working electrode surface area was determined with a reversible system (K₃Fe(CN)₆ in 1M KCl aqueous solution), employing the Randles-Sevcik equation:

$$(3) \quad i_p = 2.69 \times 10^5 n^{3/2} A D^{1/2} C \nu^{1/2}$$

where D is the diffusion coefficient of Fe(CN)₆^{+3/+2} (0.76 × 10⁻⁵ cm² s⁻¹), n indicates the exchanged electrons, C the K₃Fe(CN)₆ concentration (4mM) and ν is the scanning rate.

3.2.4.4 Spectroelectrochemical mediated titration

All experiments were performed under N₂ atmosphere at room temperature. Potentials were measured using a combination Pt wire and Ag/AgCl reference electrode calibrated against a pH 7 quinhydrone solution ($E^0 = +284$ mV vs NHE at pH 7). The redox potential was adjusted by addition of microliter aliquots of Ti^{III} citrate and K₂S₂O₈. The FAD redox potentials were measured using ca. 15 μM enzyme in 50 mM Tris buffer (pH 8.0) in a 2 ml cuvette under continuous stirring. The solution potentials were stabilized using the Fe and Co complexes (5 μM each) as mediators: [Co(*trans*-diammac)]ClO₄)₃ ($E^0 = -555$ mV vs. NHE), [Co(*cis*-diammac)](ClO₄)₃ (-503 mV), [Co(AMMEsar)]Cl₃ (-380 mV), [Co(sep)]Cl₃ (-296 mV), [Co(AMMEN₅Ssar)]Cl₃ (-220 mV), [Co(CLME-N₄S₂sar)]Cl₃ (-134 mV), [Co((NMe₃)₂sar)]Cl₅ (+10 mV), [Fe(tacn)₂]Br₃ (+144 mV) and Fe(NOTA) (+195 mV) (Bernhardt *et al.*, 2006). Changes in the UV-Vis spectrum were monitored

continuously with an Ocean Optics USB4000 fiber optic spectrometer. Equilibrium was established when no further change in either the optical absorbance or solution potential was detectable. The formal potential for the first electron of FAD reduction (E_1) was determined at 465 nm using the equation:

$$(4) A = \frac{c_{ox}\epsilon_{ox}10^{\frac{E-E_1}{59}} + c_{red}\epsilon_{red}}{1 + 10^{\frac{E-E_1}{59}}}$$

At the same time the potential of both electron transfer (E_1 and E_2) were determined at 465 nm using the equation:

$$(5) A = \frac{(c_{ox}\epsilon_{ox}10^{\frac{(E-E_1)}{59}} + c_{sq}\epsilon_{sq} + c_{red}\epsilon_{red}10^{\frac{(E_2-E)}{59}})}{1 + 10^{\frac{(E-E_1)}{59}} + 10^{\frac{(E_2-E)}{59}}}$$

In the above equations E is the potential, A is the absorption, $c_{ox}\epsilon_{ox}$ and $c_{ox}\epsilon_{ox}$ are the limiting absorbance values of the XDH at 293 K in its oxidized and reduced forms respectively.

4 Results and Discussion

4.1 Mesoporous materials

On planar surfaces only a limited amount of protein can be adsorbed. Therefore despite the advantage of the high transparency of transparent conductive materials the amount of the immobilized protein is close to that of a monolayer and requires high sensitive techniques to be optically detected. For this purpose three dimensionally structured electrodes are presented in this work. For the investigation of such materials different kind of static and microfluidic (spectro)electrochemical cells were designed, constructed and optimized (see section 3.1.2).

4.1.1 Direct electron transfer of cyt c in mpITO

Equilibration of a mpITO electrode in an aqueous solution of cyt c solution results in a quick and efficient surface interaction of the protein, as revealed by the cyclic voltammetry (CV), which displayed a reversible response up to scan rates as high as 1 V s^{-1} . Only a minimal decrease was obtained after the cyt c solution has been exchanged by a protein-free 5 mM phosphate buffer (pH 7.0), demonstrating the strong binding of cyt c in the mesoporous electrode (Figure 22). The pair of voltammetric peaks is almost symmetric and the currents increase linearly with the square root of the scan rate, which gives evidence for a reversible, diffusion-controlled redox process in the pores (Figure 22, inset) (Laviron, 1979).

The CV shows the characteristic full width at half-maximum for a one-electron-exchange process of around 90 mV, at a scan rate of 50 mV s^{-1} . However, the peak broadens at higher scan rates. In the absence of cyt c in the pores no peak current was observed. The CV signals were stable and unchanged for more than a week when the cyt c-loaded electrodes were kept in buffer solution at $4 \text{ }^\circ\text{C}$. For the cyt c in the pores, the formal potential (E^0) was determined to be $9 \pm 1 \text{ mV}$ (Figure 22, solid line), whereas for cyt c in solution E^0 was found to be $14 \pm 1 \text{ mV}$ (Figure 22, dashed line). These values are very similar to those reported for cyt c immobilized on planar ITO (El Kasmi *et al.*, 2002) or gold electrodes (Ge *et al.*, 2002; Jin *et al.*, 1997).

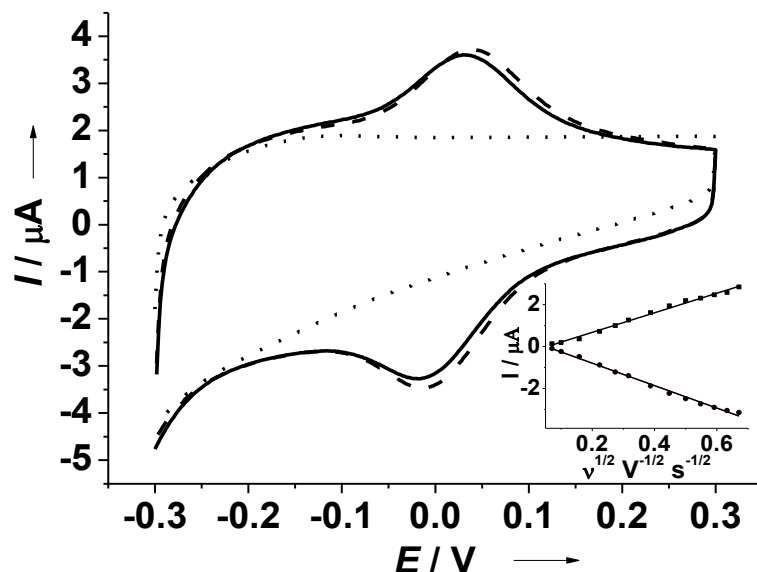


Figure 22. Cyclic voltammograms of a mPITO electrode, obtained in a potassium phosphate buffer (5 mm, pH 7.0) at 50 mVs^{-1} without addition of cyt *c* (dotted line), in the presence of 10 mM cyt *c* in solution (dashed line), and after immobilization of cyt *c* (solid line). The inset shows the dependency of the peak current on the square root of scan rate.

From the CV at different scan rates, the electrochemical transfer coefficient α was calculated to be 0.55 and the apparent heterogeneous rate constant was estimated to be $1.20 \pm 0.02 \text{ s}^{-1}$ (Laviron, 1979). The rate constant is lower than that determined for cyt *c* on planar ITO electrode (18 s^{-1} (El Kasmi *et al.*, 2002)), but very close to those measured for cyt *c* bound in other mesoporous materials (SnO_2 : $1 \pm 0.03 \text{ s}^{-1}$ (Topoglidis *et al.*, 2003)); silica: (1.33 s^{-1} (Zhang *et al.*, 2007)), on colloidal Au ($1.21 \pm 0.08 \text{ s}^{-1}$ (Ju *et al.*, 2002)), and in NaY zeolite ($0.78 \pm 0.04 \text{ s}^{-1}$ (Dai *et al.*, 2004)). The total amount of loaded protein increases with the cyt *c* concentration in the initial solution used for incubation. As measured by UV-Vis absorption spectroscopy, both quantities are directly correlated with the concentration range under investigation (Figure 23, solid triangles). However, the electrochemical experiments reveal a drastic decrease of the fraction of electroactive proteins with the amount of adsorbed cyt *c* (Figure 23, open triangles). Moreover, broader voltammetric redox peaks at high cyt *c* concentration suggest an agglomeration of the proteins in the pores, which evidently impairs electronic communication with the electrode.

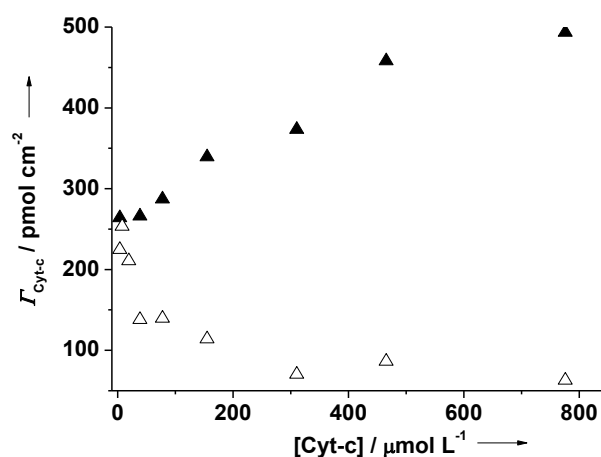


Figure 23. Adsorbed (solid triangles) and electroactive (open triangles) cyt c surface coverage of mpITO for different protein loading solutions, in a potassium phosphate buffer (5 mM, pH 7.0), determined spectroscopically and electrochemically, respectively.

As shown, both experimentally and theoretically, rotational diffusion of immobilized cyt c is an essential determinant for the dynamics of the interfacial redox process, since the preferred binding domain exhibits only a relatively poor electronic coupling with the electrode (Kranich *et al.*, 2008; Paggi *et al.*, 2009). Instead, a high electronic coupling is associated with a medium-affinity binding site, such that a fast interfacial electron transfer requires a rotational motion of the immobilized protein. It is very likely that this mobility is severely restricted for cyt c immobilized inside the narrow pores as compared to the protein adsorbed on the surface of planar ITO electrodes.

A good compromise between the amount of adsorbed and the fraction of electroactive protein was achieved with a loading solution of 10 μM cyt c. Taking into account the geometrical area of the mpITO-coated slide (0.237 cm^2), under these condition a surface concentration of approximately 250 pmol cm^{-2} was voltammetrically determined, with nearly 100 % electroactive species. Assuming a spherical shape for cyt c with a surface area of approximately 7 nm^2 (Topoglidis *et al.*, 1998), the enzyme coverage of 250 pmol cm^{-2} is approximately 10 times larger than the theoretical value for a densely packed cyt c monolayer and 15 times larger than that determined for cyt c immobilized on a planar ITO electrode (El Kasmi *et al.*, 2002). This high value for the mpITO electrode implies that cyt c effectively penetrates into the network of pores of the approximately 170 nm-thick ITO layer.

The low ionic strength in the loading condition was essential since it was found that an attempt to immobilize cyt c directly in a higher ionic strength buffer solution (100 mM sodium phosphate pH 7.0) led to a 30% smaller protein loading.

After 1 hour incubation of the cyt *c* modified mpITO in solutions with high ionic strength larger than 250 mM, desorption takes place as reflected by a decrease in the CV peaks. No effect was noted at lower ionic strengths. The main reason of the cyt *c* immobilization in the mesoporous structure of the mpITO film is therefore likely a largely stabilized by electrostatic interactions. A further contribute of the protecting environment created by the porosity is not to be excluded. In this respect, the performance of the mpITO electrode is better than that of self-assembled monolayer (SAM)-coated metal electrodes for which efficient desorption of electrostatically bound cyt *c* is already induced at significantly lower ionic strengths.

After removal of the electrostatically bound cyt *c*, the mpITO electrode gave rise to a CV that is essentially the same as that for the original material prior to the first protein loading. However, readsorption of the protein from a cyt *c* containing solution did not lead to the same amount of immobilized electroactive protein as a freshly prepared mpITO electrode. Presumably, a small fraction of electroinactive and minor contributions of denatured protein could not be removed by incubation with concentrated electrolyte solutions, thereby blocking adsorption for subsequent reloading cyt *c*. However after stringent electrode pretreatment including washing with detergents and alcohol (see the methods section 3.2.2.4), the original loading capacity could be restored. The washing sequence was therefore used as standard pretreatment of the electrode.

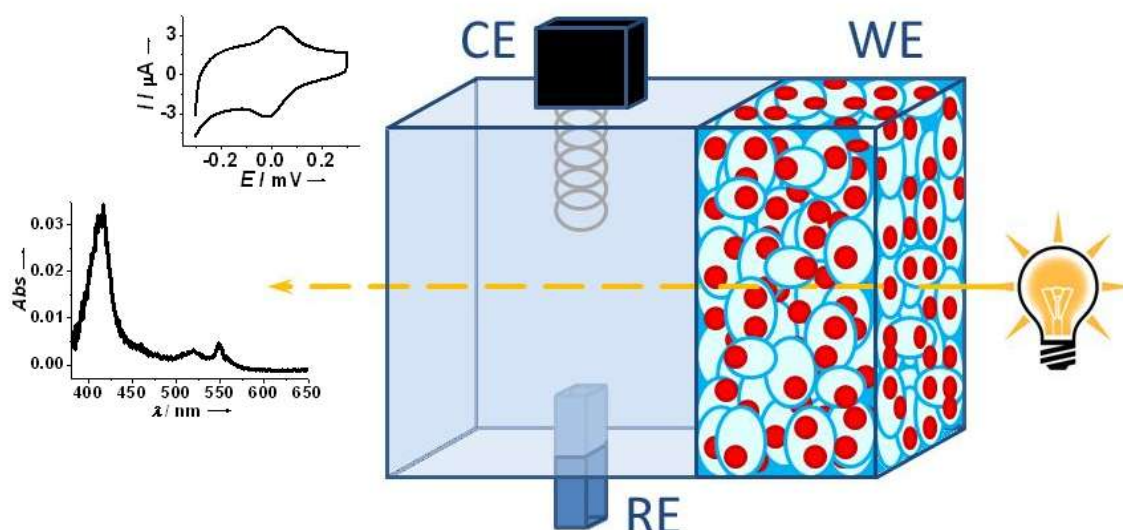


Figure 24. Schematic representation of the spectroelectrochemical cell. The cyt *c* (red circles) is immobilizer in the porosity of the mpITO. WE indicates the working electrode, CE the counter electrode and RE the reference electrode. The cell may combine optical and electrochemical measurement of an analyte in the electrode porosity as well as in the solution.

The immobilization strategy employed is clearly very facile, with the cyt *c* adsorption most probably being based upon electrostatic interactions between negatively charged groups on the ITO surface and positively charged surface lysine and/or arginine residues.

4.1.2 UV-Vis spectroelectrochemistry of cyt *c* in mpITO

The optical properties of ITO allow monitoring of cyt *c* immobilized on mpITO films on glass slides simultaneously to UV-Vis spectroscopy. Upon varying the electrode potential, the oxidation state of the adsorbed cyt *c* was reversibly switched from the ferric to the ferrous form, as indicated by the shift of the Soret band from 410 to 416 nm and the formation of the characteristic 520 nm and 550 nm bands in the Q-band region (Figure 25 left).

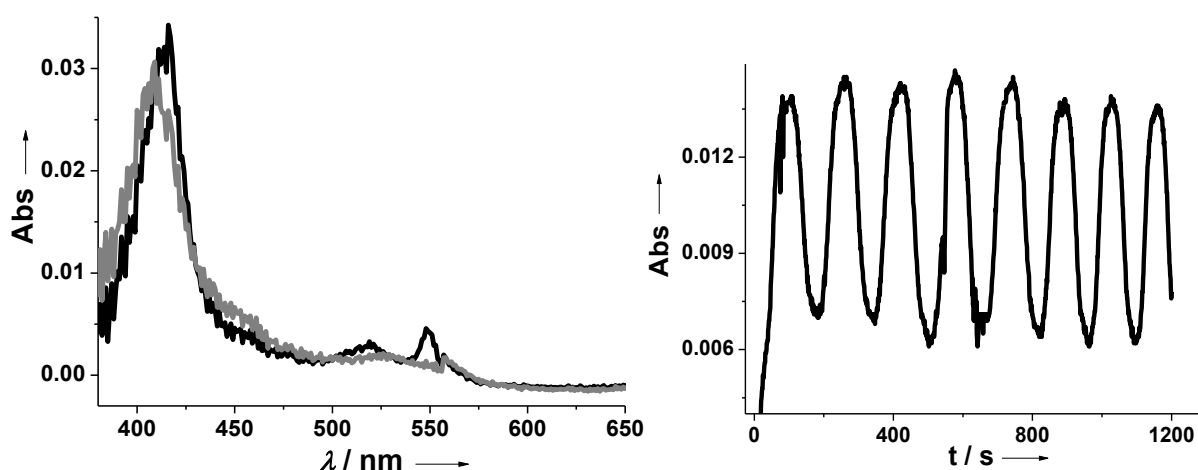


Figure 25. (Left) Absorption spectra of cyt *c* adsorbed on a mpITO electrode at +0.2 V (gray) and at -0.2 V (black), corresponding to the ferric and ferrous form of cyt *c*, respectively; (right) absorbance changes at 416 nm of a mpITO electrode loaded with cyt *c* in contact with a protein-free buffer, pH 7.0).

The absorption spectra also allow determining the surface concentration of cyt *c*, on the basis of the extinction coefficients for the oxidized (ferric) and reduced (ferrous) form. Thus, for a loading solution of 10 μM cyt *c*, surface concentrations of 260 ± 10 and 250 ± 10 pmol cm^{-2} were obtained for the oxidized and reduced cyt *c*, respectively. Since within the error margins the concentrations for the oxidized and reduced cyt *c* are the same, these results indicate that the adsorbed protein is fully redox active. This finding, as well as the value determined for the cyt *c* surface concentration, is in very good agreement with the results derived from CV

measurements. In Figure 25 (right), the absorbance at 416 nm is plotted during the continuous potential sweep, displaying a cyclic oxidation and reduction of the enzyme in the porous structure and indicating a reversible process.

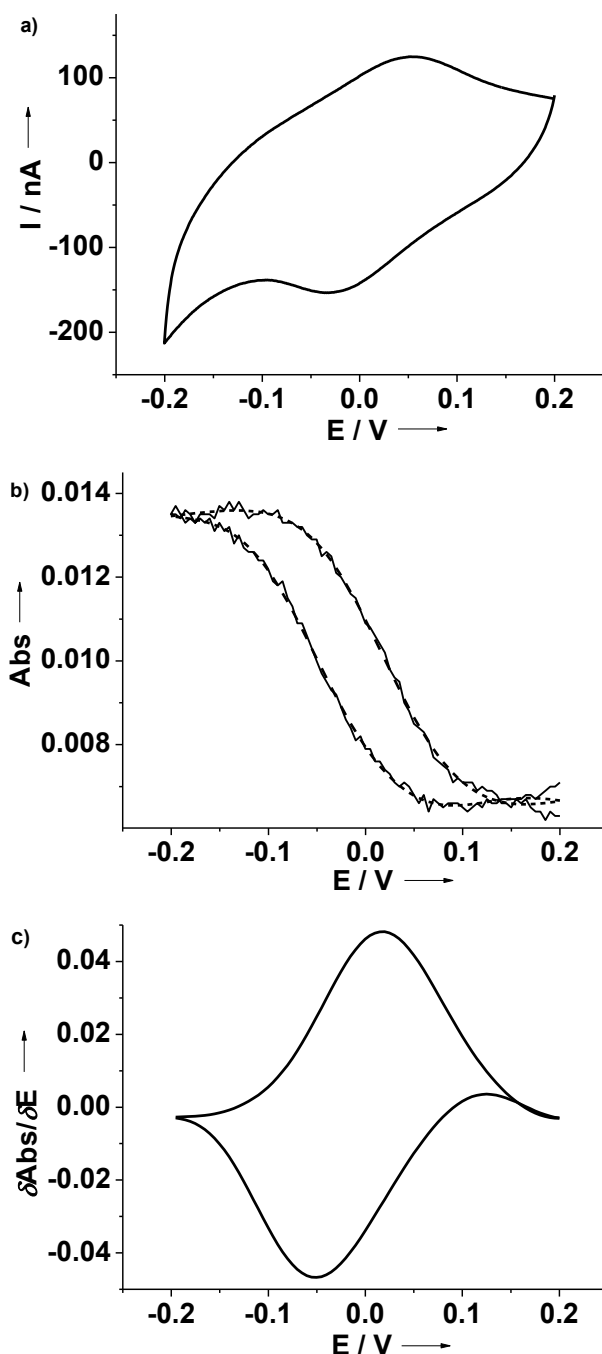


Figure 26. a) CV, b) CVA, and c) DCVA obtained for cyt *c* adsorbed on a mpITO electrode (scan rate = 5 mV s^{-1} ; 5 mM phosphate buffer, pH 7.0). The absorbance was monitored at 416 nm (see Figure 25 right). The DCVA was calculated from the CVA after applying a Fourier transform smoothing algorithm (dashed line in b).

The absorbance at 416 nm following the cyclic variation of electrode potential, known as cyclic voltabsorptogram (CVA) (Bowden *et al.*, 1982), and the

corresponding derivative (DCVA) yield a formal reduction potential of 5 ± 4 mV (Figure 26), very close to that obtained by CV (Figure 22).

4.1.3 Resonance Raman spectroelectrochemistry in mpITO

Resonance Raman (RR) spectroscopy was performed in order to provide information about the structural integrity of the heme pocket. RR spectroscopy is based on inelastic scattering, or Raman scattering, of monochromatic light by and other low-frequency modes in a system. It allows, using the Soret absorption of the cyt *c*, to selectively study the events at the heme environment. Different RR spectra are associated to the oxidized and reduced state of the cyt *c* and besides to the active and inactive state.

RR spectra of cyt *c* adsorbed on mpITO electrodes were measured as a function of the applied potential. The spectra provide no indications for contributions from non-native states of the protein at relative concentrations of more than 5 % (Oellerich *et al.*, 2002) and all spectra could be well described by a superposition of the component spectra of the native ferric and ferrous form of cyt *c* as well as of the component spectrum of bare ITO, which has been determined in separate experiments in the absence of cyt *c* (Figure 27a). Quantitative analysis of the spectra afforded the relative concentrations of the ferrous and ferric species, which were then are plotted as a function of the electrode potential (Figure 27b).

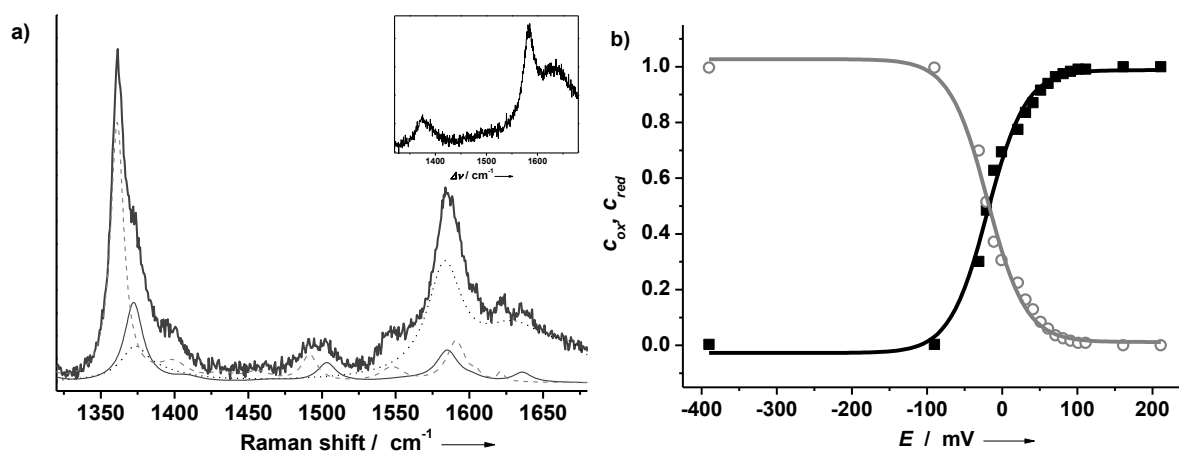


Figure 27. a) RR spectrum of cyt *c*/mpITO measured at 0.0 V; the component spectra of the ferrous and ferric form of the native protein are indicated by the dashed and solid lines, respectively. The dotted line and the inset represents the spectral contribution of ITO; b) Relative concentrations of the ferric (solid squares) and ferrous forms (open circles) of cyt *c* as a function of applied potential. The solid lines refer to the fit of the Nernst equation to the experimental data.

The results reveal a nearly ideal behavior since the apparent number of transferred electrons is very close to one ($n = 0.97$). For cyt *c* electrostatically adsorbed on metal electrodes coated with SAMs of carboxyl-terminated thiols, experimentally determined n values were typically between 0.8 and 0.9, which was attributed to heterogeneous protein adsorption. Conversely, the present results for cyt *c* on mpITO thus suggest a highly homogeneous surface distribution of the protein. The formal potential derived from RR spectroscopy analysis was found to be approximately -16 mV, which is slightly more negative than that derived from the (spectro)electrochemical measurements, but is still within the reported limits.

4.1.4 Spectroelectrochemical studies of cyt *c* in mpITBO

A general problem in the production of mpITO is the limited amount of cheaper component, 10 wt % tin, in respect to the expensive component, indium. Furthermore the elevated production temperature implies a compromise between the conductivity and regular porosity (von Graberg *et al.*, 2011).

To avoid phase segregation of *tin-rich* ITO, a low-temperature approach with high control over the In/Sn molar ratio was reported recently, based on the molecular single-source precursor indium tin tris-*tert*-butoxide (ITBO; Scheme 1) containing indium and tin in the molar ratio of 1:1, which facilitates the formation of *tin-rich* ITO with an identical stoichiometry in the final product (Aksu *et al.*, 2009).

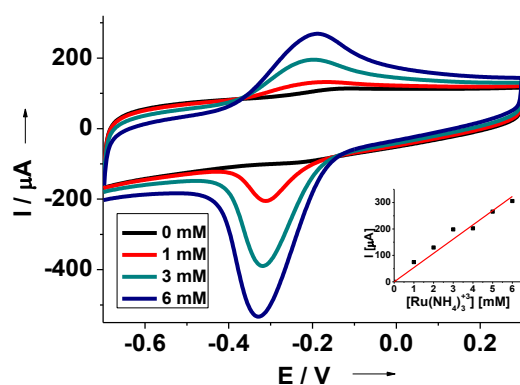


Figure 28. Cyclic voltammograms of a mpITBO_F127 electrode obtained in a potassium phosphate buffer solution (50 mM, 500mM, pH 7.0) in absence (black line) and presence of 1mM (red line), 3mM (cyan line) and 6mM (blue line) of $\text{Ru}(\text{NH}_3)_6^{+3}$, scan rate 100mV/s. The inset shows the dependency of the peak current on the $\text{Ru}(\text{NH}_3)_6^{+3}$ concentration.

Due to the recent development of such material, initial electrochemical experiments with the small mobile redox mediator $\text{Ru}(\text{NH}_3)_6^{2+/3+}$ were performed.

mpITBOs shows a fast reduction and oxidation. The standard rate constants were calculated to be $4 \pm 2 \times 10^{-3} \text{ cm s}^{-1}$ and $3 \pm 1 \times 10^{-3} \text{ cm s}^{-1}$ (Nicholson, 1965) for mpITBO_F127 and mpITBO_KLE respectively, much higher value than those for a crystalline mpITO, produced from conventional tin and indium precursors ($6 \pm 2 \times 10^{-4} \text{ cm s}^{-1}$) as described in the chapter 3.2.2.1.

This electrochemical efficiency and the optical transparency of the mpITBOs (Figure 18) lend themselves to application for protein (spectro)electrochemical study. Equilibration of a mpITBO electrode in an aqueous solution of cyt c solution results in an efficient protein loading, as revealed by the CVs after substitution of the cell solution with a cyt c-free buffer solution. They displayed a reversible response at low scan rate, with a formal potential of $-6 \pm 5 \text{ mV}$ (vs. Ag/AgCl/ 1M KCl). As in the case of mpITO a small concentration of cyt c in the initial solution was selected for incubation (see chapter 4.1.1). Assuming a spherical shape for cyt c with a surface area of ca. 7 nm^2 (Topoglidis *et al.*, 1998), the spectroscopic characterization of the immobilized protein reveals a higher protein loading of the ITBO_KLE ($\Gamma_{\text{cyt } c} \sim 1900 \text{ pmol cm}^{-2}$, $\sim 0.7 \text{ nm}$ film thickness) than the ITBO_F127 ($\Gamma_{\text{cyt } c} \sim 2400 \text{ pmol cm}^{-2}$, $\sim 1.5 \text{ nm}$ film thickness), taking into account the different film thickness.

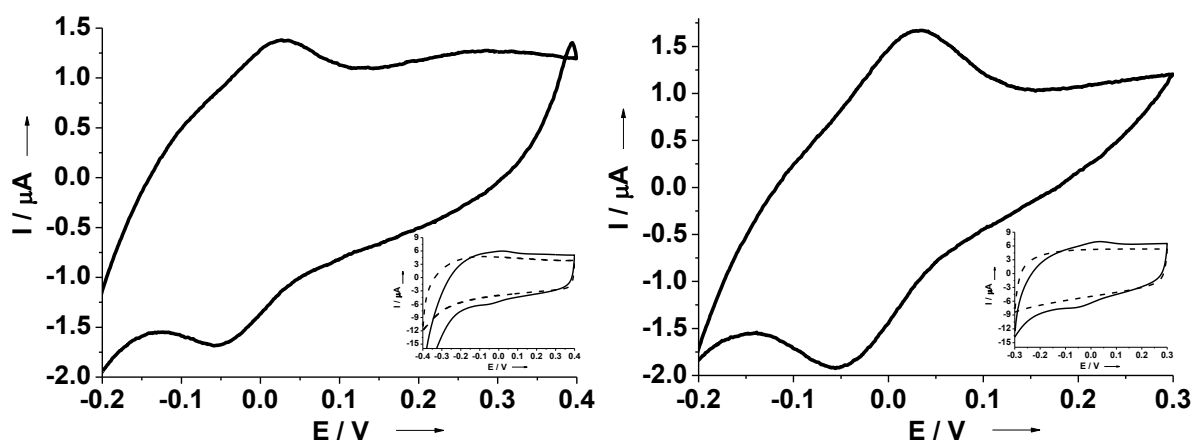


Figure 29. Background-subtracted cyclic voltammograms of mpITBO electrodes (left mpITBO_KLE and right mpITBO_F127), obtained in a potassium phosphate buffer (5 mM, pH 7.0) at 5 mVs^{-1} after immobilization of cyt c. The insets show the raw CVs at the same condition before (dashed line) and after (solid line) immobilization of cyt c.

The increase of the protein amount in thicker films may be due to the effective deep localization of the protein inside the three-dimensional structure. The cyt c incorporation takes much more time for ITBO_KLE than for ITBO_F127 (Figure 30). For ITBO_KLE it takes about a week to reach a maximum amount of immobilized

protein, whereas for ITBO_F127 the maximum amount is reached in less than 2 h. It should be noted that for the two templates the formation of different mesostructures in silicas have been reported.

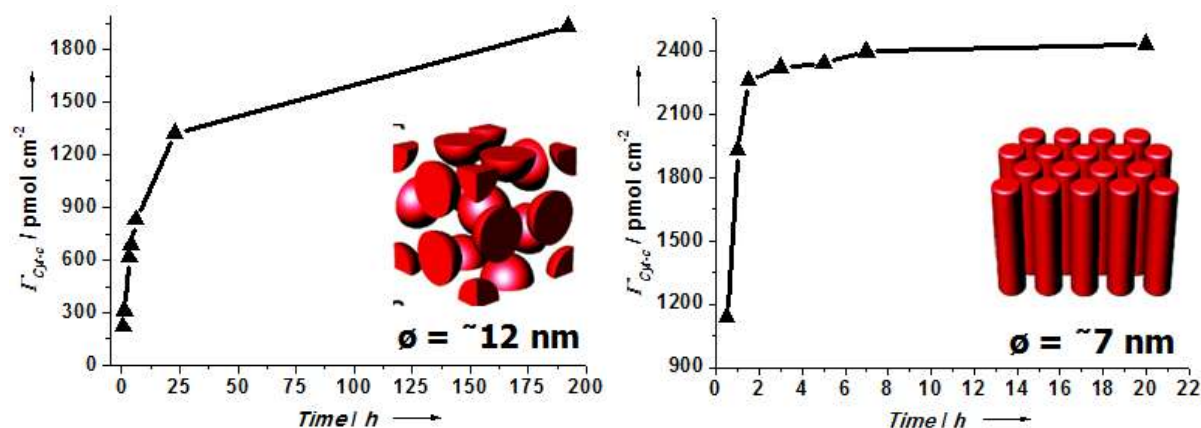


Figure 30. Cytochrome c surface loading of (left) ITO_KLE and (right) ITO_F127 for different protein incubation times in a 15 μ M cyt c solution determined spectroscopically in protein-free potassium phosphate buffer (5 mM, pH 7.0). The close-packed spherical pores formed by KLE and two-dimensional hexagonal arrangement of cylindrical pores formed by F127, as well as the pore sizes are depicted.

For KLE the formation of close-packed spherical pores connected via smaller micropores was reported (Thomas *et al.*, 2003), while for F127 typically a two-dimensional hexagonal arrangement of cylindrical pores is found (Grosso *et al.*, 2001). Similarly also the formation of spherical and cylindrical (“worm-like”) pores can be observed in ITBO_KLE and ITBO_F127, respectively (Aksu *et al.*, 2011). Thus, although ITBO_KLE possesses a larger mesopore diameter, the pores are harder to access for the protein, as the connectivities between those pores are much smaller. In both cases the finally immobilized cyt c is able to exchange electrons directly with the conductive electrode material. Cathodization (-0.3 V vs Ag/AgCl, 1 M KCl) of the modified electrode, for a couple of minutes, reduces completely the present protein, within the margins of error. In the same way cytochrome c is reoxidized, applying a positive potential around $+0.3$ V. This process is fully reversible and thus can be exploited to study the protein in a potentiostatically controlled redox state.

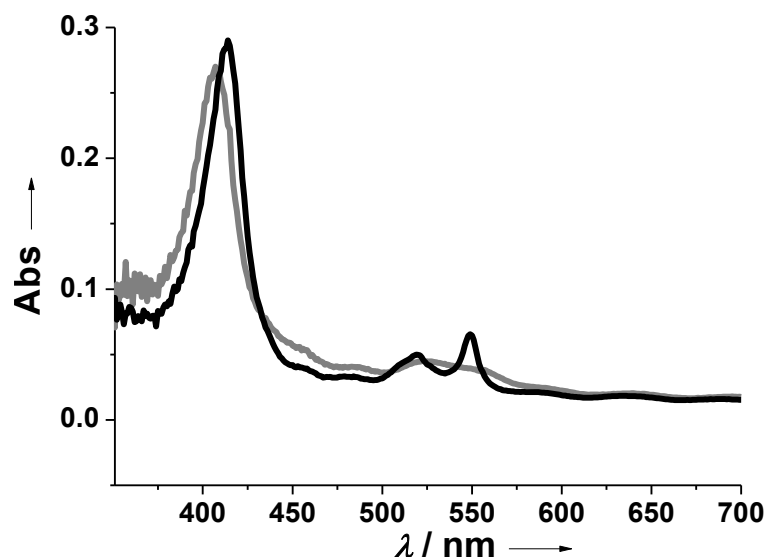


Figure 31. Absorption spectra of Cyt *c* adsorbed on a mpITBO_F127 electrode at +0.2 V (gray line) and at -0.2 V (black line), corresponding to the ferric and ferrous form of cyt *c*, respectively.

The optical properties of ITBO allow monitoring of the state of cyt *c* by UV-Vis simultaneously with electrochemistry. The oxidation state of the immobilized cyt *c* was reversibly switched from the ferric to the ferrous form upon varying the electrode potential between +0.2 and -0.2 V (vs AgAgCl/1 M KCl). Oxidized and reduced cyt *c* display characteristic absorption spectra. As it was observed for mpITO the switch from oxidized (ferric) to reduced (ferrous) state is indicated by the shift of the Soret band from 410 to 416 nm and the evolution of the 520 and 550 nm bands in the Q-band region (Figure 31).

4.1.5 Superoxide biosensor

To assess the performance of mesoporous indium tin oxide based materials as a support for a biosensor, the reactivity of cyt *c* adsorbed on mpITO towards O_2^- was studied. In nature, cyt *c* shows an excellent reactivity to many reductants and oxidants. In the past it has been demonstrated that a biosensor relied on the reaction of cyt *c* with O_2^- [Equation (1)] can be used for superoxide anion radical detection (Scheller *et al.*, 1999; McNeil *et al.*, 1995; Ge and Lisdat, 2002; Hill *et al.*, 1985; McNeil *et al.*, 1989; Wollenberger, 2005). Superoxide anion radicals were generated by enzymatic reaction of xanthine oxidase (XOD) with oxygen and hypoxanthine. A constant concentration was achieved when superoxide formation and disproportionation were in steady state [Equation (6)] (McCord *et al.*, 1968).

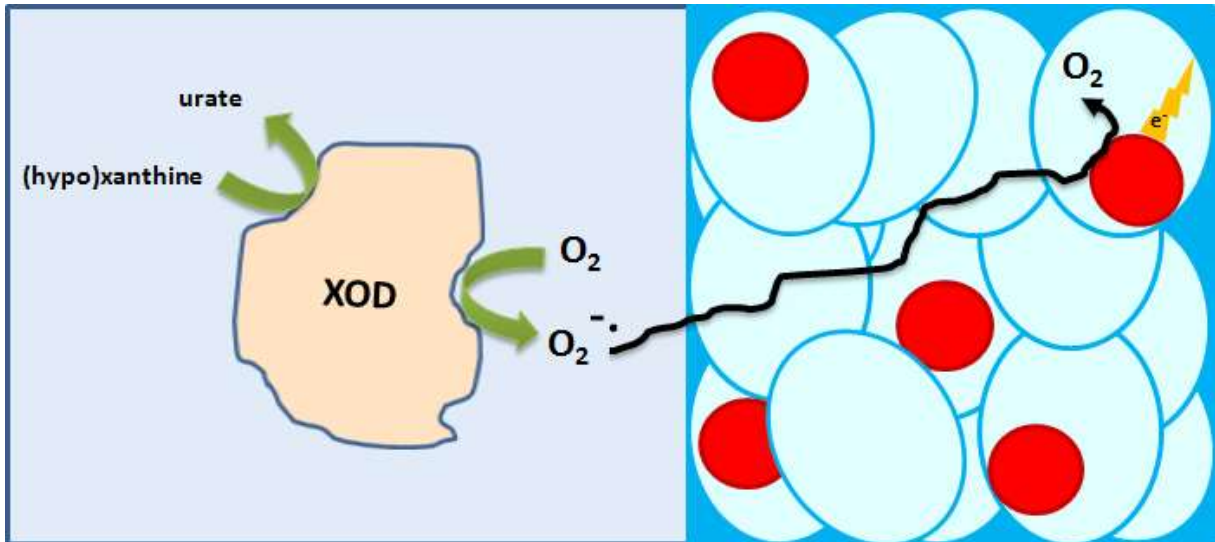
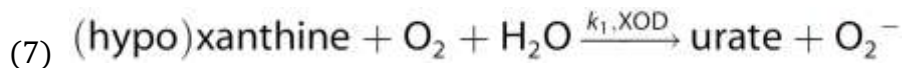


Figure 32. Schematic representation of cyt c (red circles) immobilized in the porosity of the mpITO, shown on the right. The enzymatic generation of superoxide, by XOD in the bulk solution, is shown on the left. The catalytic oxidation of the superoxide diffusing in the porosity and the subsequent electron transfer between cyt c and the conductive ITO pore wall is also depicted.

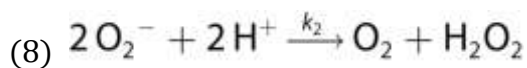
Under steady state conditions, this process can be described according to

$$(6) \quad \frac{d[\text{O}_2^-]}{dt} = k_1 [\text{XOD}] - 2k_2 [\text{O}_2^-]^2 = 0$$

where k_1 is the rate constant of the XOD-catalyzed reaction given in [Equation (7)]:



and k_2 is the rate constant of the disproportionation reaction given in [Equation (8)]:



The concentration of superoxide in solution is considered to be proportional to the square root of the enzymatic activity (McCord *et al.*, 1968) as given in [Equation (9)]:

$$(9) \quad [\text{O}_2^-]_{\text{st}} = \sqrt{\frac{k_1 [\text{XOD}]}{2k_2}}$$

At +150 mV, the adsorbed cyt *c* is oxidized by heterogeneous electron transfer and reduced by O_2^- . This reaction gives rise to a catalytic oxidation current (Figure 32). After addition of superoxide dismutase (SOD), as a consequence of the consumption of superoxide by SOD, the current drops rapidly. This indicates therefore that only the specific reaction with superoxide in solution is responsible for the detected signal (Figure 33, inset).

In the proposed case of a cyt *c*-modified mpITO electrode, a linear dependence of the catalytic current and the square root of the XOD concentration was obtained in the range of 1 – 20 $mU L^{-1}$ with a linear regression of $I \text{ (nA)} = -0.73 + 30.55 [XOD] \text{ (mU L}^{-1}\text{)}$ and $R^2=0.994$. From this dependence and using the spontaneous disproportionation rate of O_2^- of $2.3 \times 10^5 M^{-1} s^{-1}$ (Behar *et al.*, 1970; Ge *et al.*, 2002), the linear measuring range of the steady state O_2^- concentration of 0.13 to 0.67 μM was estimated with a sensitivity of about 100 $A M^{-1} m^{-2}$ (Figure 33). Note that at the blank mpITO electrodes, lacking the (adsorbed) protein, no current-time traces were generated when superoxide was generated in solution. Also, addition of hypoxanthine in the absence of XOD did not show any catalytic response.

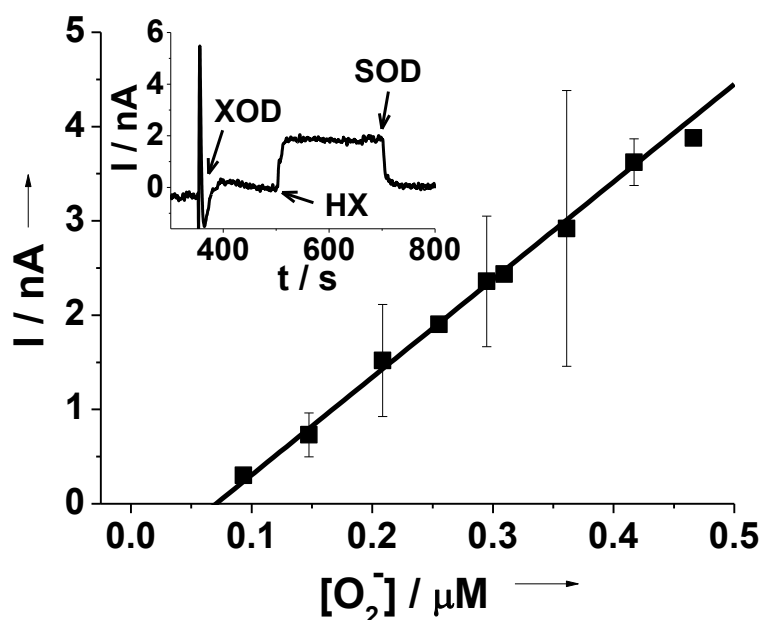


Figure 33. Linear dependence of the current signal on the superoxide concentration. Amperometric indication of superoxide using a cyt *c*/mpITO electrode. The inset shows the current response after addition of xanthine oxidase, starting the superoxide production with 200 mM hypoxanthine solution and later scavenging the superoxide radicals by superoxide dismutase (5 mM sodium phosphate buffer at pH 7.0, applied potential +150 mV vs. Ag/AgCl, 1m KCl).

After rinsing the electrochemical cell with buffer solution (5 mM phosphate buffer) to remove all residual reagents, the mpITO electrode was still loaded with cyt *c* and displayed the characteristic electrochemical performance of the native immobilized cyt *c*, such that it could be used again for detection of superoxide anions. Although optimization of the cyt *c*/mpITO electrode for application to real samples is still necessary, in the present state of development the functionality of the device could be demonstrated.

4.1.6 Reversible electro-system for biochemical switchable optical device

The elevated light transmission of the indium tin oxide based materials lends itself to application in the field of the optical detective systems. Optical adsorption changes of a protein immobilized in nanostructured materials upon reaction with an analyte can be utilized for the detection (Hulko *et al.*, 2011). However very tiny changes are associated to such a detective system. On the other hand the optical detection of a color developing dye may overcome such problems. The accumulation of a product with high extinction coefficient, upon enzyme mediated reaction of the dye with the analyte, may enhance the sensitivity of the method.

The ability of cyt *c* to oxidize a dye like TMB by hydrogen peroxide in a mesoporous matrix has been explored in our opto-bioelectronic device cyt *c*/mpITO (Figure 34).

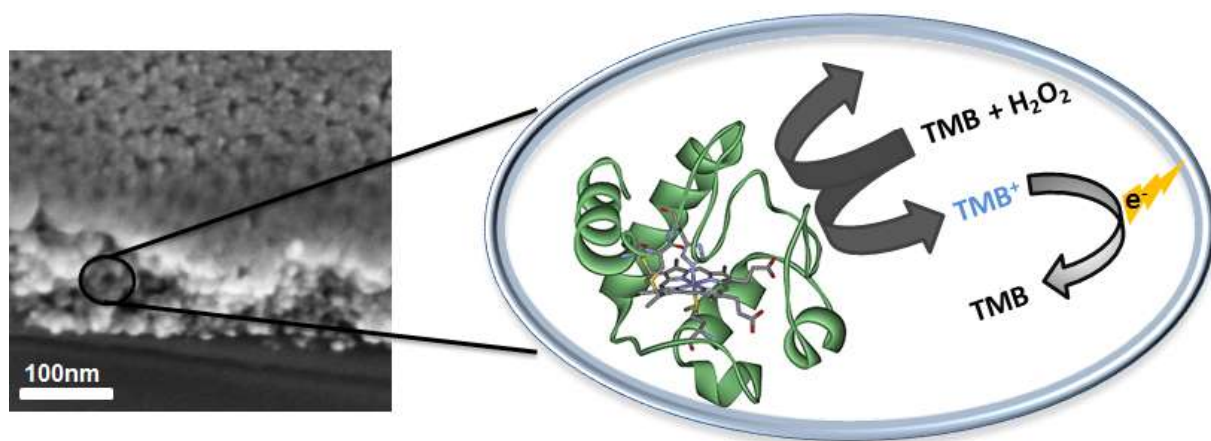


Figure 34. Side-view, by scanning electron microscopy of a mpITO film and a schematic representation of a nanoreactor consisting of a cytochrome *c* molecule entrapped in an ITO pore. The catalytic oxidation of TMB, by cyt *c*, in presence of hydrogen peroxide is also depicted as well as the electrochemical regeneration of the dye by electron exchange with the conductive ITO pore wall.

The easily accessible cyt *c* immobilized in mpITO is able to catalyze the oxidation of the chromogenic electron donor TMB by H₂O₂ in the bulk solution. In Figure 35 the increase of the absorption at the wavelengths of the intermediate (370 and 650 nm) and the very slow formation of the fully oxidized product (450 nm) are shown. In less than half an hour a constant value is reached. Cyt *c* is firmly entrapped in the mesopores and for several days maintains a stable output signal as a result of the contact with a solution containing hydrogen peroxide and TMB (Figure 35 inset b).

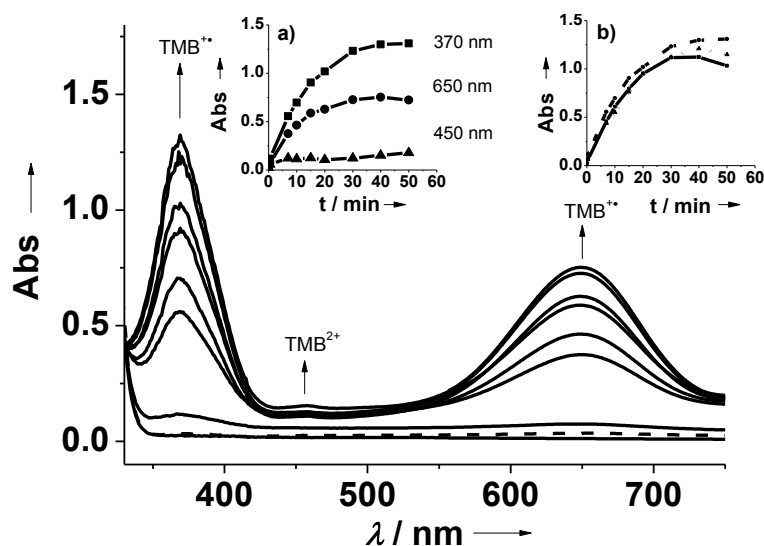


Figure 35. Absorption spectra of 1 mL TMB solution (1 mM) in contact with a cyt *c* modified mpITO film after 0, 30 s, 7, 10, 15, 30, 40, 50 minutes from the addition of 100 μ M H₂O₂ (100 mM sodium phosphate pH 7.0). The dashed line shows the same experiment with a cyt *c*-free mpITO film. The inset a) shows the trend of the different wavelengths associated to the TMB process, and b) shows the trend at 370 nm for the first (bold line), second (dotted line) and third (dashed line) day.

As indicated in the scheme in Figure 36, the colorless TMB in a mild acidic solution (pH 4–7) can undergo two successive one-electron electro-oxidation processes. The first step yields an intermediate product TMB-free radical in the first step, which forms a colored charge-transfer complex with another TMB radical ($\lambda = 370, 652$ nm) (Misono *et al.*, 1997). A second step forms slowly the completely oxidized product quinonediimine ($\lambda = 450$ nm) (Josephy *et al.*, 1982; Jiao *et al.*, 2004; Yang *et al.*, 2005). The formation of a radical cation and the two-step mechanism were demonstrated for TMB using spectrophotometric and EPR data (Marquez *et al.*, 1997; Josephy *et al.*, 1982). TMB reacts directly very slowly with H₂O₂, as depicted by the dashed line in Figure 35.

The optimum pH for the formation of the blue intermediate is displayed in mild acidic conditions. The lower activity at high pH values is in analogy to the catalytic

cycle of *horseradish* peroxidase and also reflects the influence of hydroxyl ions on the TMB charge-transfer complex formation.

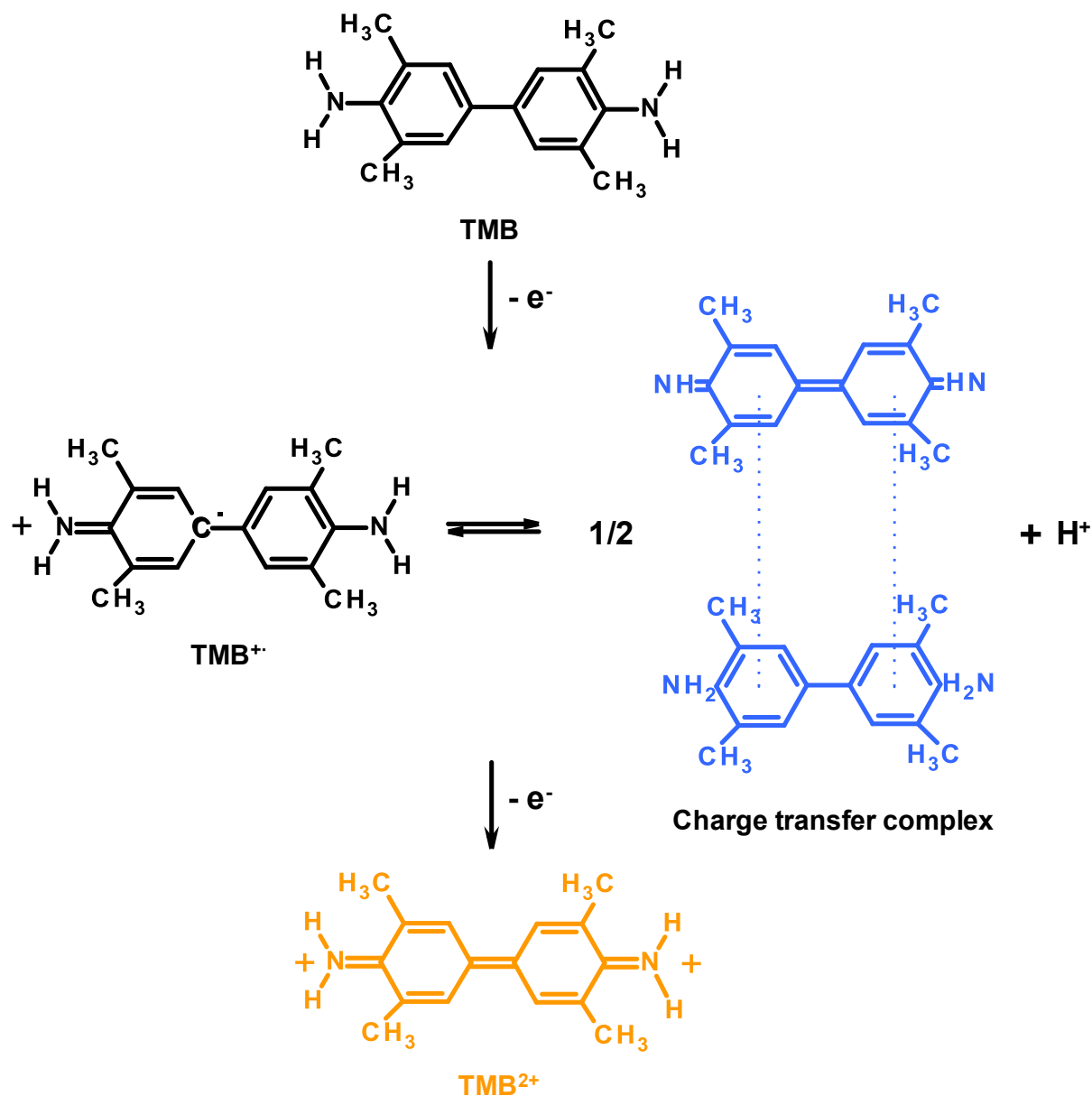


Figure 36. The scheme of 3, 3', 5, 5'-tetramethylbenzidine (TMB) undergoing two successive one-electron reduction–oxidation processes. The intermediate product TMB-free radical is in equilibrium with the colored charge transfer complex which is detected in at 370 nm.

In an attempt to develop a more compact system, avoiding problems connected to TMB diffusion and side reactions in the bulk, TMB was first immobilized into the mpITO. In addition to the enzymatic reduction, TMB can also be electrochemically oxidized and reduced. After TMB was assembled on the mpITO film electrode, two pairs of redox waves, centered at 0.24 and 0.50 V, can be obtained at low scan rate

(Figure 37b). The current waves obviously result from the two consecutive one electron exchanges of the immobilized TMB mediator. Scanning at higher rate, the variation of the adsorbed TMB^+ calculated by mean of the optical absorption at 370 nm shows a cyclic oxidation and reduction of TMB (Figure 37a), with a negligible formation of TMB^{2+} . The repetitive oxidation and reduction cycles for an elevated number of cycles over a period of 20 minutes indicate a stable reversible process (Figure 37a inset).

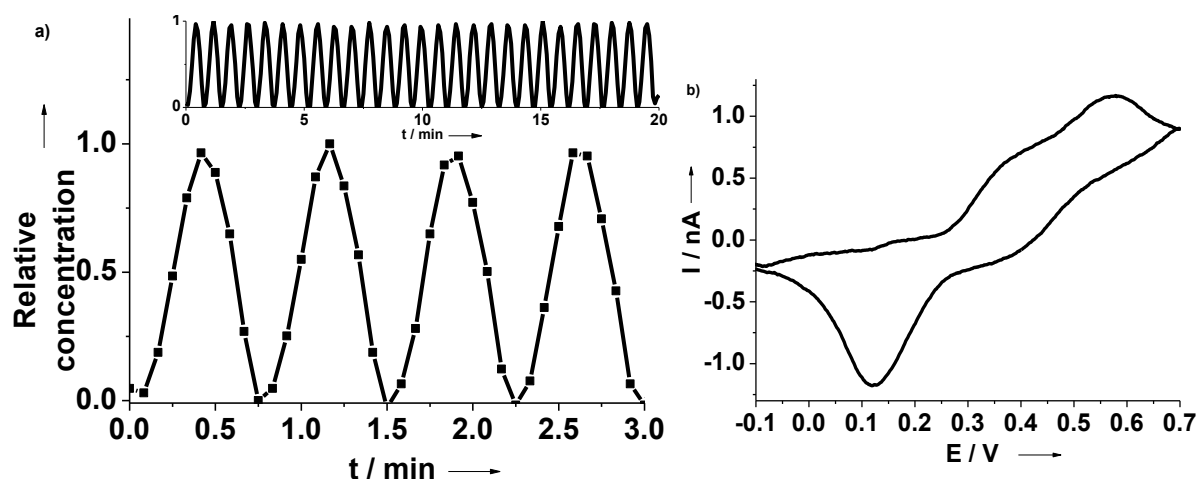


Figure 37. a) Absorption measurements at 370 nm for the relative concentration of oxidized dye in a TMB modified mpITO electrode. The inset shows the same process over a period of 20 minutes (5 mM sodium phosphate buffer, pH 7.0. Applied potential range (scan rate = 50 mV s^{-1} , potential limits = -0.4 V and $+0.7 \text{ V}$) and in parallel. b) Cyclic voltammogram of a mpITO electrode after modification with TMB, obtained in a sodium phosphate buffer (100 mM, pH 7.0) at 10 mVs^{-1} .

Finally TMB was sequentially immobilized after the cyt *c* modification of mpITO. A spectroelectrochemical flow through cell was constructed to provide a holder for the mpITO coated glass slide, an optical window, an electrical contact as well as solution in and outlets (Figure 13). The adsorption of TMB at 370 nm was recorded versus the time for subsequent three injections of H_2O_2 (Figure 38). A stable adsorption could be observed when the buffer is flowing in the cell. Immediately after the injection of the sample solution, the adsorption increases rapidly due to the cyt *c*-catalyzed reaction of hydrogen peroxide and the dye. Once the higher level of colored intermediate is reached, the signal shows no significant changes, within the limits of the noise, also after injection of fresh H_2O_2 -free buffer. Upon application of a reducing potential at the mpITO a sharp drop of the adsorption to initial level is displayed because of the

reduction of TMB back to the transparent form. The potential was therefore switched on in order to reset the system and to prepare it to the next injection.

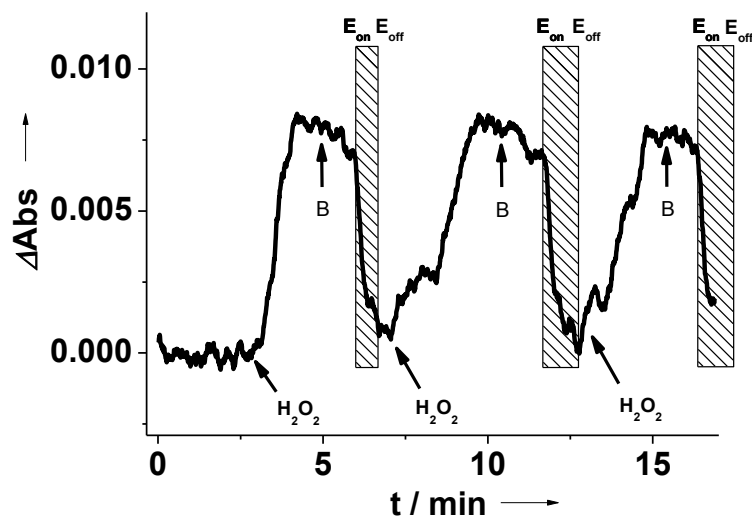


Figure 38. Absorbance changes at 370 nm of a TMB/cyt *c* modified mpITO. The moment of H₂O₂ addition and the potential apply are marked. The experiment is performed in 5 mM potassium phosphate buffer, pH 7.0; the added H₂O₂ solution was 10 μM; the moments when a potential of -0.5 V vs. Ag/AgCl, 1 M KCl was switched on and off is indicated with “E_{on}” and “E_{off}”; B indicates the moment when a fresh H₂O₂-free buffer was flowed.

This work is the first reported study of the immobilization of catalytically active proteins in a mesoporous transparent and conducting film together with a color developing dye for the optical read out in response of an external signal. The peroxidase activity of the protein was employed to oxidize a dye to its optical detectable form. The dye co-immobilized with cyt *c* could also be reset to the earlier state by application of reducing potential.

4.1.7 Spectroelectrochemical studies of *h*SO-HD in mpITO

The negative charged surface of ITO, IEP 3.0 (Koreeda *et al.*, 2004) due to the surplus of In(OH)₃-like and InOOH-like surface species (Milliron *et al.*, 2000), which promote the interaction with cyt *c*, creates an unfavorable environment for negatively charged proteins.

Therefore in order to show spectroelectrochemical evidence for the direct electron exchange of an isolated HD from *h*SO, the mpITO was modified by a cationic polymer. In such a way a situation comparable to the surface condition of gold nanoparticles investigated with *h*SO and reported in the next chapter (4.2) is obtained. In recent SERR spectroelectrochemical experiments (Sezer *et al.*, 2010)

HD has also identified as the electron transfer mediator between the surface absorbed *h*SO and an aminated electrode.

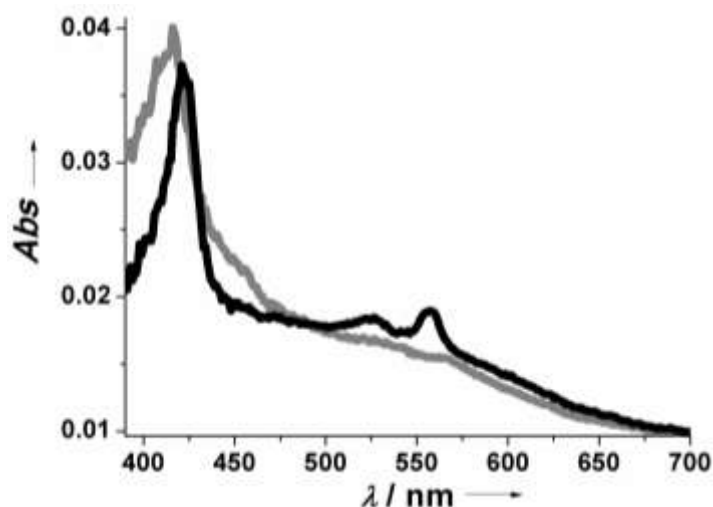


Figure 39. Absorption spectra of HD adsorbed on a poly-L-lysine modified mpITO electrode at +0.1 V (gray) and at -0.4 V (black), corresponding to the ferric and ferrous form of HD, respectively.

Protein load was not observed when a clean mpITO was used, due to incorrect surface charge. On the other hand a high protein loading of 330 pmol cm^{-2} , calculated from the absorption spectra is reached when a poly-L-Lysine modified mpITO was used (Figure 39). The high conductivity and the optical transparency of ITO allow monitoring redox transformation and UV-Vis spectroscopy of immobilized HD simultaneously.

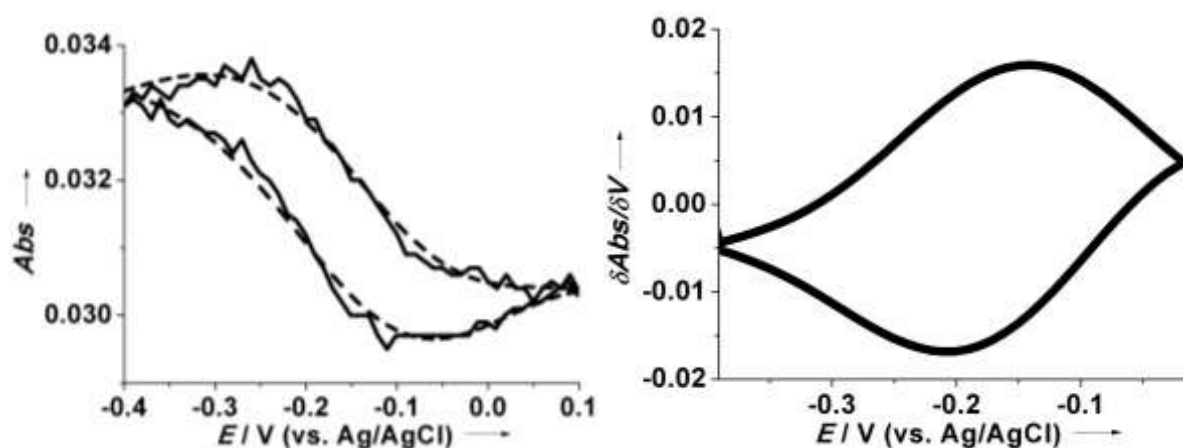


Figure 40. (Left) Cyclic voltabsorptogram (CVA) and (right) derivative cyclic voltabsorptogram (DCVA) obtained for HD adsorbed on a poly-L-Lysine modified mpITO electrode (scan rate= 5 mV s^{-1} ; 5 mM phosphate buffer, pH 7.0). The absorbance was monitored at 416 nm. The dashed line was calculated from the CVA applying a Fourier transform smoothing algorithm.

Upon varying the electrode potential, the oxidation state of the adsorbed HD was reversibly switched from the ferric to the ferrous form, as indicated by the red shift of the Soret band and the formation of two bands in the Q-band region. The derivative cyclic voltabsorptogram (DCVA), calculated from the cyclic voltabsorptogram (CVA) at 421 nm, shows a formal potential of the HD of -146 ± 3 mV (Figure 40).

Since within the error margins the formal potential calculated spectroelectrochemically is identical to the results derived from CV measurements (see section 4.2.1), these results suggest that the HD is the protein part of the *h*SO involved in the electron exchange with the electrode surface modified with positive charged polymers.

4.1.8 Catalytic activity of *h*SO on planar ATO

The research toward the replacing of the rare and expensive indium in transparent conducting films and the possibility to work with negative charged proteins is of great interest. A promising material is the antimony-doped tin oxide (ATO) (Batzill *et al.*, 2005). Sb is a common *n*-type dopant, for the enhancement of the conductivity, in tin oxide (Stjerna *et al.*, 1994).

Since so far protein electrochemistry on such transparent conductive oxide is very poor previous electrochemical experiments were performed. At planar ATO (pIATO) a fast and quasi-reversible reduction and oxidation of the small mobile positive charged ($\text{Ru}(\text{NH}_3)_6^{2+/3+}$) and negative charge ($\text{Fe}(\text{CN})_6^{3-/4-}$) redox mediators is shown (Figure 41a and b). The standard rate constants were calculated to be $3 \pm 1 \times 10^{-3} \text{ cm s}^{-1}$ for both mediators (Nicholson, 1965). The formal potential was -287 ± 1 mV and 262 ± 2 mV for $\text{Ru}(\text{NH}_3)_6^{2+/3+}$ and for $\text{Fe}(\text{CN})_6^{3-/4-}$ respectively. The pIATO films display a comparable rate constants as amorphous mpITBO films and higher than those for a crystalline mpITO with $\text{Ru}(\text{NH}_3)_6^{2+/3+}$ (see chapter 4.1.4). But unlikely to indium based tin oxides, surprisingly the ATO film in addition to positive charged mediators display electron exchange also with a negative charged redox couple ferri/ferrocyanide. The electrochemical parameters of all the studied transparent conductive oxides are summarized in the table 1 in the chapter 5.

Furthermore the electrochemistry of an uncharged molecule, dopamine, was tested at pIATO. Dopamine shows a non reversible oxidation and a reduction peak centered at around 160 mV (Figure 41c).

The possibility to work with negative charged molecules opens new doors to use proteins which fail to communicate with indium based tin oxide films without surface modification as shown in chapter 4.1.7.

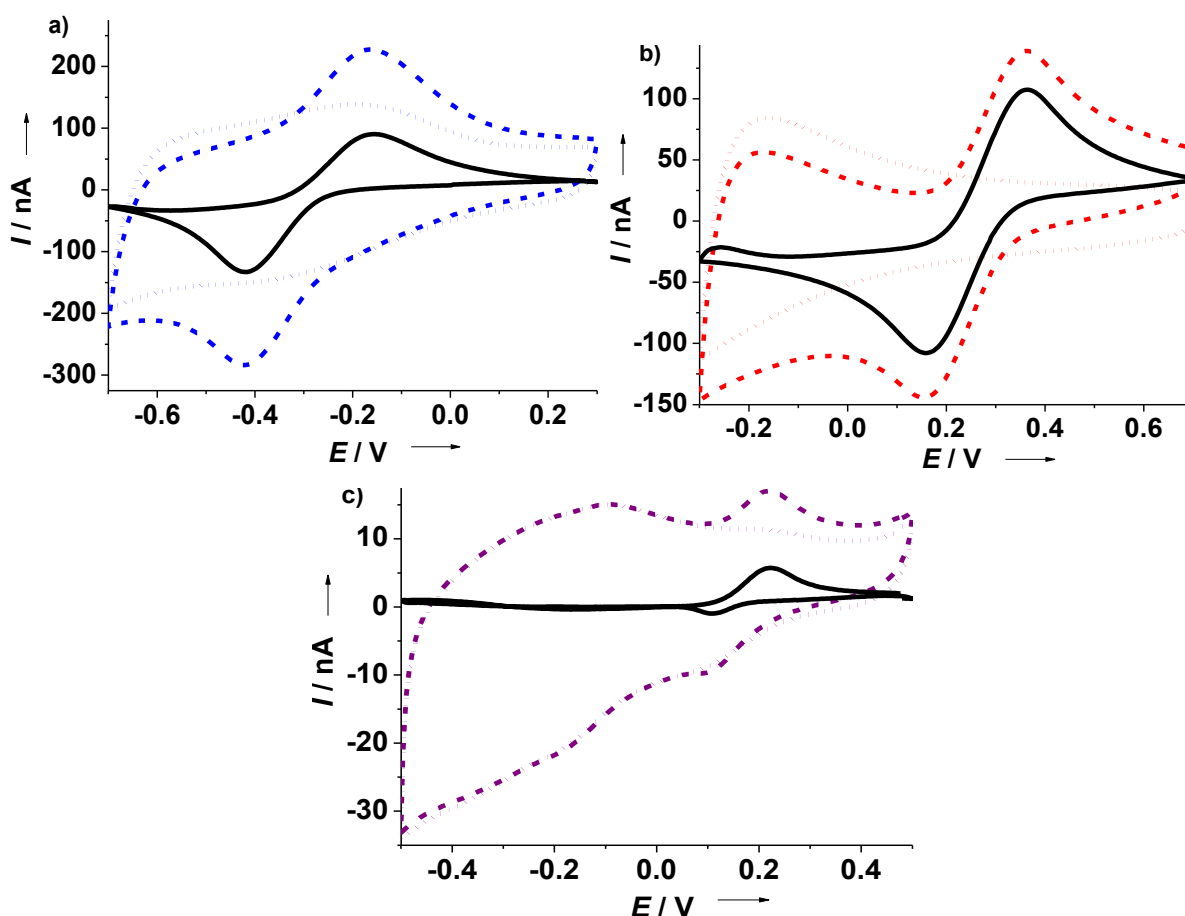


Figure 41. Cyclic voltammograms of a pIATO electrode obtained in a potassium phosphate buffer solution a) 50 mM, 0.1 M KCl, pH 7.0 in absence (blue dotted line) and presence of 2 mM of $\text{Ru}(\text{NH}_3)_6^{+3}$ (blue dashed line) at 0.6 V s^{-1} , b) 50 mM, 1 M KCl, pH 7.0 in absence (red dotted line) and presence of 2mM of $\text{Fe}(\text{CN})_6^{3-/4-}$ at 0.6 V s^{-1} (red dashed line) and c) 50 mM, 1 M KCl, pH 7.0 in absence (purple dotted line) and presence of 10mM of dopamine at 0.05 V s^{-1} (purple dashed line). The black curves show the background-subtracted cyclic voltammograms of each substance at pIATO.

In order to investigate the behavior of anionic proteins, human sulfite oxidase (*hSO*) has been adsorbed on the pIATO. Likely the film, lacking a tridimensional structure and high surface area, is able to absorb only few amount of protein. However the presence of the protein on the surface was indicated by its electrocatalytic activity with the substrate. Catalytic oxidation current was showed in presence of sulfite (Figure 42a). Unfortunately no cyclic voltammetrical peaks could

be seen, even at low scan rate as well as no change were detected in the absorption spectra through the pIATO film.

Nevertheless the protein immobilized on pIATO displayed a high long time stability and is able to work in elevated ionic strength. It showed no change in electroactivity after a period of 12 days stored in 5mM Tris buffer at 4 °C and it worked even in 750mM Tris buffer. It has to be mentioned that the stationary oxidation current reach a steady state at applied potential of about 0V (Figure 42b) and no direct sulfite oxidation is shown until the applied potential exceed the 0.2 V.

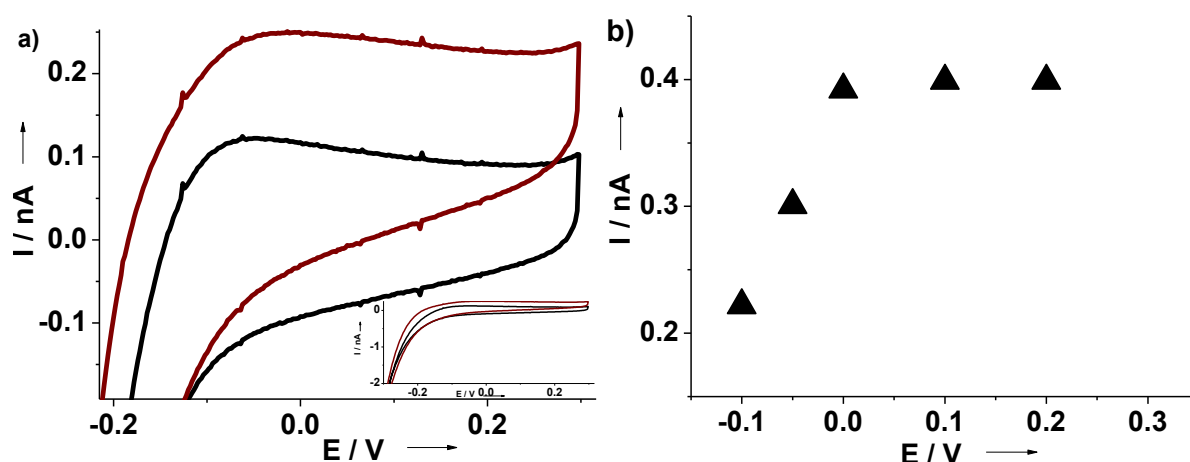


Figure 42. a) CV of a pIATO modified with hSO with (brown curve) and without (black curve) 200 μM sulfite, in a 750 mM Tris buffer solution pH 8.4 at 2 mV s^{-1} . The inset shows the full CV. b) Stationary oxidation current response of the same electrode at different applied potential in a buffer Tris buffer pH 8.4 solution 750 mM containing 200 μM SO_3^{2-} .

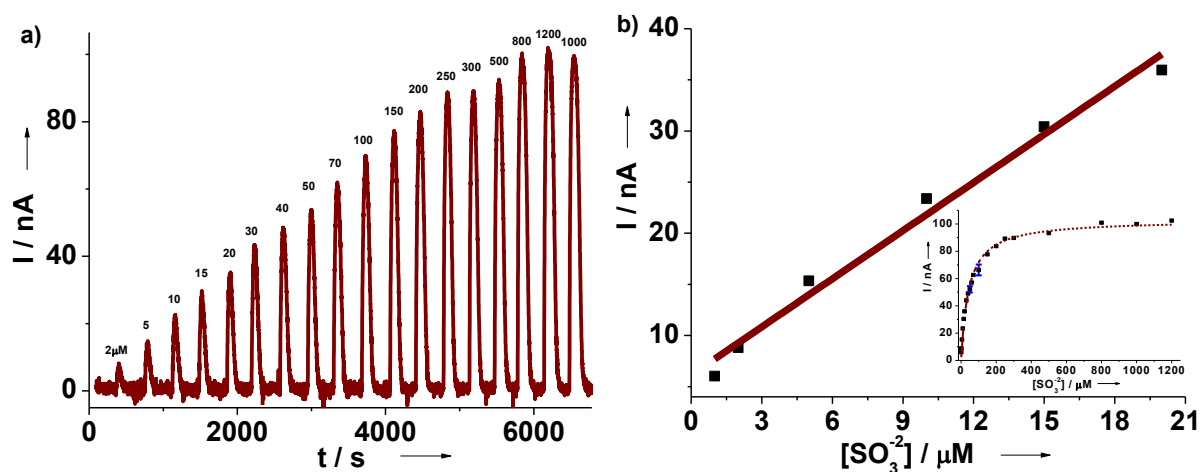


Figure 43. a) Oxidation current detected with a pIATO modified with hSO at different SO_3^{2-} concentrations. b) Linear dependence of the current signal on the sulfite concentration. The inset shows the current response peaks obtained using the same modified electrode in a flow system after addition of different sulfite concentration. In 750 mM Tris buffer solution at pH 8.4 and applied potential 0 V.

As shown in the Figure 43 for pIATO/hSO inserted in a fluidic system the detected oxidation current increases as the concentration of sulfite increases. The current follow a Michaelis-Menten relationship to the sulfite concentration with a $K_{m, app.}$ of $43 \pm 3 \mu\text{M}$ and a I_{max} of $103 \pm 2 \text{ nA}$ (Figure 43). At the same time a linear range, between 1 and 20 μM sulfite concentration, is displayed by oxidation current and sulfite concentration. The linearity is defined by the equation $I_p = a + b [\text{SO}_3^{2-}]$ where a is $6 \pm 1 \mu\text{M}$ and b is $1.8 \pm 0.1 \mu\text{A}/\mu\text{M}$. The R^2 was equal to 0.98.

4.2 Direct electrochemistry and catalytic activity of *h*SO on AuNP

4.2.1 Direct Electrochemistry of *h*SO

The incubation of an AuNP-modified electrode in an aqueous solution of *h*SO results in the formation of a protein film on the surface. After exchange of the protein solution by a protein-free buffer solution cyclic voltammetry was carried out, either in low and high ionic strength, to study the direct (unmediated) electron exchange between the protein and the electrode. An oxidation and a reduction peak were observed, centered at -145 ± 5 mV, demonstrating the interaction of *h*SO with the positive charged AuNPs (Figure 3a and b) comparable with previous reported data (Sezer *et al.*, 2010).

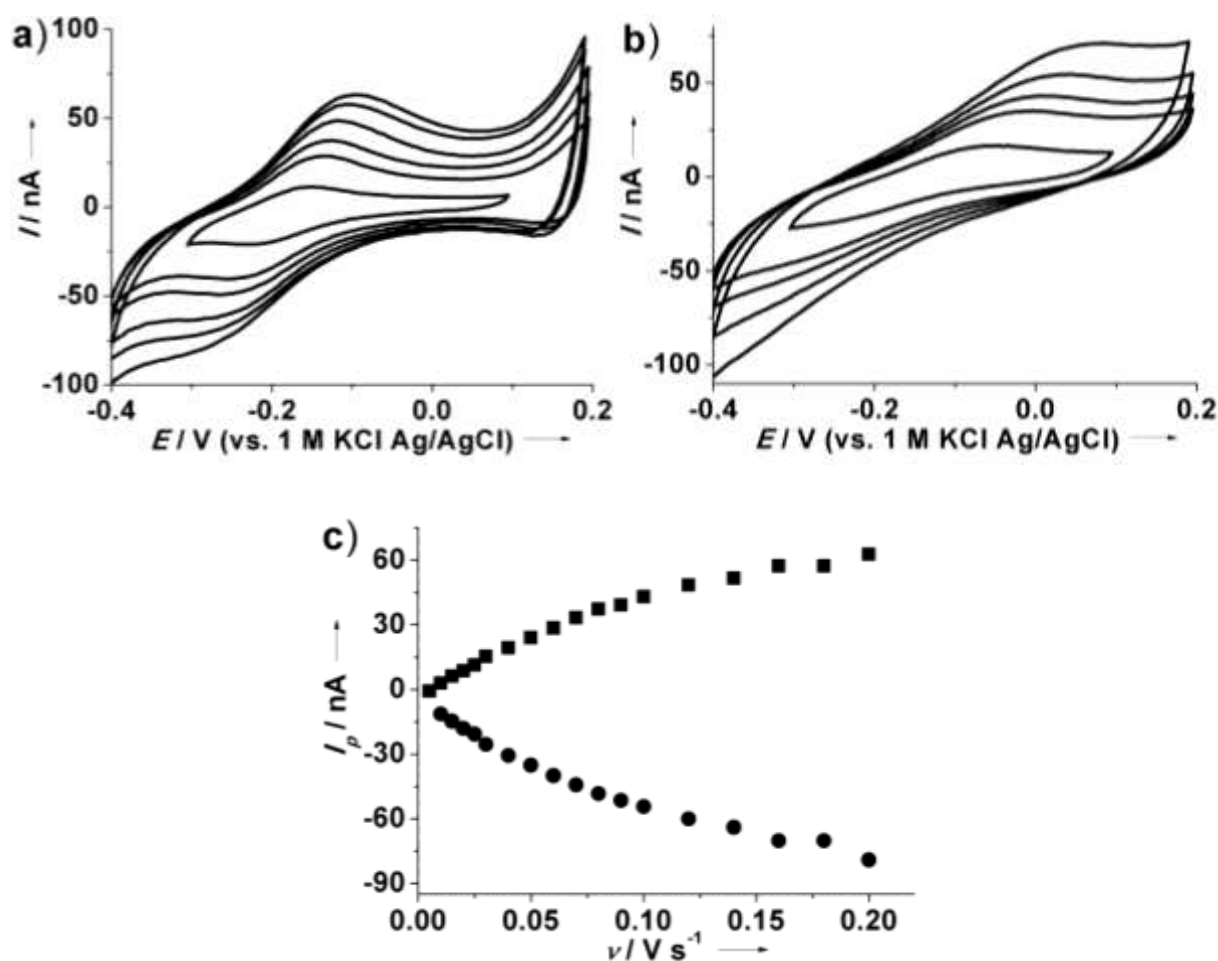


Figure 44. Cyclic voltammogram of *h*SO on an AuNP-modified gold electrode in a a) 5mM and b) 750mM Tris buffer pH 8.4 for various scan rates (25, 60, 80, 120, 200 $mV s^{-1}$). In c) is showed the dependency of the oxidation (square) and reduction (circle) peak current on the scan rate.

The formal potential derived from CV measurements is similar to that calculated spectroelectrochemically for an isolated HD from *h*SO on mpITO (see chapter 4.1.7). These results indicate that the HD in the protein is involved in the electron exchange with the electrode surface. From the peak area of the anodic wave an electroactive protein surface concentration of 30 fmol cm^{-2} was calculated. In absence of *h*SO no peak appeared. The peak separation and the peak current increase with increasing scan rate. The nonlinear dependency of the peak current from the scan rate indicates that a weakly adsorbed species contribute to the redox process at the electrode surface (Figure 44c). Presumably the mobility of the HD, which shuttle electrons from the MD to the electrode, is responsible for this behavior in contrast of the simple Laviron's model on diffusionless electrochemical system (Laviron, 1979). By increasing the buffer concentration an increase of peak separation is observed, which indicates a slower heterogeneous electron transfer between protein and electrode. A better orientation for the intra molecular electron transfer may be the reason for this phenomenon supported also by the higher catalytic activity at elevated ionic strength which will be discussed in the next chapters (see paragraph 4.2.3).

4.2.2 Surface enhanced resonance Raman spectroscopy

Surface enhanced resonance Raman (SERR) spectroscopy can be used to selectively monitor the HD structural state of immobilized *h*SO if the excitation line matches with the Soret band adsorption of the heme cofactor and the surface plasmon resonance of the metallic support. To achieve this two-fold resonance violet light excitation and nanostructured Ag supports are necessary. SERR spectro-electrochemical measurements of *h*SO were thus performed using electrochemically roughened Ag electrodes as bulk support. SERR spectra were recorded for *h*SO adsorbed on Ag-MUA/MU-AuNP-PEI surfaces and compared to the spectra in the absence of nanoparticles on Ag-MUA/MU-PEI surfaces (Figure 45a). In both systems the spectra were identical to the RR spectra in solution and to the ones on Ag electrodes coated with amino-terminated SAMs, measured in a previous work (Sezer *et al.*, 2010). Hence is possible to conclude that no denaturation of the heme environment occurs upon enzyme adsorption. The SERR intensities of HD on Ag-MUA/MU-PEI are 3 times lower than in the case of HD on Ag-C₈(NH₂)/C₆(OH) SAM coated electrodes, which can be rationalised by the larger distance of the heme

from the Ag surface due to the different coating thickness (ca. 1.5 nm for C₈(NH₂) and 4 nm for MUA-PEI).

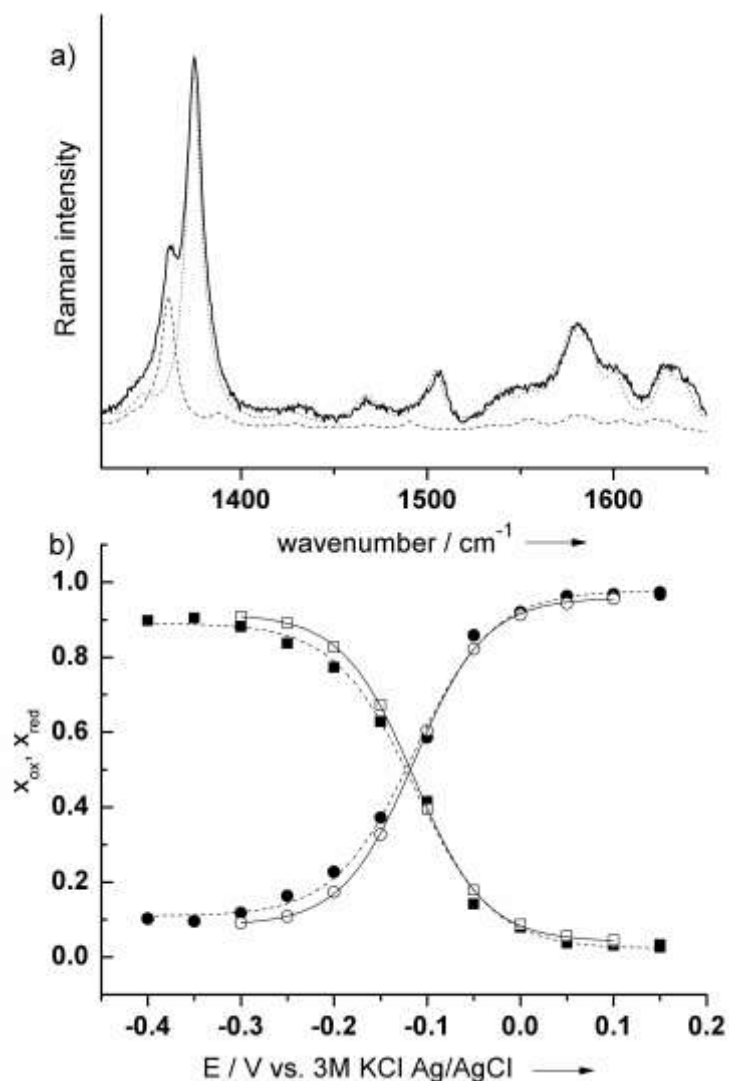


Figure 45. a) SERR spectrum of hSO at open circuit. The dashed and dotted lines represent the component spectra of the reduced and oxidized species respectively. b) Molar fraction of reduced X_{red} (circles) and oxidized X_{ox} (squares) HD adsorbed on Ag-MUA/MU-PEI (open symbols) and Ag-MUA/MU-AuNP-PEI (solid symbols) electrodes, with an experimental error in the order of 0.01, as a function of potential E/V .

Interestingly comparable SERR intensities were measured for Ag-MUA/MU-PEI and Ag-MUA/MU-AuNP-PEI systems although in the latter case the protein is distinctly further away from the electrode surface. An explanation of this effect can be a plasmon coupling of the AuNPs with the surface plasmon resonances of the Ag support observed also previously for Au island films on rough Ag supports (Feng *et al.*, 2010). As a result a similar surface enhancement is achieved at the AuNP surface.

The molar fractions of reduced and oxidised HD were in the following determined with SERRS in the potential range from -0.4 to +0.2 V vs. Ag/AgCl, 3M KCl. For the Ag-MUA/MU-PEI-*h*SO system at 750 mM Tris buffer concentration a sharp redox transition with a midpoint potential of -114 mV was determined (Figure 45b), which is close to the value of -110 mV obtained for *h*SO on C₈(NH₂)/C₆(OH) SAMs at the same ionic strength (Sezer *et al.*, 2010). The main fraction of the enzyme on the surface remained redox active as only 10% of HD could not be reduced at very negative potentials. The apparent number of electrons *n*, derived from a Nernstian analysis, was determined to be 0.65, which is lower than in the case of SAM coated electrodes where under these conditions *n* = 0.9 was measured (Sezer *et al.*, 2010). However, this lower value is in agreement with previous measurements of redox proteins on polyelectrolyte coated electrodes (Weidinger *et al.*, 2006) and can be explained by the much more heterogeneous arrangement of NH₂ groups in the case of PEI in comparison to the highly ordered SAM coatings.

For the Ag-MUA/MU-AuNP-PEI system the same midpoint potential (-115 mV) with a slightly lower *n* value (*n* = 0.6) was observed (Figure 45). Also the amount of redox active HD remains the same indicating a good electrical communication between the AuNPs and the electrode.

4.2.3 Catalytic activity of *h*SO

When the AuNP-PEI/*h*SO modified gold electrode was immersed in a sulfite solution the peaks of the CV disappeared and a drastic increase in the oxidation current is observed for potentials higher than about -150 mV (Figure 46). Since sulfite does not directly oxidize at bare and AuNP-modified gold electrode in this potential region the observed electrocatalytic oxidation can be attributed to the presence of *h*SO. For comparison the gold electrode modified with PEI, but without NPs has also been loaded with *h*SO. As for SERR experiment an electroactive amount comparable to the AuNPs modified electrode is obtained. Nevertheless the electrocatalytic sulfite oxidation current was significantly smaller without AuNPs (dashed black curve in Figure 46). The reduction current visible, when the AuNPs were present, in the more negative potential region is to be assigned to the higher catalytic activity of the AuNPs confined on the electrode surface towards reduction of oxygen (El-Deab *et al.*, 2002; El-Deab *et al.*, 2003) in respect to the gold electrode (Haruta, 1998; Zhang *et al.*, 2003) which is in this case additionally blocked by the SAM layer.

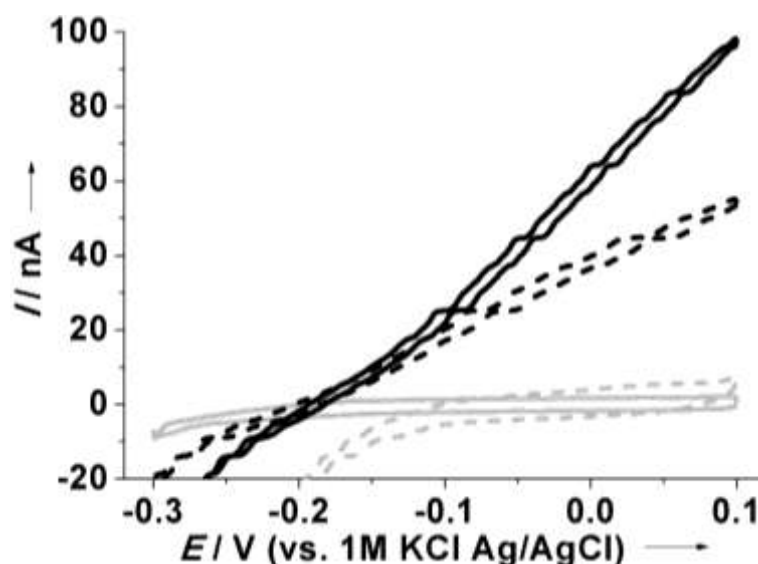


Figure 46. Cyclic voltammogram of a *hSO*/AuNP-functionalized (solid black line), *hSO*/PEI-functionalized (dashed black line), AuNP-functionalized (dashed grey line) and bare (solid grey line) SAM-modified gold electrode in a 750mM Tris buffer pH 8.4, 200 μ M SO_3^{2-} solution at 2 mV s^{-1} .

To avoid the influence of oxygen the following hydrodynamic voltammograms were recorded in inert atmosphere. The hydrodynamic voltammograms were recorded in order to obtain a substrate diffusion limited experiment at different applied potential (Figure 47 left). A high response to sulfite was detected starting from -0.1 V vs. Ag/AgCl, 1M KCl corresponding to the potential range where roughly all the electroactive HD of the protein are oxidized by the electrodes (see Figure 44a). The stationary oxidation current increases with increasing applied potential. Due to the considerable low electron transfer rate no leveling-off is obtained, but rather a continuous increase with the increasing potential. Above 0.1 V however a direct sulfite oxidation may also occur (Figure 47 left, open squares). Therefore in order to avoid direct sulfite oxidation, as side reaction, a potential of 0 V was used for the following amperometric experiments. This potential further ensures minimization of unspecific oxidization from other interfering compounds at high potentials.

The pH plays an important role in the overall mechanism and interactions of this system. The formal potential of the molybdenum center has a strong pH dependency since two protons are involved in the catalytic cycle whereas the heme has no virtually pH dependence (Sullivan Jr. *et al.*, 1993; Elliott *et al.*, 2002). At the same time the interaction of the MD and the HD depending on the respective charge is expected to be pH influenced. Likely the interaction of negative charged *hSO* on the

countercharged NPs surface is also affected by pH influencing the final heterogeneous electron transfer.

Variation of the solution pH results in drastic changes of the catalytic response of AuNPs-PEI/*h*SO on sulfite addition. A basic pH is the most favorable for a high response (Figure 47 right). This is in agreement with the pH optimum of the protein in solution (Carrie A. *et al.*, 2000) and confined on an electrode surface (Aguey-Zinsou *et al.*, 2003; Spricigo *et al.*, 2010; Kalimuthu *et al.*, 2010).

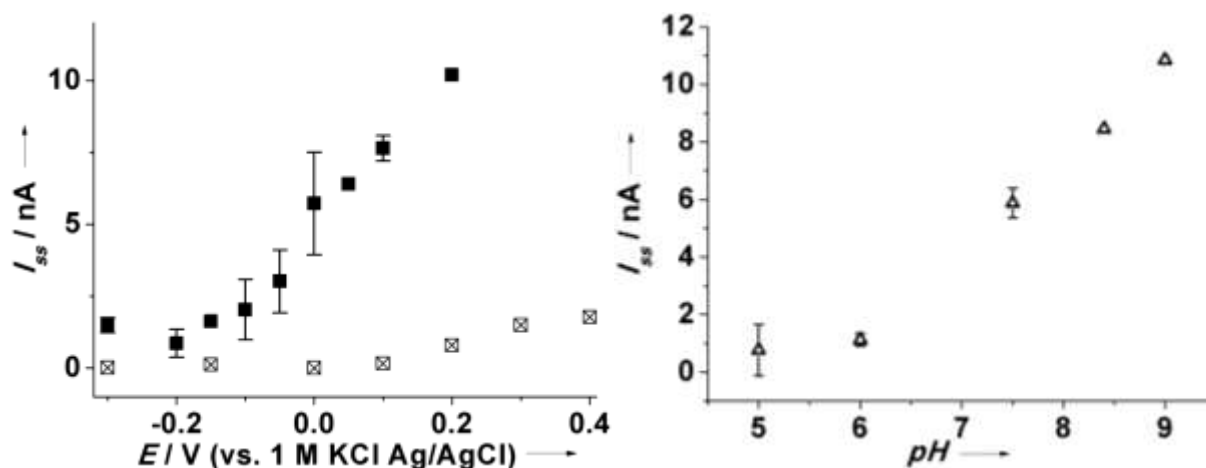


Figure 47. Stationary oxidation current response I_{ss}/nA of a AuNPs modified electrode with (solid square) and without (open square) *h*SO functionalization (left) at different applied potential E/V in a buffer pH 8.4 solution and (right) at different pH conditions at 0V in an oxygen-free Tris buffer solution 750 mM containing $200\mu\text{M SO}_3^{2-}$.

The bearing of the ionic strength was investigated by means of different buffer concentration. As showed in Figure 48, with all other conditions being equal, the catalytic current strongly depends on the buffer concentration. From a Tris concentration of 25 mM the current begins to be detectable, reaching an increase of 2000% at 750mM. Interestingly at such an elevated ionic strength no detectable loss of electroactive protein occurred. The last data supported the mechanism reported by Sezer (Sezer *et al.*, 2010) for immobilized *h*SO on amino functionalized silver electrode. From molecular modeling it has been suggested that a high ionic strength increases the mobility of the HD while the enzyme is immobilized via the dimerization domain to the SAM surface. The flexible loop connecting the HD allows alternating contact with the MD and the electrode surface, thereby promoting the intramolecular and heterogeneous electron transfer (Pacheco *et al.*, 1999).

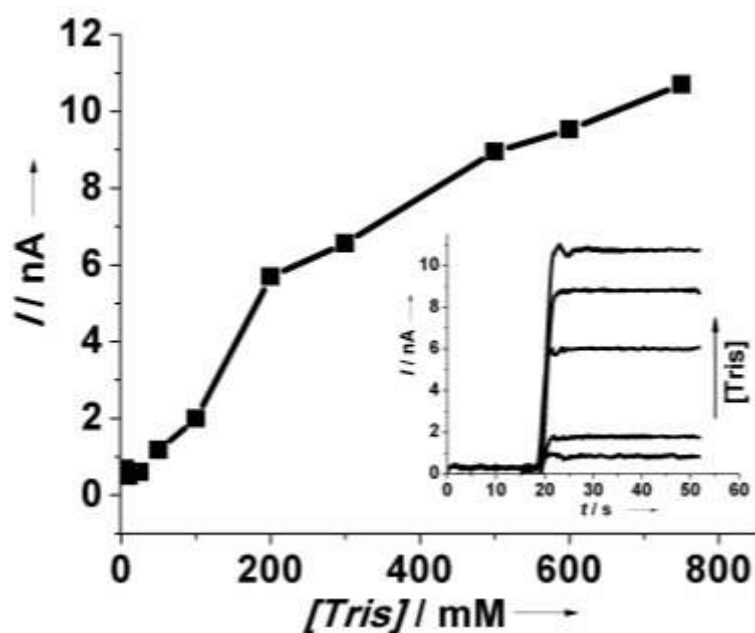


Figure 48. Current response at different Tris buffer pH 8.4 concentration. The inset shows amperometric curves obtained at 0V in a 200 μ M SO_3^{2-} oxygen-free solution containing 25, 100, 200, 500 and 750mM Tris.

4.2.4 Sulfite biosensor

The AuNP-PEI/*h*SO electrode was applied for sulfite detection at high ionic strength condition applying a constant low potential. Figure 49 shows the amperometric response to subsequent addition of sulfite to the constantly stirred 750 mM Tris pH 8.4 buffer solution at an applied potential of 0 V versus Ag/AgCl, 1M KCl. After each sulfite injection a rapid increase of current is observed that reached a steady state within 2 s (zoom in Figure 49). The current increased linearly with sulfite concentration with a sensitivity of 1.85 nA μM^{-1} . This is in a similar order of magnitude of other enzyme-based sulfite biosensors, such as the cytochrome *c* mediated *h*SO (Spricigo *et al.*, 2009) and bacterial sulfite dehydrogenase (Kalimuthu *et al.*, 2010) or chicken SO-polytyramine-modified glassy carbon electrode (Situmorang *et al.*, 1999), but higher than other mediated SO-based biosensors (Svitel *et al.*, 1998; Spricigo *et al.*, 2010).

The high sensitivity allowed measurement down to 0.5 μM sulfite. A linear dependence of the current as a function of sulfite concentration could be seen in a range between 0.5 and 5.4 μM (inset in Figure 49). The short response time of the AuNPs/*h*SO system enabled nearly immediate detection. The possibility to work at

elevated ionic strength promises its employs in real samples as a sulfite biosensor or as component of a biofuel cell and more complex bioelectronic systems.

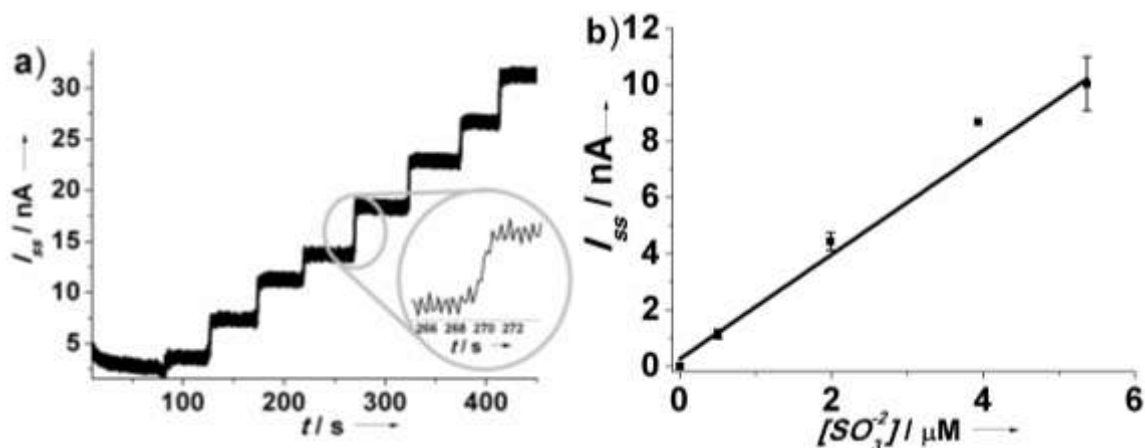


Figure 49. a) Current response I/nA after subsequent additions of SO_3^{2-} in stirring 750 mM Tris buffer solution at pH 8.4 and applied potential 0 V. One of the current steps is zoomed to emphasize the quick increase of current. b) Linear dependency of the stationary current signal I_{ss}/nA on the sulfite concentration $[SO_3^{2-}]/\mu M$ defined by the equation $I_p = a + b [SO_3^{2-}]$ where a is $0.2 \pm 0.2 \mu M$ and b is $1.8 \pm 0.1 \mu A/\mu M$.

In addition the possibility that oxygen may act as electron acceptor and as competitor to the electrode was investigated since this enzyme is also capable to transmit electrons, extracted from sulfite, to different artificial mediators (ferricyanide, 2,6-dichlorophenol indophenol and methylene blue) besides the natural electron acceptor cytochrome *c* (Cohen *et al.*, 1971a; Cohen *et al.*, 1971b).

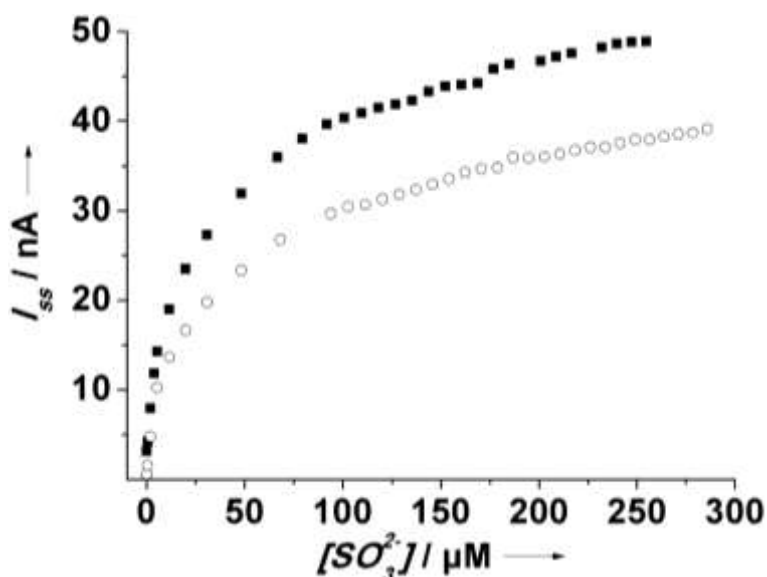


Figure 50. Stationary oxidation current I_{ss}/nA at different sulfite concentration $[SO_3^{2-}]/\mu M$ in presence (open circles) and absence (solid square) of oxygen in stirred 750 mM Tris buffer solution at pH 8.4 and applied potential 0 V.

As shown in figure 9, for different sulfite concentrations, a decrease of catalytic current is visible for sulfite. A $K_{m, app.}$ of $101 \pm 13 \mu\text{M}$ and $72 \pm 14 \mu\text{M}$ with a I_{max} of $60 \pm 2 \text{ nA}$ and $70 \pm 4 \text{ nA}$ were estimated for measurement in air and in nitrogen atmosphere, respectively.

The $K_{m, app.}$ values were comparable to that calculated for *hSO* on antimony-doped tin oxide electrodes (see chapter 4.1.8), but much higher than the Michaelis-Menten constant for native protein in solution ($17 \mu\text{M}$ (Garret *et al.* 1998)).

Since the assembly of *hSO* does not involve cross-linking or protecting membranes the stability of the described sensor is restricted to a few days. Further effort should be focused towards the improvement of the long term stability.

4.3 Electrochemistry of XDH and mAOH1

4.3.1 Direct Electrochemistry of immobilized proteins

Equilibration of a drop of XDH from *R. Capsulatus* on freshly prepared EP-GC, results in a protein immobilization displaying a durable and stable electrical signal. On the contrary, its equilibration on a freshly cleaned glassy carbon shows no detectable direct electron transfer between the protein cofactors and the electrode.

The phenomenon may be attributed to the coupling of the enzyme with the oxygen functionality created during the cathodization process. The carbon surface area seems to be unchanged upon pretreatment and a similar surface area for the pretreated and untreated GC electrode was calculate, $(6.8 \pm 0.5) \times 10^{-2} \text{ cm}^2$ and $(6.4 \pm 0.8) \times 10^{-2} \text{ cm}^2$ respectively.

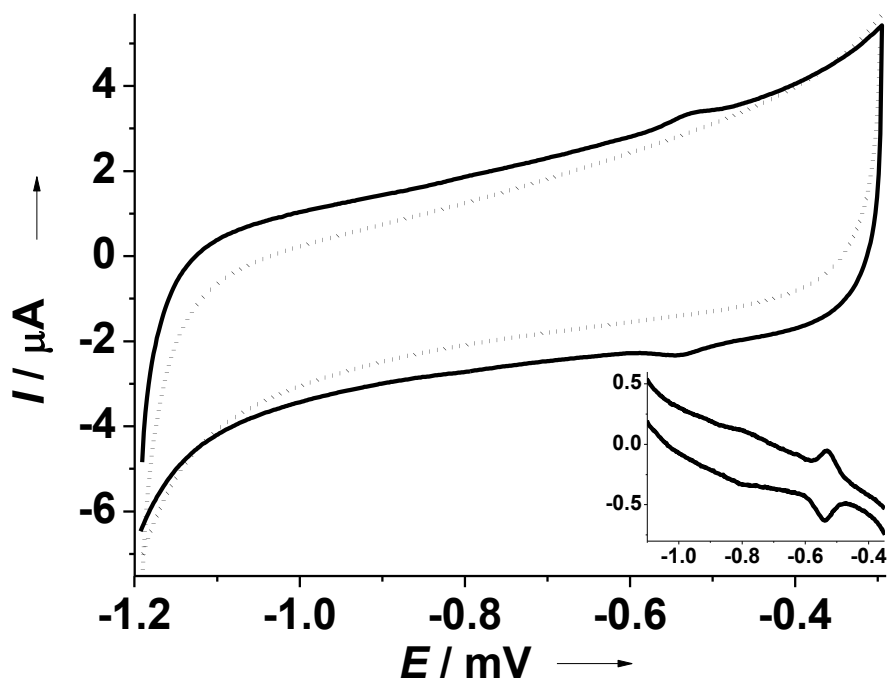


Figure 51. Cyclic voltammogram of XDH immobilized on an EP-GCE (solid line) and of bare EP-GCE (dotted line) in a 50mM Tris buffer pH 8.0 at scan rate of 50mV/s. The inset shows the background-subtracted CV.

Figure 51 shows the cyclic voltammogram (CVs) of a XDH modified EP-GC, it exhibits a couple of reversible and symmetric peaks at scan rate of 50 mV s^{-1} , with a peak current ratio ($I_{\text{ox}}/I_{\text{red}}$) of 0.9. The anodic and cathodic peaks are centered at -535 mV. The half-peak width (i.e. the width of the peak at half its height) for these peaks are around 50 mV which is close to the theoretical value ($\sim 90 \text{ mV} / n$) for a

reversible 2 electrons exchange process. At more negative potentials, the immobilized enzyme shows a broadened and small peak centered around -800 mV. No voltammetric response was displayed at electrochemically pretreated electrode modified with the same procedure but equilibrated with a drop of buffer without the enzyme.

In order to have more defined peak, square wave voltammetry (SWV) was employed to ensure a higher sensitivity and less capacitive charge current effects. At pH 8.0 several SWVs (Figure 52 left) result in a peak at -532 ± 5 mV and second smaller one at -781 ± 9 mV.

Upon the immobilization of two recombinant XDH variant, bearing one of the cysteines bounding to the FeSII (Cys39 and Cys63) substituted by a serine, an additional peak appears in the SWVs. This third peak is shown at -633 mV and -622 mV, for the XDHC39S and the XDHC63S respectively (Figure 52 right). The less negative response can be assigned to the FAD cofactor, the more negative one to the Mo cofactor whereas the additional peak appearing in the SWV voltammograms of the variants is attributed to the second and more exposed of the two iron sulfur cluster.

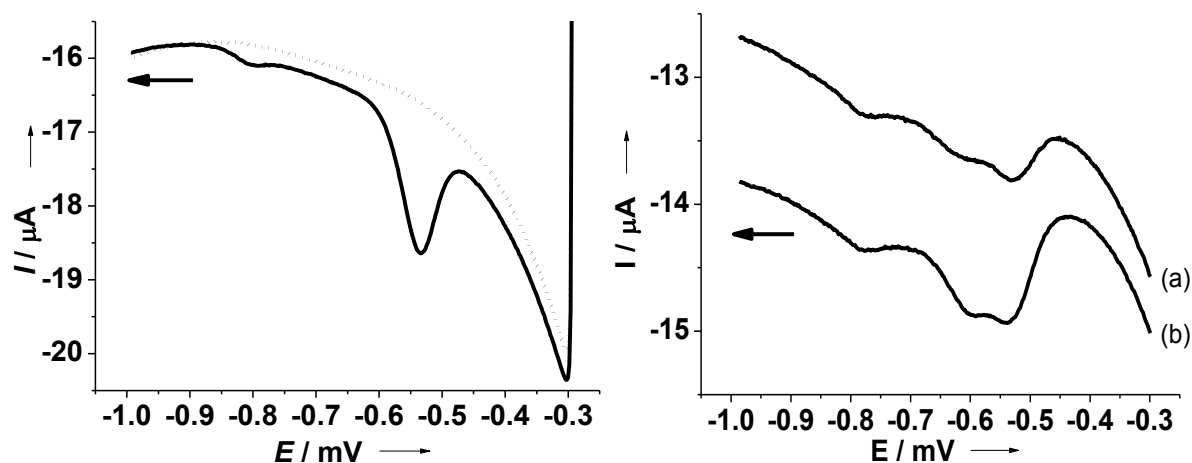


Figure 52. (Left) Square wave voltammetry of XDHwt immobilized on an EP-GCE (solid line) and of bare EP-GCE (dotted line). (Right) Square wave voltammetry of XDH C39S (a) and C63S (b) immobilized on an EP-GCE. Experimental condition were 50mM Tris buffer solution pH 8.0, potential step 4mV, square wave amplitude 25 mV, and square wave frequency 25 Hz. The arrow indicates the scanning direction.

For comparison another member of the xanthine oxidase family and high homologues to the XDH was immobilized on the EP-GCE. The *mAOH1* (mouse aldehyde oxidase homolog 1) has an elevated degree of similarity and presumably a relative identical structure with the XDH. As expected for such a similarity, the protein

shows two different peaks which for analogy may be associated to the Moco and FAD cofactor.

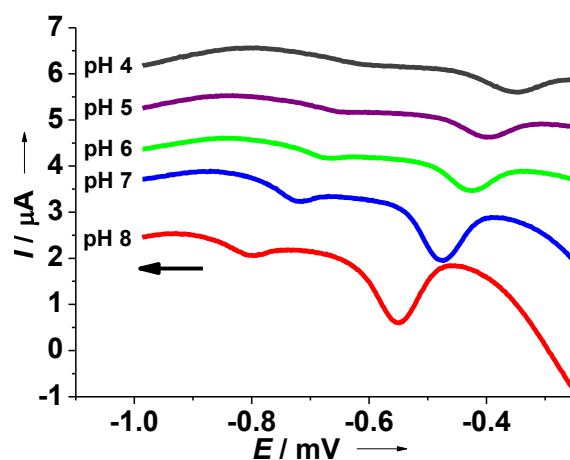


Figure 53. (Left) Square wave voltammetry of *mAOH1* immobilized on an EP-GCE at different pH condition in 50mM Tris buffer solution pH 8.0, potential step 4mV, square wave amplitude 25 mV, and square wave frequency 25 Hz. The arrow indicates the scanning direction.

Figure 54 describes the peak potentials trend with different pH solution within the pH studied range 4.0 - 8.0. For XDHWt The peak potential shifts linearly to cathodic direction with a slope of $-51 \pm 1 \text{ mV pH}^{-1}$ and $-49 \pm 4 \text{ mV pH}^{-1}$ for the FAD and the Moco respectively. A similar slope is displayed from the corresponding peaks in the case of XDHC63S and the FeSII shows a slope of $-51.4 \pm 0.7 \text{ mV pH}^{-1}$, whereas *mAOH1* shows a slope of $-45 \pm 3 \text{ mV pH}^{-1}$ and $-40 \pm 3 \text{ mV pH}^{-1}$ for the FAD and the Moco respectively. Although the *mAOH1* depart partially from the XDHS variations, all these potential slopes are close to the theoretical value of 59 mV pH^{-1} expected for the process proton/electron ratio of 1.0. FAD center undergoes clearly a one-electron reduction to the semiquinone forms accompanying one-proton addition to the group; for the molybdenum center the pH dependency is associated to ionizable groups in the vicinity, perhaps within the molybdenum coordination sphere itself, as was also reported by optical absorption changes (Ryan *et al.*, 1995); in the case of the iron sulfur center it is likely that the proton maybe bound to the nearby groups which can interact electrostatically with the cluster as in was found in the xanthine oxidase (Porrás *et al.*, 1982; Wu *et al.*, 2007).

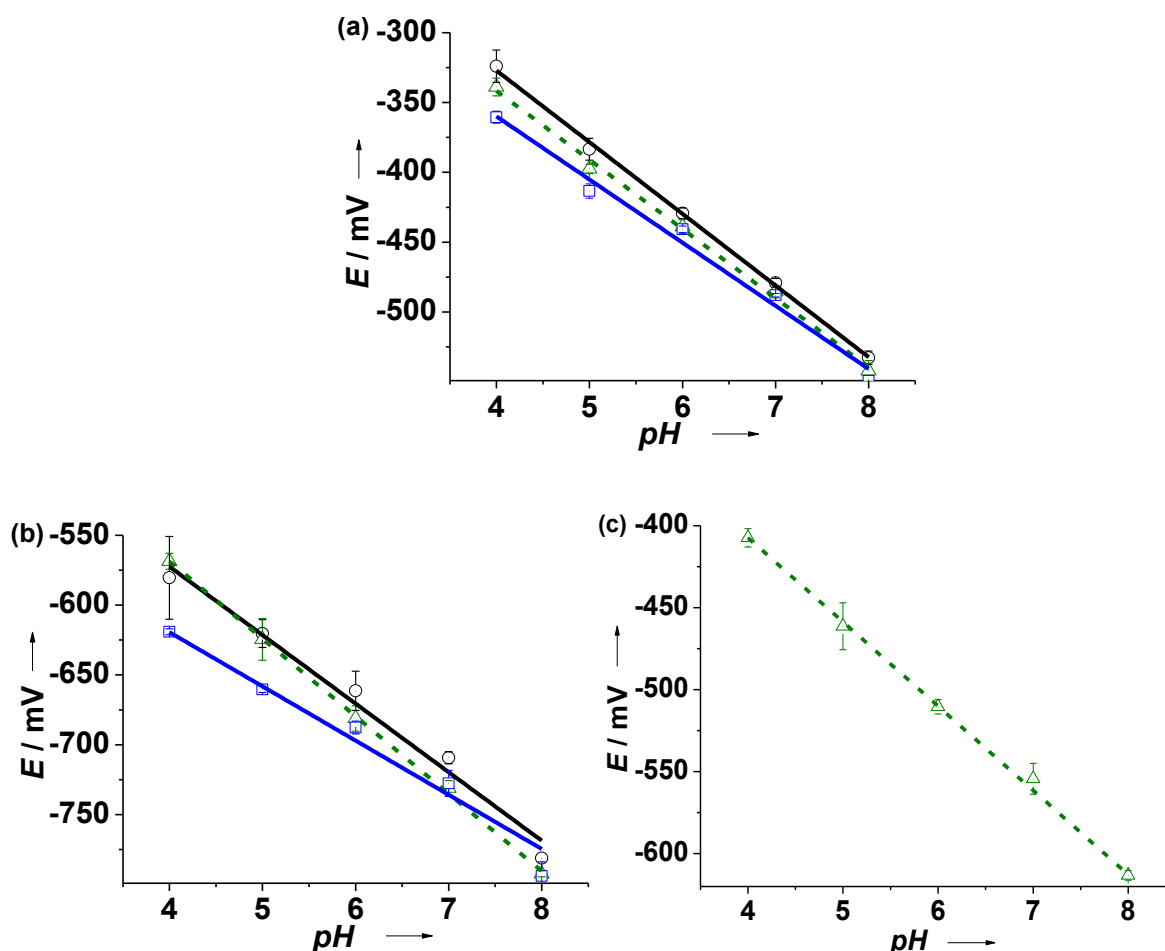


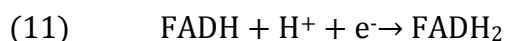
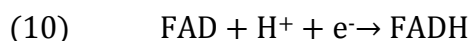
Figure 54. pH dependency of the FAD (a), Moco (b) and FeSII (c) potentials for the XDH wild type (black line), XDH C63S (green dashed line) and *mAOH1* (blue line).

4.3.2 Mediated spectroelectrochemical titration of XDHwt

R. capsulatus XDH in its fully oxidized state has an absorption maximum at 465 nm associated to the absorption of the oxidized FAD, slightly red-shifted in comparison with the bovine XO, probably due to different environments of FAD in the two proteins (Leimkühler *et al.*, 2003).

The flavin and FeS centers dominate the UV-Vis absorption spectrum of the oxidized enzyme. The absorption attributable to the molybdenum center is quite small compared to the changes associated with reduction of the FAD and iron-sulfur centers of the enzyme (Hille, 1996; Ryan *et al.*, 1995).

FAD cofactor undergoes a two successive electron transfer (Cable *et al.*, 2005):



It is known that the FAD-semiquinone, FADH[•], shows an absorption maximum around 630 nm (Hunt *et al.*, 1993).

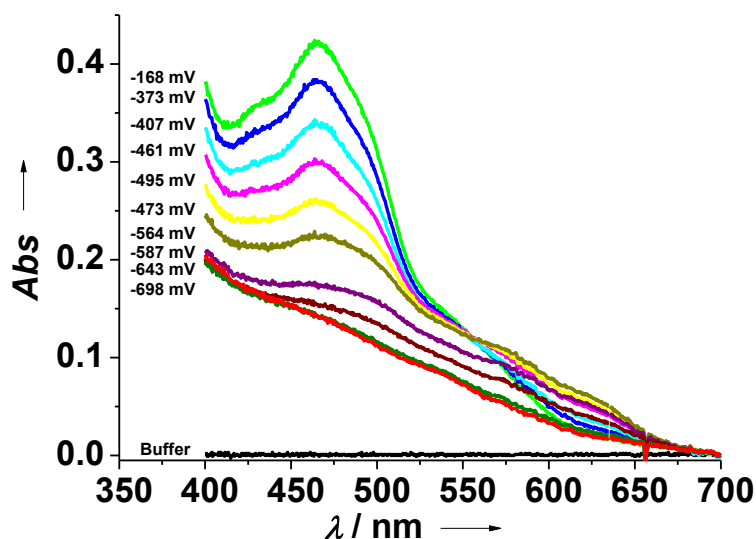


Figure 55. XDH adsorption at different solution potential in presence of 5 μM mediators (see experimental part 3.2.4.4).

Therefore to measure the potential of the FAD/FADH[•] and FADH[•]/FADH₂ couples in XDH, an electrometrical titration in presence of several cobalt and iron complexes as mediators was performed. The solution was made anaerobic and reduced stepwise by addition of Ti^{III} followed by measurement of the absorption spectrum and the redox potential.

One series of absorption spectra for XDHwt measured at various redox potentials is shown in Figure 55. Moving to more negative potentials the absorption maximum at 465 nm decreases, meanwhile a shoulder with a maximum at 623 nm appears, but decreasing back later. This latter absorption indicates the formation of the blue neutral flavin semiquinone (Hunt *et al.*, 1993).

Figure 56a shows the titration curves (plots of optical changes vs. redox potential) for XDHwt at 465 nm and figure 5c at 623 nm. In each case two sets of data are shown: circles mark the values measured during the reduction, whereas the stars correspond to the data taken while the system was reoxidized by dithionite addition.

The formation of a stable semiquinone could be clearly observed. Modeling the absorption data at 465 nm by equation (4) a midpoint potential for the first half reaction $E_{\text{FAD}/\text{FADH}^{\bullet}} = -479 \pm 20 \text{ mV}$ was obtained.

This result is expected to have a large error due to the optical contribution of the two iron-sulfur centers in the region around 460 nm.

At the same time analyzing the trend of the adsorption at 623 nm by equation (5) a formal potential of -453 ± 16 and -608 ± 27 for the first and the second half reaction, respectively, was calculate (Figure 56b). Both potential result ca. 80mV higher than the value, corrected for the theoretical shift due to the different solution pH, reported by Hunt (Hunt *et al.*, 1993) for milk xanthine dehydrogenase, but in good agreement in respect to the separation between flavin half-potentials.

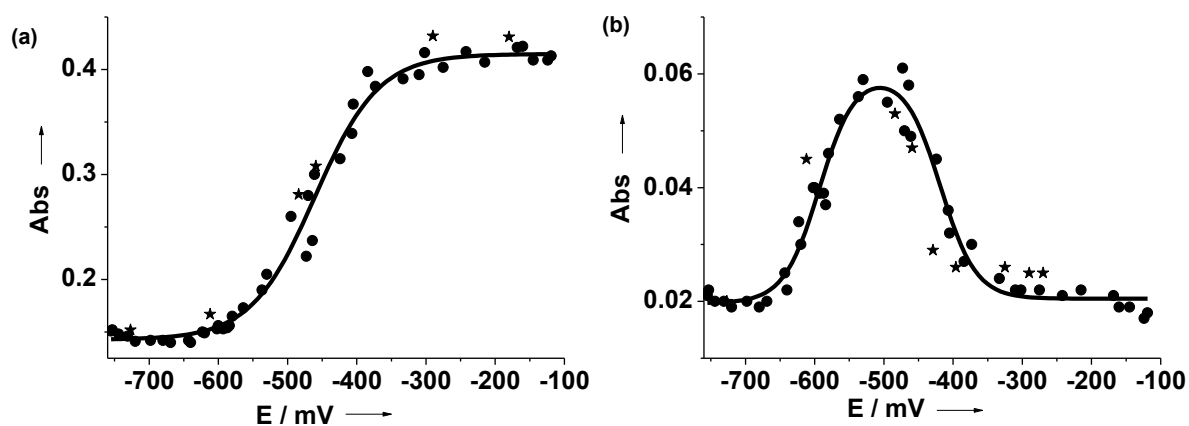


Figure 56. (a) Adsorption changes at 465 nm and (b) at 623 nm after reduction (circles) and reoxidation (stars) upon addition of Ti(III) and $S_2O_8^{2-}$ respectively.

5 Summary

This work contributed to different aspects within the research field of protein spectro- and electro-chemistry on nanostructured materials. In this respect novel optical transparent materials were exploited for the investigation of redox proteins and biosensing systems. For this purpose several measuring set up were designed, constructed and optimized.

One aspect was related to the investigation of mesoporous transparent and conductive metal oxides, as supporting materials, in combination with cytochrome *c* and *human* sulfite oxidase for the development of biosensing systems. A further aspect was the investigation of electrode surfaces modified with spherical gold nanoparticles for the enhancement of the catalytic electroactivity of *human* sulfite oxidase with the purpose of sulfite biosensing. Finally, the direct electronic communication of protein with high structure complexity such as xanthine dehydrogenase from *Rhodobacter capsulatus* and its high homologues *mouse* aldehyde oxidase homolog 1 and the two formal potential of the FAD cofactor were spectroelectrochemically determined. An overall view of the methods and strategy employed in this thesis for protein spectroelectrochemical investigation are summarized in Figure 57.

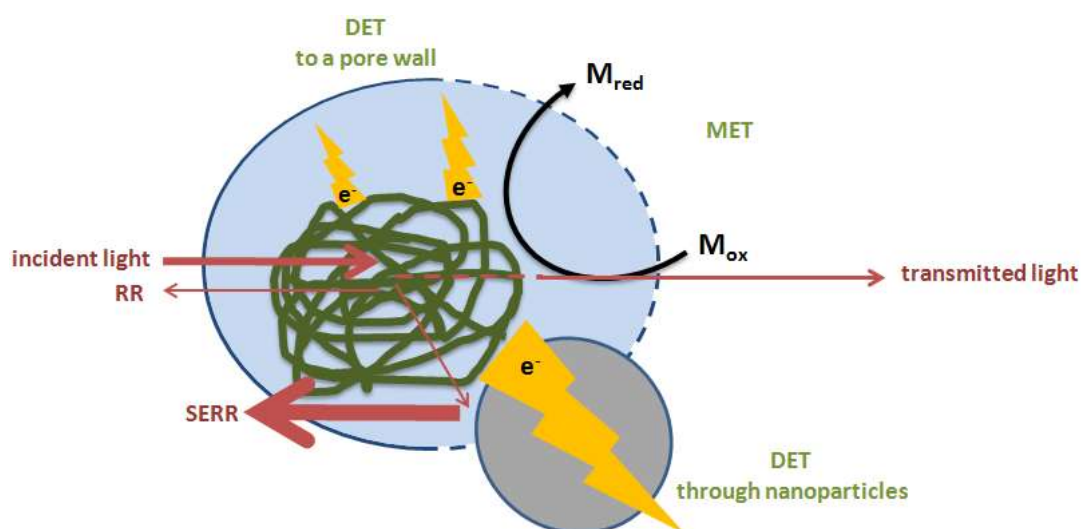


Figure 57. General representation of the different strategies and methods employed in this work. The different possibilities of electron transfer reactions via mediators, porous materials and nanoparticles are illustrated. Further the opportunity of optical detection by absorption UV-Vis spectroscopy, resonance Raman (RR) and surface enhanced resonance Raman (SERR) are also depicted. DET stay for direct electron transfer, MET for mediated electron transfer, while M_{red} and M_{ox} for the reduced and oxidized form of a mediator molecule, respectively.

The first part of the work is dedicated to the spectroelectrochemical characterization of the redox protein cytochrome *c* (cyt *c*) immobilized on a recently developed mesoporous tin-doped (mpITO) and *tin-rich* (mpITBO) indium oxide and antimony-doped oxide (ATO). Due to the high conductivity and optical transparency, electrochemical methods could be combined with spectroscopic approaches.

Equilibration of mpITO and *tin-rich* mpITBO in a cyt *c* solution resulted in stable protein adsorption. Immobilization of the native protein into the porous structure was quickly achieved with long-term stability and no detectable denaturation. The structural integrity of the heme pocket was demonstrated by resonance Raman (RR) spectra, which displayed a remarkable signal-to-noise ratio. This good spectral quality is noteworthy since RR spectroscopic characterization of immobilized proteins usually requires the additional signal amplification of the surface-enhanced Raman effects provided by rough Ag surfaces. These materials evidently overcome this restriction due to the substantially increased surface concentration. Film thickness was found to be proportional to the protein loading which is likely due to the deep localization of the immobilized cyt *c*. The immobilization time was highly influenced by the pore shape and size. The surface charge instead plays an important role in the ability of the material to selectively immobilize charged proteins.

Due to the high loading and durable immobilization of cyt *c*, even at high ionic strength, and the accessibility of the protein for small molecules, the cyt *c*/mpITO device represents a system appropriate for biosensor development. As shown for the detection of superoxide in solution upon enzymatic generation of superoxide in the electrochemical cell, a steady-state amperometric response was observed. The sensitivity was much higher than for recently reported sensors employing cyt *c* covalently bound to alkanethiol-modified gold electrodes (Chen *et al.*, 2008), but lower than for sensors whereupon cyt *c* has been assembled in multilayers using electrostatic interaction (Beissenhertz *et al.*, 2004). Although this electrostatic immobilization resulted in increased sensitivity, in contrast to the system proposed in this work, the biosensors already showed a serious loss of protein from the electrode within two days of storage or a few measurements (Beissenhertz *et al.*, 2004).

The particular properties showed by the mpITO in combination with cyt *c* open the possibility to develop several more complex catalytic systems. An electrochemical switchable protein-based optical device was designed with the core part composed of

cyt *c* immobilized on a mesoporous indium tin oxide film. Although it could be possible the direct optical observation of the redox changes at the catalytic centers, in this proposed switchable system a color developing redox sensitive dye was used. Optical changes of the protein are generally very tiny due to the restriction of the protein amount, which can be immobilized (Hulko *et al.*, 2011; Panicco *et al.*, 2008). In contrast a dye allows enhancing the optical output due to its larger extinction coefficient and to the possibility of product accumulation. The cyt *c*-catalyzed oxidation of the dye by hydrogen peroxide was spectroscopically investigated. When the dye is co-immobilized with the protein, its redox state is easily controlled by application of an electrical potential at the supporting material. This enables to electrochemically reset the system to the initial state and repetitive signal generation. The present work contributes to the development of reusable sensing systems with a visual evaluation of the detection process related to an analyte.

Further investigation was extended to negative charged proteins which do not have good interaction with the negative charged indium tin oxide based films. A strategy based on the charge inversion, by a positive charged polymer, was implemented. It allows direct spectroelectrochemical investigation of the isolated domain containing the *b5*-type heme cofactor from *human* sulfite oxidase (*hSO*).

In case of more complex negative enzymes a novel transparent conductive material, the antimony-doped tin oxide (ATO), was considered. This transparent and conductive metal oxide shows quick direct electron exchange with small redox molecules (Table 1). Unlike to the indium tin oxide based materials the negative charged redox mediator showed a reversible electrochemistry on ATO films. In addition ATO films resemble the indium tin oxide based materials in the reversible electrochemistry of a positive charged mediator. The charge seems in the case of ATO films to be not relevant in the electrochemical processes. Similar behaviors are showed either with a planar and a mesoporous ATO film.

It should be pointed out that the negative charged *hSO*, which show no adsorption on the other metal oxides, could be adsorbed on ATO film. An increase of the oxidation current when sulfite was in contact with an ATO modified with *hSO* was detected at potential lower than that associated to a direct oxidation of the substrate.

	$\text{Ru}(\text{NH}_3)_6^{2+/3+}$		$\text{Fe}(\text{CN})_6^{3-/4-}$	
	E^0 / mV	K /cm s ⁻¹	E^0 / mV	K /cm s ⁻¹
mpITO (PIB3000)	-226 ± 6	$(6 \pm 2) \cdot 10^{-4}$	n/a	n/a
planar ITO	-223 ± 13	n.d.	n/a	n/a
mpITBO (F127)	-282 ± 14	$(4 \pm 2) \cdot 10^{-3}$	n/a	n/a
mpITBO (KLE)	-261 ± 14	$(3 \pm 1) \cdot 10^{-3}$	n/a	n/a
planar ATO	-287 ± 1	$(3 \pm 1) \cdot 10^{-3}$	262 ± 2	$(3.2 \pm 0.9) \cdot 10^{-3}$
mpATO (PBD-10k)	-309 ± 8	$(3 \pm 1) \cdot 10^{-3}$	242 ± 8	$(2.1 \pm 0.1) \cdot 10^{-3}$

Table 1. Formal potential (E^0) of two mediators, corresponding to the mean value of the oxidation and reduction peak potential, and heterogeneous electron transfer constant (K), calculated by the method of Nicholson (Nicholson 1965), at different metal oxide electrodes. For mesoporous materials the block co-polymer used in the synthesis are reported in parenthesis. The working solution were 2 mM $\text{Ru}(\text{NH}_3)_6\text{Cl}_2$ in potassium phosphate buffer solution 50 mM, 0.1 M KCl, pH 7.0 and 2 mM $\text{K}_3\text{Fe}(\text{CN})_6$ in potassium phosphate buffer solution 50 mM, 1 M KCl, pH 7.0. Reference electrode Ag/AgCl, 1M KCl. (n.d. = non determinable, n/a = not applicable).

A bioelectrocatalytic sulfite conversion was likely displayed and the oxidation current could be correlated to the substrate concentration. This combined system has interesting features, e.g. for biosensing and for integration to novel opto- and electrochemical biodevices. These features are the possibility to work at elevated ionic strength and the long term stability combined to the high conductivity and transparency of the supporting material. Furthermore the low working potential employed (0 V) could ensures reduced interferences in case of biosensing application and a high driving force in biofuel cell devices. Although the electrocatalysis of an enzyme immobilized on ATO surface was shown for the first time, further development of the three dimensional structure in the supporting metal oxide is required. Porosity of appropriate size will enable the entrapment higher protein amount permitting then to increase the conversion capability and to extend the investigation to optical methods.

The present work contributes to the extension of opto- and electrochemical studies of proteins on different supporting materials, included novel materials with low or no content of the rare and expensive indium. The differentiation of the supporting material enables to control the surface chemistry, the geometry of the porosity and

the working potential window. These characteristics are of high interest for the combination of these metal oxides with a large variety of proteins and enzymes. Thereby fundamental studies of the biomolecules but also the construction of new devices will be therefore likely.

The second part of this thesis pertains to the development of a sulfite biosensing system, based on direct electron transfer of an immobilized *human* sulfite oxidase (*hSO*) to a gold nanoparticles modified electrode.

The small mobile protein domain containing the *b5*-type heme cofactor was spectroelectrochemically found to be responsible for the electron shuttle between the catalytic active molybdenum center and the electrode. The structural integrity of the heme pocket was demonstrated by surface enhanced resonance Raman spectroscopy. The spectroscopic studies further displayed that almost all the immobilized enzyme molecules are reachable for a direct electron transfer with the electrode. The *hSO* direct electron transfer was possible also at a very high ionic strength, where other systems based on mediated electron transfer or on layer-by-layer technique need a membrane protection. Gold nanoparticles (AuNPs) enhance the electrocatalytic activity of the immobilized protein in respect to the AuNPs-free electrode. Basic pH condition, elevated ionic strength, oxygen-free solution and very low applied potential (0 V) were the optimum conditions for sulfite biosensing. At the current status the detection of sulfite was possible in a range between 0.5 and 5.4 μM with a high sensitivity ($1.85 \text{ nA } \mu\text{M}^{-1}$). This system based on *hSO* and gold nanoparticles shows remarkable advantages such as the possibility to work at low applied potential, avoiding sulfite direct oxidation, and to work at very high ionic strength without leaking of protein. In addition the short response time enables nearly immediate detection. Therefore these properties could make the system proposed in this work useful for the development of bioelectronic devices and its application in real samples.

Although the above mentioned ATO film and the AuNP-modified electrode show comparable properties with respect to immobilization stability of *hSO* and small overpotential for electrocatalytic sulfite oxidation, the two supporting material could accomplish different tasks. ATO offers the possibility to couple optical and electrochemical methods which are of considerable interest in the basic investigation of the enzyme. On contrary the AuNPs provide features like the wide opportunity to

build several three dimensional architectures, high handiness and device miniaturization possibilities which address the requirement in the biosensor and biofuel cells.

Finally in the third part protein with high structure complexity such as the xanthine dehydrogenase from *R. capsulatus* (XDH) and its high homologues the *mouse* aldehyde oxidase homolog 1 (*mAOH1*) were electrochemically and spectroelectrochemically studied.

An electrochemical pretreatment was employed to generate oxygen functionality on a glassy carbon electrode. The oxygen functionality created in this way promoted the protein immobilization on the electrode surface. It could be demonstrated that the FAD as well as the molybdenum cofactor (Moco), as terminal cofactors of the electron pathway inside the proteins, are able to directly exchange electrons with the electrode. Both cofactors showed the typical potential shift usually associated to one electron exchange per each proton exchanged. Although FAD should show two different formal potentials for each electron exchange, it displayed via direct electrochemistry only one peak which contains both electron exchanges. This behavior of the cofactors is also reported here for the first time with *mAOH1*, which is a member of the xanthine oxidase family and structurally a XDH-like protein.

Only in the case of XDH mutants bearing a serine substituted to the cysteines bound to the second iron sulfur cluster in the electron internal pathway (FeSII) a further electrochemical signal appeared. Based on previous investigation and EPR measurement this third signal could be assigned to this most exposed FeSII (Aguey-Zinsou *et al.*, 2003). The other iron sulfur cluster, which is the first in the electron internal pathway (FeSI), was probably too buried for any direct electron transfer. For comparison the data from the present work are listed in Table 2 with an overview of the published potentials, determined by direct electrochemistry at different electron surfaces. In every investigation the FAD signal was displayed, when possible. These signals match with the potential measured at the EP-GC electrode, within negligible discrepancy. The signal of the molybdenum center was reported only in some cases and is located in the far negative region. Furthermore this work showed that it is possible to observe the potential of the second iron sulfur cluster, which was until now rarely reported. It has to be remarked that the lack of a clear electro-oxidation of the substrate in the present work, as well as in the previous

published electrochemical studied, raises doubts about the actual native conformation of the enzyme on the electrode surfaces.

	Enzyme	Working electrode	FAD	FeSII	Moco
(Rodrigues <i>et al.</i> , 1991)	XOD	GC or Hg	-463		
(Wang <i>et al.</i> , 2004)	XOD	Au + SWNT	-532		
(Liu <i>et al.</i> , 2005)	XOD	PG + DNA	-508		-612
(Bernhardt <i>et al.</i> , 2006)	XOD	EPPG + DDAB	-479		
(Zhou <i>et al.</i> , 2006)	XOD	PG + TiO ₂	-519		-605
(Wu <i>et al.</i> , 2007)	XOD	GC + SWCNT	-520	-600	-820
(Shan <i>et al.</i> , 2009)	XOD	GC + Laponite	-533		
(Correia dos Santos <i>et al.</i> , 2004)	AOR	GC or PG	n/a	-507	-767
(Aguey-Zinsou <i>et al.</i> , 2003)	XDH	EPPG	-537	-637	-747
This work	XDH	EP-GC	-532	-622	-781
This work	<i>mAOH1</i>	EP-GC	-549		-794

Table 2. Up dated list of redox potentials electrochemically determined for protein members of the xanthine oxidase family. The working electrodes are also reported. For clarity all the potentials are reported at pH 8, against a Ag/AgCl, 1M KCl reference. (n/a = not applicable).

In order to separate the two successive electron transfer steps of the FAD cofactor in the XDH structure a mediated spectroelectrochemical titration was performed. The changes in the solution potential, by chemical mean, showed an evolution of the adsorption spectra of the XDH. The fully oxidized state has an UV-Vis absorption maximum at 465 nm dominated by the flavin and FeS. In contrast the FAD-semiquinone shows an absorption maximum around 630 nm. A stable semiquinone was detected and is a characteristic for the XDH. In xanthine oxidase, in contrast, no stable semiquinone was found (Hunt *et al.*, 1993). The absorption changes around 630 nm were used for the calculation of the two distinct potentials of the FAD/FADH[•] and FADH[•]/FADH₂ couples in XDH. Several transparent iron and cobalt complexes were used as mediators in solution in order to avoid disturbances from their UV-vis absorption. Interestingly the arithmetic mean of the two potential is identical, within the error margins, with the potential measured for FAD by direct electrochemistry.

This work provides insights into the fundamental enzymatic electron pathway of proteins from the xanthine oxidase family by combination of the direct electrochemical and the mediated spectroelectrochemical investigations. Knowledge

about these processes may not only be relevant for further studies of XDH from *R. capsulatus* and *mouse* AOH1 but also for a deep understanding of the different members of the molybdo-containing enzymes. Due to the dimensional restriction of the porous material currently available these complex enzymes could not be immobilized in mesoporous transparent and conductive oxides. Further improvement of porosity in such material will lead to the possibility to entrap high amount of enzymes. Then direct or mediated electrochemical investigation combined with optical methods described in this work, like UV-Vis, resonance Raman as well as surface enhanced resonance Raman could be achieved employing very tiny amount of these enzymes. Therefore the results reported in this work could provide a base for the future research on spectroelectrochemistry of more complex proteins and enzymes confined on surfaces and likely more new fascinating biodevices.

6 References

- Abass, A., 2000. Development of an amperometric sulfite biosensor based on sulfite oxidase with cytochrome c, as electron acceptor, and a screen-printed transducer. *Sens. Actuators, B* 62, 148-153.
- Adelhelm, P., Stockburger, M., 1989. Cytochrome c at charged interfaces. 1. Conformational and redox equilibria at the electrode/electrolyte interface probed by surface-enhanced resonance Raman spectroscopy. *Biochemistry* 28, 6710-6721.
- Aguey-Zinsou, K.-F., Bernhardt, P.V., Kappler, U., McEwan, A.G., 2003. Direct electrochemistry of a bacterial sulfite dehydrogenase. *J. Am. Chem. Soc.* 125, 530-535.
- Aguey-Zinsou, K.F., Bernhardt, P.V., Leimkühler, S., 2003. Protein film voltammetry of *Rhodobacter capsulatus* xanthine dehydrogenase. *J. Am. Chem. Soc.* 125, 15352-8.
- Aksu, Y., Driess, M., 2009. A Low-Temperature Molecular Approach to Highly Conductive *Tin-rich* Indium Tin Oxide Thin Films with Durable Electro-Optical Performance. *Angew. Chem., Int. Ed.* 48, 7778-7782.
- Aksu, Y., Frasca, S., Wollenberger, U., Driess, M., Thomas, A., 2011. A Molecular Precursor Approach to Tunable Porous *Tin-rich* Indium Tin Oxide with Durable High Electrical Conductivity for Bioelectronic Devices. *Chem. Mater.* 23, 1798-1804.
- Allen, P.M., Allen, H., Hill, O., Walton, N.J., 1984. Surface modifiers for the promotion of direct electrochemistry of cytochrome c. *J. Electroanal. Chem.* 178, 69-86.
- Arion, V.B., Rapta, P., Telser, J., Shova, S.S., Breza, M., Luspai, K., Kozisek, J., 2011. Syntheses, electronic structures, and EPR/UV-vis-NIR spectroelectrochemistry of nickel(II), copper(II), and zinc(II) complexes with a tetradentate ligand based on S-methylisothiosemicarbazide. *Inorg. Chem.* 50, 2918-2931.
- Armstrong, F.A., Hill, H.A.O., Walton, N.J., 1988. Direct electrochemistry of redox proteins. *Acc. Chem. Res.* 21, 407-413.
- Armstrong, F.A., 1990. Probing metalloproteins by voltammetry, in: *Bioinorganic Chemistry*. eds. Springer-Verlag, Berlin/Heidelberg.
- Armstrong, F.A., 2002. Voltammetry of proteins, in: *Encyclopedia of Electrochemistry*. eds. Wiley VCH Weinheim, pp. 13-29.
- Astashkin, A.V., Raitsimring, A.M., Feng, C., Johnson, J.L., Rajagopalan, K.V., Enemark, J.H., 2002. Pulsed EPR studies of nonexchangeable protons near the Mo(V) center of sulfite oxidase: direct detection of the alpha-proton of the coordinated cysteinyl residue and structural implications for the active site. *J. Am. Chem. Soc.* 124, 6109-6118.
- Balasubramanian, N., Subrahmanyam, A., 1989. Electrical and optical properties of reactively evaporated indium tin oxide (ITO) films-dependence on substrate temperature and tin concentration. *J. Phys. D: Appl. Phys.* 22, 206-209.

- Batzill, M., Diebold, U., 2005. The surface and materials science of tin oxide. *Prog. Surf. Sci.* 79, 47-154.
- Behar, D., Czapski, G., Rabani, J., Dorfman, L.M., Schwarz, H.A., 1970. Acid dissociation constant and decay kinetics of the perhydroxyl radical. *J. Phys. Chem.* 74, 3209-3213.
- Beissenhirtz, M.K., Scheller, F.W., Lisdat, F., 2004. A Superoxide Sensor Based on a Multilayer Cytochrome c Electrode. *Anal. Chem.* 76, 4665-4671.
- Beissenhirtz, M.K., Scheller, F.W., Stöcklein, W.F.M., Kurth, D.G., Möhwald, H., Lisdat, F., 2004. Electroactive Cytochrome c Multilayers within a Polyelectrolyte Assembly. *Angew. Chem., Int. Ed.* 43, 4357-4360.
- Bernad, S., Mäntele, W., 2006. An innovative spectroelectrochemical reflection cell for rapid protein electrochemistry and ultraviolet/visible/infrared spectroscopy. *Anal. Biochem.* 351, 214-218.
- Bernhardt, P.V., 2006. Enzyme Electrochemistry - Biocatalysis on an Electrode. *Aust. J. Chem.* 59, 233-256.
- Bernhardt, P.V., 2009. Communication with the Mononuclear Molybdoenzymes: Emerging Opportunities and Applications in Redox Enzyme Biosensors, in: Davis, J. (Ed.), *Engineering the Bioelectronic Interface*. Royal Society of Chemistry, Cambridge, pp. 1-24.
- Bernhardt, P.V., Chen, K.-I., Sharpe, P., 2006. Transition metal complexes as mediator-titrants in protein redox potentiometry. *J. Biol. Inorg. Chem.* 11, 930-936.
- Bernhardt, P.V., Honeychurch, M.J., McEwan, A.G., 2006. Direct electrochemically driven catalysis of bovine milk xanthine oxidase. *Electrochem. Commun.* 8, 257-261.
- Bertini, I., Cavallaro, G., Rosato, A., 2006. Cytochrome c: occurrence and functions. *Chem. Rev.* 106, 90-115.
- De Biase, P.M., Paggi, D.A., Doctorovich, F., Hildebrandt, P., Estrin, D.A., Murgida, D.H., Marti, M.A., 2009. Molecular basis for the electric field modulation of cytochrome C structure and function. *J. Am. Chem. Soc.* 131, 16248-16256.
- Bon Saint Côme, Y.A., Lalo, H., Wang, Z., Etienne, M., Gajdzik, J., Kohring, G.-W., Walcarius, A., Hempelmann, R., Kuhn, A., 2011. Multiscale-tailored bioelectrode surfaces for optimized catalytic conversion efficiency. *Langmuir.* 27, 12737-12744.
- Bowden, E.F., Cohen, D.J., Hawkrige, F.M., 1982. Anaerobic thin-layer electrochemical cell for planar optically transparent electrodes. *Anal. Chem.* 54, 1005-1008.
- Bowden, E.F., Hawkrige, F.M., Blount, H.N., 1984. Interfacial electrochemistry of cytochrome c at tin oxide, indium oxide, gold, and platinum electrodes. *J. Electroanal. Chem.* 161, 355-376.
- Bowden, E.F., Hawkrige, F.M., Chlebowski, J.F., Bancroft, E.E., Thorpe, C., Blount, H.N., 1982. Cyclic voltammetry and derivative cyclic voltabsorptometry of purified horse heart cytochrome c at tin-doped indium oxide optically transparent electrodes. *J. Am. Chem. Soc.* 104, 7641-7644.

- Brody, M.S., Hille, R., 1995. The reaction of chicken liver sulfite oxidase with dimethylsulfite. *Biochim. Biophys. Acta* 1253, 133-135.
- Brody, M.S., Hille, R., 1999. The kinetic behavior of chicken liver sulfite oxidase. *Biochemistry* 38, 6668-6677.
- Burgess, B.K., Lowe, D.J., 1996. Mechanism of Molybdenum Nitrogenase. *Chem. Rev* 96, 2983-3012.
- Bushnell, G.W., Louie, G.V., Brayer, G.D., 1990. High-resolution three-dimensional structure of horse heart cytochrome c. *J. Mol. Biol.* 214, 585-595.
- Byrne, R.S., Hänsch, R., Mendel, R.R., Hille, R., 2009. Oxidative half-reaction of arabidopsis thaliana sulfite oxidase: generation of superoxide by a peroxisomal enzyme. *J. Biol. Chem.* 284, 35479-35484.
- Cable, M., Smith, E.T., 2005. Identifying the $n = 2$ reaction mechanism of FAD through voltammetric simulations. *Anal. Chim. Acta* 537, 299-306.
- Calvo, E.J., Wolosiuk, A., 2004. Supramolecular Architectures of Electrostatic Self-Assembled Glucose Oxidase Enzyme Electrodes. *ChemPhysChem* 5, 235-239.
- Campanella, L., Favero, G., Tomassetti, M., 1997. A modified amperometric electrode for the determination of free radicals. *Sens. Actuators, B* 44, 559-565.
- Campàs, M., Prieto-Simón, B., Marty, J.-L., 2009. A review of the use of genetically engineered enzymes in electrochemical biosensors. *Semin. Cell Dev. Biol* 20, 3-9.
- Caroppi, P., Sinibaldi, F., Fiorucci, L., Santucci, R., 2009. Apoptosis and human diseases: mitochondrion damage and lethal role of released cytochrome C as proapoptotic protein. *Curr. Med. Chem.* 16, 4058-4065.
- Carrie A., T., Tyler N., G., Rajagopalan, K.V., 2000. Optimization of Expression of Human Sulfite Oxidase and Its Molybdenum Domain. *Arch. Biochem. Biophys.* 338, 281-287.
- Caruana, D.J., Howorka, S., 2010. Biosensors and biofuel cells with engineered proteins. *Mol. Biosyst.* 6, 1548-1556.
- Chambers, J.P., Arulanandam, B.P., Matta, L.L., Weis, A., Valdes, J.J., 2008. Biosensor recognition elements. *Curr. Issues Mol. Biol.* 10, 1-12.
- Chen, D., Wang, G., Li, J., 2007. Interfacial Bioelectrochemistry: Fabrication, Properties and Applications of Functional Nanostructured Biointerfaces. *J. Phys. Chem. B* 111, 2351-2367.
- Chen, X.J., West, A.C., Cropek, D.M., Banta, S., 2008. Detection of the superoxide radical anion using various alkanethiol monolayers and immobilized cytochrome c. *Anal. Chem.* 80, 9622-9629.
- Chopra, K.L., Major, S., Pandya, D.K., 1983. Transparent conductors—A status review. *Thin Solid Films* 102, 1-46.

- Cohen, H.J., Fridovich, I., 1971a. Hepatic sulfite oxidase. Purification and properties. *J. Biol. Chem.* 246, 359-366.
- Cohen, H.J., Fridovich, I., 1971b. Hepatic sulfite oxidase. The nature and function of the heme prosthetic groups. *J. Biol. Chem.* 246, 367-373.
- Collinson, M., Bowden, E.F., 1992. UV-visible spectroscopy of adsorbed cytochrome c on tin oxide electrodes. *Anal. Chem.* 64, 1470-1476.
- Correia dos Santos, M.M., Sousa, P.M.P., Gonçalves, M.L.S., Romão, M.J., Moura, I., Moura, J.J.G., 2004. Direct electrochemistry of the *Desulfovibrio gigas* aldehyde oxidoreductase. *Eur. J. Biochem.* 271, 1329-38.
- Coury Jr., L.A., Murray, R.W., Johnson, J.L., Rajagopalan, K.V., 1991. Electrochemical study of kinetics of electron transfer between synthetic electron acceptors and reduced myoglobin protein sulfite oxidase. *J. Phys. Chem.* 95, 6034-6040.
- Çubukçu, M., Timur, S., Anik, Ü., 2007. Examination of performance of glassy carbon paste electrode modified with gold nanoparticle and xanthine oxidase for xanthine and hypoxanthine detection. *Talanta* 74, 434-439.
- Dai, Y., Zheng, Y., Swain, G.M., Proshlyakov, D.A., 2011. Equilibrium and kinetic behavior of $\text{Fe}(\text{CN})_6^{3-/4-}$ and cytochrome c in direct electrochemistry using a film electrode thin-layer transmission cell. *Anal. Chem.* 83, 542-548.
- Dai, Z., Liu, S., Ju, H., 2004. Direct electron transfer of cytochrome c immobilized on a NaY zeolite matrix and its application in biosensing. *Electrochim. Acta* 49, 2139-2144.
- Deng, Z., Gong, Y., Luo, Y., Tian, Y., 2009. WO_3 nanostructures facilitate electron transfer of enzyme: application to detection of H_2O_2 with high selectivity. *Biosens. Bioelectron.* 24, 2465-2469.
- Deriu, D., Pagnotta, S.E., Santucci, R., Rosato, N., 2007. Spectroscopic and electrochemical characterization of cytochrome c encapsulated in a bio sol-gel matrix. *Biometals* 21, 417-423.
- Dronov, R., Kurth, D.G., Möhwald, H., Scheller, F.W., Lisdat, F., 2007. A self-assembled cytochrome c/xanthine oxidase multilayer arrangement on gold. *Electrochim. Acta* 53, 1107-1113.
- Dronov, R., Kurth, D.G., Möhwald, H., Spricigo, R., Leimkühler, S., Wollenberger, U., Rajagopalan, K.V., Scheller, F.W., Lisdat, F., 2008. Layer-by-layer arrangement by protein-protein interaction of sulfite oxidase and cytochrome c catalyzing oxidation of sulfite. *J. Am. Chem. Soc.* 130, 1122-1123.
- Dryhurst, G., Kadish, K.M., Scheller, F.W., Renneberg, R., 1982. *Biological Electrochemistry*. Academic Press, New York.
- Dunsch, L., 2011. Recent Advances in in situ multi-spectroelectrochemistry. *J. Solid State Electrochem.* 15, 1631-1646.
- Eddowes, M.J., Hill, H.A.O., 1977. Novel method for the investigation of the electrochemistry of metalloproteins: cytochrome c. *J. Chem. Soc., Chem. Commun.* 771b.

- Eddowes, M.J., Hill, H.A.O., 1979. Electrochemistry of horse heart cytochrome c. *J. Am. Chem. Soc.* 101, 4461-4464.
- Eilers, T., Schwarz, G., Brinkmann, H., Witt, C., Richter, T., Nieder, J., Koch, B., Hille, R., Hänsch, R., Mendel, R.R., 2001. Identification and biochemical characterization of *Arabidopsis thaliana* sulfite oxidase. A new player in plant sulfur metabolism. *J. Biol. Chem.* 276, 46989-46994.
- El Kasmi, A., Leopold, M.C., Galligan, R., Robertson, R.T., Saavedra, S.S., El Kacemi, K., Bowden, E.F., 2002. Adsorptive immobilization of cytochrome c on indium/tin oxide (ITO): electrochemical evidence for electron transfer-induced conformational changes. *Electrochem. Commun.* 4, 177-181.
- Elion, G., 1989. The purine path to chemotherapy. *Science* 244, 41-47.
- Elliott, S.J., McElhaney, A.E., Feng, C., Enemark, J.H., Armstrong, F.A., 2002. A Voltammetric Study of Interdomain Electron Transfer within Sulfite Oxidase. *J. Am. Chem. Soc.* 124, 11612-11613.
- El-Deab, M. S., Ohsaka T., 2002. An extraordinary electrocatalytic reduction of oxygen on gold nanoparticles-electrodeposited gold electrodes. *Electrochem. Commun.* 4, 288-292.
- El-Deab, M. S., Ohsaka T., 2003. Electrocatalysis by nanoparticles: oxygen reduction on gold nanoparticles-electrodeposited platinum electrodes. *J. Electroanal. Chem.* 553, 107-115.
- Enroth, C., Eger, B.T., Okamoto, K., Nishino, T., Nishino, T., Pai, E.F., 2000. Crystal structures of bovine milk xanthine dehydrogenase and xanthine oxidase: Structure-based mechanism of conversion. *Proc. Natl. Acad. Sci. U. S. A.* 97, 10723-10728.
- Fan, J.C.C., Goodenough, J.B., 1977. X-ray photoemission spectroscopy studies of Sn-doped indium-oxide films. *J. Appl. Phys.* 48, 3524-3531.
- Fattakhova-Rohlfing, D., Brezesinski, T., Rathouský, J., Feldhoff, A., Oekermann, T., Wark, M., Smarsly, B.M., 2006. Transparent Conducting Films of Indium Tin Oxide with 3D Mesopore Architecture. *Adv. Mater.* 18, 2980-2983.
- Fedurco, M., 2000. Redox reactions of heme-containing metalloproteins: dynamic effects of self-assembled monolayers on thermodynamics and kinetics of cytochrome c electron-transfer reactions. *Coord. Chem. Rev.* 209, 263-331.
- Feng, C., Kedia, R.V., Hazzard, J.T., Hurley, J.K., Tollin, G., Enemark, J.H., 2002. Effect of solution viscosity on intramolecular electron transfer in sulfite oxidase. *Biochemistry* 41, 5816-5821.
- Feng, J.-J., Gernert, U., Hildebrandt, P., Weidinger, I.M., 2010. Induced SER-Activity in Nanostructured Ag-Silica-Au Supports via Long-Range Plasmon Coupling. *Adv. Funct. Mat.* 20, 1954-1961.
- Feng, J.-J., Hildebrandt, P., Murgida, D.H., 2008. Silver nanocoral structures on electrodes: a suitable platform for protein-based bioelectronic devices. *Langmuir* 24, 1583-6.

- Ferapontova, E.E., Christenson, A., Hellmark, A., Ruzgas, T., 2004. Spectroelectrochemical study of heme- and molybdopterin cofactor-containing chicken liver sulphite oxidase. *Bioelectrochemistry* 63, 49-53.
- Ferapontova, E.E., Ruzgas, T., Gorton, L., 2003. Direct electron transfer of heme- and molybdopterin cofactor-containing chicken liver sulfite oxidase on alkanethiol-modified gold electrodes. *Anal. Chem.* 75, 4841-4850.
- Fischer, M., Thöny, B., Leimkühler, S., 2010. The biosynthesis of folate and pterins and their enzymology, in: *Comprehensive Natural Products II: Chemistry and Biology*, 7. pp. 599-648.
- Frasca, S., von Graberg, T., Feng, J.-J., Thomas, A., Smarsly, B.M., Weidinger, I.M., Scheller, F.W., Hildebrandt, P., Wollenberger, U., 2010. Mesoporous Indium Tin Oxide as a Novel Platform for Bioelectronics. *ChemCatChem* 2, 839-845.
- Frost & Sullivan, 2006. *Biosensors in Medical Diagnostics (Technical Insights)*.
- Garret, R. M., Johnson, J. L., Graf, T. N., Feigenbaum, A., Rajagopalan, K.V. 1998. Human sulfite oxidase R160Q: Identification of the mutation in a sulfite oxidase-deficient patient and expression and characterization of the mutant enzyme. *Proc. Natl. Acad. Sci. U.S.A.* 95, 6394-6398.
- Ge, B., Lisdat, F., 2002. Superoxide sensor based on cytochrome c immobilized on mixed-thiol SAM with a new calibration method. *Anal. Chim. Acta* 454, 53-64.
- Ge, Y., Turner, A.P.F., 2008. Too large to fit? Recent developments in macromolecular imprinting. *Trends Biotechnol.* 26, 218-224.
- van Gelder, B., Slater, E.C., 1962. The extinction coefficient of cytochrome c. *Biochim. Biophys. Acta* 58, 593-595.
- von Graberg, T., Hartmann, P., Rein, A., Gross, S., Seelandt, B., Röger, C., Zieba, R., Traut, A., Wark, M., Janek, J., Smarsly, B.M., 2011. Mesoporous tin-doped indium oxide thin films: effect of mesostructure on electrical conductivity. *Sci. Technol. Adv. Mater.* 12, 025005.
- Granqvist, C.G., Hultåker, A., 2002. Transparent and conducting ITO films: new developments and applications. *Thin Solid Films* 411, 1-5.
- Grochol, J., Dronov, R., Lisdat, F., Hildebrandt, P., Murgida, D.H., 2007. Electron transfer in SAM/cytochrome/polyelectrolyte hybrid systems on electrodes: a time-resolved surface-enhanced resonance Raman study. *Langmuir* 23, 11289-11294.
- Grosso, D., Balkenende, A.R., Albouy, P.A., Ayral, A., Amenitsch, H., Babonneau, F., 2001. Two-Dimensional Hexagonal Mesoporous Silica Thin Films Prepared from Block Copolymers: Detailed Characterization and Formation Mechanism. *Chem. Mater.* 13, 1848-1856.
- Gu, M.B., Mitchell, R.J., Kim, B.C., 2004. Whole-cell-based biosensors for environmental biomonitoring and application. *Adv. Biochem. Eng. Biotechnol.* 87, 269-305.

- Guerrieri, A., Cataldi, T.R.I., Hill, H.A.O., 1991. Direct electrical communication of cytochrome c and cytochrome b5 at basal plane graphite electrodes modified with lauric acid or laurylamine. *J. Electroanal. Chem.* 297, 541-547.
- Gupta, L., Mansingh, A., Srivastava, K., 1989. Band gap narrowing and the band structure of tin-doped indium oxide films. *Thin Solid Films* 176, 33-44.
- Hagen, W.R., 1989. Direct electron transfer of redox proteins at the bare glassy carbon electrode. *Eur. J. Biochem.* 182, 523-530.
- Hall, R.H., 2002. Biosensor technologies for detecting microbiological foodborne hazards. *Microbes Infect.* 4, 425-432.
- Hänsch, R., Lang, C., Riebeseel, E., Lindigkeit, R., Gessler, A., Rennenberg, H., Mendel, R.R., 2006. Plant sulfite oxidase as novel producer of H₂O₂: combination of enzyme catalysis with a subsequent non-enzymatic reaction step. *J. Biol. Chem.* 281, 6884-6888.
- Harrison, R., 2002. Structure and function of xanthine oxidoreductase: where are we now? *Free Radical Biol. Med.* 33, 774-797.
- Haruta, M., 1998. Size- and support-dependency in the catalysis of gold. *Catal. Today* 36, 153-166.
- Heineman, W.R., Hawkrige, F.M., Blount, H.N., 1984. Spectroelectrochemistry at Optically Transparent Electrodes. II. Electrodes Under Thin-Layer and Semi-infinite Diffusion Conditions and Indirect Coulometric Titrations, in: *Electroanalytical Chemistry*. A. J. Bard, Dekker, New York.
- Hill, H.A.O., Lawrance, G.A., 1989. Some consequences of mixed and dilute surface modification of gold electrodes for protein electrochemistry. *J. Electroanal. Chem.* 270, 309-318.
- Hill, H.A.O., Tew, D.G., Walton, N.J., 1985. An opsonised microelectrode: Observation of the respiratory burst of a single human neutrophil. *FEBS Lett.* 191, 257-263.
- Hille, R., 1996. The Mononuclear Molybdenum Enzymes. *Chem. Rev.* 96, 2757-2816.
- Hille, R., 2002. Molybdenum enzymes containing the pyranopterin cofactor: an overview. *Met. Ions Biol. Syst.* 39, 187-226.
- Hille, R., Nishino, T., 1995. Flavoprotein structure and mechanism. 4. Xanthine oxidase and xanthine dehydrogenase. *FASEB J.* 9, 995-1003.
- Hinnen, C., Parsons, R., Niki, K., 1983. Electrochemical and spectrophotometric studies of the adsorbed horse heart cytochrome c and cytochrome c3 from *D. Vulgaris*, miyazaki strain, at gold electrode. *J. Electroanal. Chem.* 147, 329-337.
- Hoffmann, R., Kriele, A., Obloh, H., Tokuda, N., Smirnov, W., Yang, N., Nebel, C.E., 2011. The creation of a biomimetic interface between boron-doped diamond and immobilized proteins. *Biomaterials* 32, 7325-7332.

- Hou, K., Puzzo, D., Helander, M.G., Lo, S.S., Bonifacio, L.D., Wang, W., Lu, Z., Scholes, G.D., Ozin, G.A., 2009. Dye-Anchored Mesoporous Antimony-Doped Tin Oxide Electrochemiluminescence Cell. *Advanced Materials* 21, 2492-2496.
- Howard, J.B., Rees, D.C., 1996. Structural Basis of Biological Nitrogen Fixation. *Chem. Rev.* 96, 2965-2982.
- Hulko, M., Hospach, I., Krasteva, N., Nelles, G., 2011. Cytochrome C Biosensor—A Model for Gas Sensing. *Sensors* 11, 5968-5980.
- Hunt, J., Massey, V., Dunham, W.R., Sands, R.H., 1993. Redox potentials of milk xanthine dehydrogenase. Room temperature measurement of the FAD and 2Fe/2S center potentials. *J. Biol. Chem.* 268, 18685-18691.
- Jennings, T., Strouse, G., 2007. Past, present, and future of gold nanoparticles. *Adv. Exp. Med. Biol.* 620, 34-47.
- Jiao, K., Yang, T., Wang, Z.J., 2004. Thin-layer Spectroelectrochemistry of 3, 3',5, 5'-Tetramethyl- benzidine on Pt Minigrad Optically Transparent Electrode. *Chin. Chem. Lett.* 16, 655-658.
- Jin, W., Wollenberger, U., Kärger, E., Schunck, W.-H., Scheller, F.W., 1997. Electrochemical investigations of the intermolecular electron transfer between cytochrome c and NADPH-cytochrome P450-reductase. *J. Electroanal. Chem.* 433, 135-139.
- Johnson, J.L., 2003. Prenatal diagnosis of molybdenum cofactor deficiency and isolated sulfite oxidase deficiency. *Prenat. Diagn.* 23, 6-8.
- Johnson, M.K., Rees, D.C., Adams, M.W.W., 1996. Tungstoenzymes. *Chem. Rev.* 96, 2817-2840.
- Joseph, P.D., Eling, T., Mason, R.P., 1982. The horseradish peroxidase-catalyzed oxidation of 3,5,3',5'-tetramethylbenzidine. Free radical and charge-transfer complex intermediates. *J. Biol. Chem.* 257, 3669 -3675.
- Joseph, P.D., Mason, R.P., Eling, T., 1982. Cooxidation of the clinical reagent 3,5,3',5'-tetramethylbenzidine by prostaglandin synthase. *Cancer Res.* 42, 2567-2570.
- Joshi, M.S., Johnson, J.L., Rajagopalan, K.V., 1996. Molybdenum cofactor biosynthesis in *Escherichia coli* mod and mog mutants. *J. Bacteriol.* 178, 4310-4312.
- Ju, H., Liu, S., Ge, B., Lisdat, F., Scheller, F.W., 2002. Electrochemistry of Cytochrome c Immobilized on Colloidal Gold Modified Carbon Paste Electrodes and Its Electrocatalytic Activity. *Electroanalysis* 14, 141-147.
- Kalimuthu, P., Leimkühler, S., Bernhardt, P.V., 2011. Xanthine dehydrogenase electrocatalysis: autocatalysis and novel activity. *J. Phys. Chem. B* 115, 2655-2662.
- Kalimuthu, P., Tkac, J., Kappler, U., Davis, J.J., Bernhardt, P.V., 2010. Highly sensitive and stable electrochemical sulfite biosensor incorporating a bacterial sulfite dehydrogenase. *Anal. Chem.* 82, 7374-7379.

- Kappler, U., Bailey, S., 2005. Molecular Basis of Intramolecular Electron Transfer in Sulfite-oxidizing Enzymes Is Revealed by High Resolution Structure of a Heterodimeric Complex of the Catalytic Molybdopterin Subunit and a c-Type Cytochrome Subunit. *J. Biol. Chem.* 280, 24999-25007.
- Kappler, U., Bennett, B., Rethmeier, J., Schwarz, G., Deutzmann, R., McEwan, A.G., Dahl, C., 2000. Sulfite: Cytochrome c oxidoreductase from *Thiobacillus novellus*. Purification, characterization, and molecular biology of a heterodimeric member of the sulfite oxidase family. *J. Biol. Chem.* 275, 13202-13212.
- Kavan, L., Janda, P., Krause, M., Ziegs, F., Dunsch, L., 2009. Rotating cell for in situ Raman spectroelectrochemical studies of photosensitive redox systems. *Anal. Chem.* 81, 2017-2021.
- Kirgöz, Ü.A., Timur, S., Wang, J., Telefoncu, A., 2004. Xanthine oxidase modified glassy carbon paste electrode. *Electrochem. Commun.* 6, 913-916.
- Kisker, C., Schindelin, H., Pacheco, A., Wehbi, W.A., Garrett, R.M., Rajagopalan, K.V., Enemark, J.H., Rees, D.C., 1997. Molecular basis of sulfite oxidase deficiency from the structure of sulfite oxidase. *Cell* 91, 973-983.
- Klod, S., Ziegs, F., Dunsch, L., 2009. In situ NMR spectroelectrochemistry of higher sensitivity by large scale electrodes. *Anal. Chem.* 81, 10262-10267.
- Kniemeyer, O., Heider, J., 2001. Ethylbenzene dehydrogenase, a novel hydrocarbon-oxidizing molybdenum/iron-sulfur/heme enzyme. *J. Biol. Chem.* 276, 21381-21386.
- Koetz, J., Sabine, K., 2007. *Polyelectrolytes and Nanoparticles*. Springer Berlin Heidelberg, Berlin, Heidelberg.
- Koreeda, Y., Hirata, Y., Sameshima, S., 2004. Analysis of particle connection in a two-component powder compact by electrical conductivity measurements. *J. Ceram. Process. Res.* 5, 337-342.
- Kraft, A., Hennig, H., Herbst, A., Heckner, K.H., 1994. Changes in electrochemical and photoelectrochemical properties of tin-doped indium oxide layers after strong anodic polarization. *J. Electroanal. Chem.* 365, 191-196.
- Kranich, A., Ly, H.K., Hildebrandt, P., Murgida, D.H., 2008. Direct observation of the gating step in protein electron transfer: electric-field-controlled protein dynamics. *J. Am. Chem. Soc.* 130, 9844-9848.
- Kuwana, T., Heineman, W.R., 1976. Study of electrogenerated reactants using optically transparent electrodes. *Acc. Chem. Res.* 9, 241-248.
- Laviron, E., 1979. General Expression of the Linear Potential Sweep Voltammogram in the Case of Diffusionless Electrochemical System. *J. Electroanal. Chem.* 101, 19-28.
- Léger, C., Bertrand, P., 2008. Direct Electrochemistry of Redox Enzymes as a Tool for Mechanistic Studies. *Chem. Rev.* 108, 2379-2438.

- Leimkühler, S., Hodson, R., George, G.N., Rajagopalan, K.V., 2003. Recombinant *Rhodobacter capsulatus* Xanthine Dehydrogenase, a Useful Model System for the Characterization of Protein Variants Leading to Xanthinuria I in Humans. *J. Biol. Chem.* 278, 20802-20811.
- Leimkühler, S., Kern, M., Solomon, P.S., McEwan, A.G., Schwarz, G., Mendel, R.R., Klipp, W., 1998. Xanthine dehydrogenase from the phototrophic purple bacterium *Rhodobacter capsulatus* is more similar to its eukaryotic counterparts than to prokaryotic molybdenum enzymes. *Mol. Microbiol.* 27, 853-869.
- Leimkühler, S., Wuebbens, M.M., Rajagopalan, K.V., 2011. The History of the Discovery of the Molybdenum Cofactor and Novel Aspects of its Biosynthesis in Bacteria. *Coord. Chem. Rev.* 255, 1129-1144.
- Li, Q., Luo, G., Feng, J., 2001. Direct Electron Transfer for Heme Proteins Assembled on Nanocrystalline TiO₂ Film. *Electroanalysis* 13, 359-363.
- Li, Y., Schluesener, H.J., Xu, S., 2010. Gold nanoparticle-based biosensors. *Gold Bull.* 43, 29-41.
- Liu, S., Leech, D., Ju, H., 2003. Application of Colloidal Gold in Protein Immobilization, Electron Transfer, and Biosensing. *Anal. Lett.* 36, 1-19.
- Liu, X., Peng, W., Xiao, H., Li, G., 2005. DNA facilitating electron transfer reaction of xanthine oxidase. *Electrochem. Commun.* 7, 562-566.
- Marcus, R.A., 1993. Electron transfer reactions in chemistry. Theory and experiment. *Rev. Mod. Phys.* 65, 599-610.
- Marcus, R.A., Sutin, N., 1985. Electron transfers in chemistry and biology. *Biochim. Biophys. Acta* 811, 265-322.
- Marken, F., Paddon, C.A., Asogan, D., 2002. Direct cytochrome c electrochemistry at boron-doped diamond electrodes. *Electrochem. Commun.* 4, 62-66.
- Marquez, L.A., Dunford, H.B., 1997. Mechanism of the Oxidation of 3,5,3',5'-Tetramethylbenzidine by Myeloperoxidase Determined by Transient- and Steady-State Kinetics. *Biochemistry* 36, 9349-9355.
- Massey, V., Ghisla, S., Moore, E.G., 1979. 8-Mercaptoflavins as active site probes of flavoenzymes. *J. Biol. Chem.* 254, 9640-9650.
- Matsui, M., Takahashi, N., Ozaki, J.-ichi, 2011. Adsorption of cytochrome c on nanoshell carbon. *Carbon* 13, 4505-4510.
- McCord, J.M., Fridovich, I., 1968. The reduction of cytochrome c by milk xanthine oxidase. *J. Biol. Chem.* 243, 5753-60.
- McNeil, C.J., Athey, D., Ho, W.O., 1995. Direct electron transfer bioelectronic interfaces: application to clinical analysis. *Biosens. Bioelectron.* 10, 75-83.

- McNeil, C.J., Smith, K.A., Bellavite, P., Bannister, J.V., 1989. Application of the electrochemistry of cytochrome c to the measurement of superoxide radical production. *Free Radical Res.* 7, 89-96.
- Milliron, D.J., Hill, I.G., Shen, C., Kahn, A., Schwartz, J., 2000. Surface oxidation activates indium tin oxide for hole injection. *J. Appl. Phys.* 87, 572-576.
- Min, L., Jian-xing, X., 2007. Detoxifying function of cytochrome c against oxygen toxicity. *Mitochondrion* 7, 13-16.
- Misono, Y., Ohkata, Y., Morikawa, T., Itoh, K., 1997. Resonance raman and absorption spectroscopic studies on the electrochemical oxidation processes of 3,3',5,5'-tetramethylbenzidine. *J. Electroanal. Chem.* 436, 203-212.
- Murgida, D., Hildebrandt, P., 2006. Surface-Enhanced Vibrational Spectroelectrochemistry: Electric-Field Effects on Redox and Redox-Coupled Processes of Heme Proteins, in: Kneipp, K., Moskovits, M., Kneipp, H. (Eds.), *Surface-Enhanced Raman Scattering*. Springer Berlin Heidelberg, pp. 313-334.
- Murgida, D.H., Hildebrandt, P., 2001. Heterogeneous Electron Transfer of Cytochrome c on Coated Silver Electrodes. Electric Field Effects on Structure and Redox Potential. *J. Phys. Chem. B* 105, 1578-1586.
- Nakatani, H.S., dos Santos, L.V., Pelegrine, C.P., Terezinha, S., Gomes, M., Matsushita, M., de Souza, N.E., Visentainer, J.V., 2005. Biosensor Based on Xanthine Oxidase for Monitoring Hypoxanthine in Fish Meat. *Am. J. Biochem. Biotechnol.* 1, 85-89.
- Nicholson, R.S., 1965. Theory and Application of Cyclic Voltammetry for Measurement of Electrode Reaction Kinetics. *Anal. Chem.* 37, 1351-1355.
- Niki, K., Kawasaki, Y., Kimura, Y., Higuchi, Y., Yasuoka, N., 1987. Surface-enhanced Raman scattering of cytochromes c3 adsorbed on silver electrode and their redox behavior. *Langmuir* 3, 982-986.
- Oellerich, S., Wackerbarth, H., Hildebrandt, P., 2002. Spectroscopic Characterization of Nonnative Conformational States of Cytochrome c. *J. Phys. Chem. B* 106, 6566-6580.
- Olson, J.S., Ballou, D.P., Palmer, G., Massey, V., 1974. The Mechanism of Action of Xanthine Oxidase. *J. Biol. Chem.* 249, 4363-4382.
- Ow, Y.-L.P., Green, D.R., Hao, Z., Mak, T.W., 2008. Cytochrome c: functions beyond respiration. *Nat. Rev. Mol. Cell Biol.* 9, 532-542.
- Pacheco, A., Hazzard, J.T., Tollin, G., Enemark, J.H., 1999. The pH dependence of intramolecular electron transfer rates in sulfite oxidase at high and low anion concentrations. *J. Biol. Inorg. Chem.* 4, 390-401.
- Paggi, D.A., Martín, D.F., Kranich, A., Hildebrandt, P., Martí, M.A., Murgida, D.H., 2009. Computer simulation and SERR detection of cytochrome c dynamics at SAM-coated electrodes. *Electrochim. Acta* 54, 4963-4970.
- Paleček, E., 2005. *Electrochemistry of nucleic acids and proteins: towards electrochemical sensors for genomics and proteomics*, 1st ed. Elsevier, Amsterdam ; Boston.

- Panicco, P., Astuti, Y., Fantuzzi, A., Durrant, J.R., Gilardi, G., 2008. P450 versus P420: Correlation between Cyclic Voltammetry and Visible Absorption Spectroscopy of the Immobilized Heme Domain of Cyt P450 BM3. *J. Phys. Chem. B* 112, 14063-14068.
- Paulsen, K.E., Orville, A.M., Freman, F.E., Stankovich, M.T., Lipscomb, J.D., 1992. EPR-spectroelectrochemistry of mammalian electron-transfer flavoprotein-ubiquinone oxidoreductase. *Prog. Clin. Biol. Res.* 375, 69-73.
- Pingarrón, J.M., Yáñez-Sedeño, P., González-Cortés, A., 2008. Gold nanoparticle-based electrochemical biosensors. *Electrochim. Acta* 53, 5848-5866.
- Pinkerton, T.C., Hajizadeh, K., Deutsch, E., Heineman, W.R., 1980. Optically transparent thin-layer electrochemical flow cell for liquid chromatography. *Anal. Chem.* 52, 1542-1544.
- Porras, A.G., Palmer, G., 1982. The room temperature potentiometry of xanthine oxidase. pH-dependent redox behavior of the flavin, molybdenum, and iron-sulfur centers. *J. Biol. Chem.* 257, 11617-11626.
- Rajagopalan, K.V., Johnson, J.L., 1992. The pterin molybdenum cofactors. *J. Biol. Chem.* 267, 10199-10202.
- Ram, M.K., Bertoncello, P., Ding, H., Paddeu, S., Nicolini, C., 2001. Cholesterol biosensors prepared by layer-by-layer technique. *Biosens. Bioelectron.* 16, 849-856.
- Rao, C.N.R., Kulkarni, G.U., Thomas, P.J., Edwards, P.P., 2000. Metal nanoparticles and their assemblies. *Chem. Soc. Rev.* 29, 27-35.
- Rapson, T.D., Kappler, U., Bernhardt, P.V., 2008. Direct catalytic electrochemistry of sulfite dehydrogenase: mechanistic insights and contrasts with related Mo enzymes. *Biochim. Biophys. Acta* 1777, 1319-1325.
- Renault, C., Harris, K.D., Brett, M.J., Balland, V., Limoges, B., 2011. Time-resolved UV-visible spectroelectrochemistry using transparent 3D-mesoporous nanocrystalline ITO electrodes. *Chem. Commun.* 47, 1863.
- Richard, V., Murry, C., Jennings, R., Reimer, K., 1990. Oxygen-derived free radicals and postischemic myocardial reperfusion: therapeutic implications. *Fundam. Clin. Pharmacol.* 4, 85-103.
- Rodrigues, C.G., Wedd, A.G., Bond, A.M., 1991. Electrochemistry of xanthine oxidase at glassy carbon and mercury electrodes. *J. Electroanal. Chem.* 312, 131-140.
- Romão, M.J., 2009. Molybdenum and tungsten enzymes: a crystallographic and mechanistic overview. *Dalton Trans.* 4053-4068.
- Rudolph, M.J., Johnson, J.L., Rajagopalan, K.V., Kisker, C., 2003. The 1.2 Å structure of the human sulfite oxidase cytochrome b(5) domain. *Acta Crystallogr. D Biol. Crystallogr.* 59, 1183-1191.
- Rusling, J.F., Wang, B., Yun, S., 2008. Electrochemistry of Redox Enzymes, in: *Bioelectrochemistry: Fundamentals, Experimental Techniques and Applications*. P. N. Bartlett, Wiley, Chichester, pp. 39-85.

- Ryan, M.G., Ratnam, K., Hille, R., 1995. The Molybdenum Centers of Xanthine Oxidase and Xanthine Dehydrogenase. *J. Biol. Chem.* 270, 19209 -19212.
- Salamona, Z., Tollin, G., 1991. Bioelectrochemistry and Bioenergetics: Interfacial electrochemistry of cytochrome c at a lipid bilayer modified electrode: Effect of incorporation of negative charges into the bilayer on cyclic voltammetric parameters. *Bioelectr. Bioenerg.* 26, 321-334.
- Sardar, R., Funston, A.M., Mulvaney, P., Murray, R.W., 2009. Gold nanoparticles: past, present, and future. *Langmuir* 25, 13840-13851.
- Schardinger, F., 1902. Über das Verhalten der Kuhmilch gegen Methylenblau und seine Verwendung zur Unterscheidung von ungekochter und gekochter Milch. *Z. Untersuch Nahrungs Genussmittel.* 5, 1113-1121.
- Scheller, F.W., Wollenberger, U., Lei, C., Jin, W., Ge, B., Lehmann, C., Lisdat, F., Fridman, V., 2002. Bioelectrocatalysis by redox enzymes at modified electrodes. *Rev. Mol. Biotechn.* 82, 411-424.
- Scheller, W., Jin, W., Ehrentreich-Förster, E., Ge, B., Lisdat, F., Büttemeier, R., Wollenberger, U., Scheller, F.W., 1999. Cytochrome C Based Superoxide Sensor for In Vivo Application. *Electroanalysis* 11, 703-706.
- Schrader, N., Fischer, K., Theis, K., Mendel, R.R., Schwarz, G., Kisker, C., 2003. The crystal structure of plant sulfite oxidase provides insights into sulfite oxidation in plants and animals. *Structure* 11, 1251-1263.
- Schuhmann, W., Bensen, E.M., 2003. Biosensors, in: Bard, A.J. (Ed.), *Encyclopedia of Electrochemistry*. Wiley-VCH Verlag GmbH & Co. KGaA., Weinheim, Germany, pp. 350-384.
- Schwarz, G., 2005. Molybdenum cofactor biosynthesis and deficiency. *Cell. Mol. Life Sci* 62, 2792-2810.
- Senthilkumar, M., Mathiyarasu, J., Joseph, J., Phani, K.L.N., Yegnaraman, V., 2008. Electrochemical instability of indium tin oxide (ITO) glass in acidic pH range during cathodic polarization. *Mater. Chem. Phys.* 108, 403-407.
- Sezer, M., Spricigo, R., Utesch, T., Millo, D., Leimkühler, S., Mroginski, M.A., Wollenberger, U., Hildebrandt, P., Weidinger, I.M., 2010. Redox properties and catalytic activity of surface-bound human sulfite oxidase studied by a combined surface enhanced resonance Raman spectroscopic and electrochemical approach. *Phys. Chem. Chem. Phys.* 12, 7894-7903.
- Shan, D., Wang, Y., Zhu, M., Xue, H., Cosnier, S., Wang, C., 2009. Development of a high analytical performance-xanthine biosensor based on layered double hydroxides modified-electrode and investigation of the inhibitory effect by allopurinol. *Biosens. Bioelectron.* 24, 1171-1176.
- Shan, D., Wang, Y.-N., Xue, H.-G., Cosnier, S., Ding, S.-N., 2009. Xanthine oxidase/laponite nanoparticles immobilized on glassy carbon electrode: Direct electron transfer and multielectrocatalysis. *Biosens. Bioelectron.* 24, 3556-3561.

- Shipway, A.N., Katz, E., Willner, I., 2000. Nanoparticle Arrays on Surfaces for Electronic, Optical, and Sensor Applications. *ChemPhysChem* 1, 18-52.
- Situmorang, M., Hibbert, D.B., Gooding, J.J., Barnett, D., 1999. A sulfite biosensor fabricated using electrodeposited polytyramine: application to wine analysis. *Analyst* 124, 1775-1779.
- Spence, J.T., Kipke, C.A., Enemark, J.H., Sunde, R.A., 1991. Stoichiometry of electron uptake and the effect of anions and pH on the molybdenum and heme reduction potentials of sulfite oxidase. *Inorg. Chem.* 30, 3011-3015.
- Spricigo, R., 2009. Investigations of Sulfite Oxidase and the Molybdenum Cofactor at Surfaces. *PhD Thesis*, Universität Potsdam.
- Spricigo, R., Dronov, R., Lisdat, F., Leimkühler, S., Scheller, F., Wollenberger, U., 2009. Electrocatalytic sulfite biosensor with human sulfite oxidase co-immobilized with cytochrome c in a polyelectrolyte-containing multilayer. *Anal. Bioanal. Chem.* 393, 225-233.
- Spricigo, R., Dronov, R., Rajagopalan, K.V., Lisdat, F., Leimkühler, S., Scheller, F.W., Wollenberger, U., 2008. Electrocatalytically functional multilayer assembly of sulfite oxidase and cytochrome c. *Soft Matter* 4, 972.
- Spricigo, R., Richter, C., Leimkühler, S., Gorton, L., Scheller, F.W., Wollenberger, U., 2010. Sulfite biosensor based on osmium redox polymer wired sulfite oxidase. *Colloids Surf., A* 354, 314-319.
- Sternson, L.A., 1976. Electrochemical Determination of Xanthine Oxidase-Catalyzed Oxidation of Xanthine. *Anal. Lett.* 9, 641.
- Stjerna, B., Olsson, E., Granqvist, C.G., 1994. Optical and electrical properties of radio frequency sputtered tin oxide films doped with oxygen vacancies, F, Sb, or Mo. *J. Appl. Phys.* 76, 3797.
- Sullivan Jr., E.P., Hazzard, J.T., Tollin, G., Enemark, J.H., 1993. Electron transfer in sulfite oxidase: effects of pH and anions on transient kinetics. *Biochemistry* 32, 12465-12470.
- Suzuki, H., DeLano, F.A., Parks, D.A., Jamshidi, N., Granger, D.N., Ishii, H., Suematsu, M., Zweifach, B.W., Schmid-Schönbein, G.W., 1998. Xanthine oxidase activity associated with arterial blood pressure in spontaneously hypertensive rats. *Proc. Natl. Acad. Sci. U. S. A.* 95, 4754-4759.
- Svitel, J., Stredansky, M., Pizzariello, A., Miertus, S., 1998. Composite Biosensor for Sulfite Assay: Use of Water-Insoluble Hexacyanoferrate(III) Salts as Electron-Transfer Mediators. *Electroanalysis* 10, 591-596.
- Szamocki, R., Velichko, A., Mücklich, F., Reculosa, S., Ravaine, S., Neugebauer, S., Schuhmann, W., Hempelmann, R., Kuhn, A., 2007. Improved enzyme immobilization for enhanced bioelectrocatalytic activity of porous electrodes. *Electrochem. Commun.* 9, 2121-2127.
- Temple, C.A., Graf, T.N., Rajagopalan, K.V., 2000. Optimization of expression of human sulfite oxidase and its molybdenum domain. *Arch. Biochem. Biophys.* 383, 281-287.

- Thévenot, D.R., Toth, K., Durst, R.A., Wilson, G.S., 1999. Electrochemical Biosensors: Recommended Definitions and Classification. *Pure Appl. Chem.* 71, 2333-2348.
- Thévenot, D.R., Toth, K., Durst, R.A., Wilson, G.S., 2001. Electrochemical Biosensors: Recommended Definitions and Classification. *Anal. Lett.* 34, 635.
- Thomas, A., Schlaad, H., Smarsly, B., Antonietti, M., 2003. Replication of Lyotropic Block Copolymer Mesophases into Porous Silica by Nanocasting: Learning about Finer Details of Polymer Self-Assembly. *Langmuir* 19, 4455-4459.
- Topoglidis, E., Astuti, Y., Duriaux, F., Grätzel, M., Durrant, J.R., 2003. Direct Electrochemistry and Nitric Oxide Interaction of Heme Proteins Adsorbed on Nanocrystalline Tin Oxide Electrodes. *Langmuir* 19, 6894-6900.
- Topoglidis, E., Cass, A.E.G., Gilardi, G., Sadeghi, S., Beaumont, N., Durrant, J.R., 1998. Protein Adsorption on Nanocrystalline TiO₂ Films: An Immobilization Strategy for Bioanalytical Devices. *Anal. Chem.* 70, 5111-5113.
- Topoglidis, E., Cass, A.E.G., O'Regan, B., Durrant, J.R., 2001. Immobilisation and bioelectrochemistry of proteins on nanoporous TiO₂ and ZnO films. *J. Electroanal. Chem.* 517, 20-27.
- Truglio, J.J., Theis, K., Leimkühler, S., Rappa, R., Rajagopalan, K.V., Kisker, C., 2002. Crystal Structures of the Active and Alloxanthine-Inhibited Forms of Xanthine Dehydrogenase from *Rhodobacter capsulatus*. *Structure* 10, 115-125.
- Umasankar, Y., Kumar, S.A., Chen, S.-ming, 2009. Nanostructured Materials for Electrochemical Biosensors. Nova Science Pub Inc.
- Urbanová, V., Vytras, K., Kuhn, A., 2010. Macroporous antimony film electrodes for stripping analysis of trace heavy metals. *Electrochem. Commun.* 12, 114-117.
- Wackerbarth, H., Klar, U., Gunther, W., Hildebrandt, P., 1999. Novel Time-Resolved Surface-Enhanced (Resonance) Raman Spectroscopic Technique for Studying the Dynamics of Interfacial Processes: Application to the Electron Transfer Reaction of Cytochrome c at a Silver Electrode. *Appl. Spectrosc.* 53, 283-291.
- Wang, J., Li, M., Shi, Z., Li, N., Gu, Z., 2002. Direct electrochemistry of cyt c at a glassy carbon electrode modified with single-wall carbon nanotubes. *Anal. Chem.* 74, 1993-1997.
- Wang, L., Yuan, Z., 2004. Direct Electrochemistry of Xanthine Oxidase at a Gold Electrode Modified with Single-Wall Carbon Nanotubes. *Anal. Sci.* 20, 635-638.
- Wang, S., Guo, Z., Zhang, H., 2011. Direct electrochemistry of cytochrome c entrapped in agarose hydrogel in room temperature ionic liquids. *Bioelectrochemistry* 82, 55-62.
- Wang, Y., Brezesinski, T., Antonietti, M., Smarsly, B., 2009. Ordered mesoporous Sb-, Nb-, and Ta-doped SnO₂ thin films with adjustable doping levels and high electrical conductivity. *ACS Nano* 3, 1373-1378.
- Wegerich, F., Turano, P., Allegrozzi, M., Möhwald, H., Lisdat, F., 2009. Cytochrome C mutants for superoxide biosensors. *Anal. Chem.* 81, 2976-2984.

- Weidinger, I.M., Murgida, D.H., Dong, W.-F., Möhwald, H., Hildebrandt, P., 2006. Redox processes of cytochrome c immobilized on solid supported polyelectrolyte multilayers. *J. Phys. Chem. B* 110, 522-529.
- Willit, J.L., Bowden, E.F., 1990. Adsorption and redox thermodynamics of strongly adsorbed cytochrome c on tin oxide electrodes. *J. Phys. Chem.* 94, 8241-8246.
- Wilson, H.L., Rajagopalan, K.V., 2004. The role of tyrosine 343 in substrate binding and catalysis by human sulfite oxidase. *J. Biol. Chem.* 279, 15105-15113.
- Wollenberger, U., 2005. Third generation biosensors — integrating recognition and transduction in electrochemical sensors, in: L. Gorton (Eds.) *Biosensors and Modern Biospecific Analytical Techniques*, in D. Barcelo (Eds.) *Comprehensive Analytical Chemistry Vol. XLIV, Bioanalytic*, 44. Elsevier, Amsterdam, pp. 65-130.
- Wollenberger, U., Spricigo, R., Leimkühler, S., Schröder, K., 2008. Protein Electrodes with Direct Electrochemical Communication, in: *Biosensing for the 21st Century, Advances in Biochemical Engineering/Biotechnology*. pp. 19-64.
- Wu, Y., Hu, S., 2007. Direct electron transfer of xanthine oxidase and its catalytic reduction to nitrate. *Anal. Chim. Acta* 602, 181-186.
- Xu, X., Tian, B., Zhang, S., Kong, J., Zhao, D., Liu, B., 2004. Electrochemistry and biosensing reactivity of heme proteins adsorbed on the structure-tailored mesoporous Nb₂O₅ matrix. *Analytica Chimica Acta* 519, 31-38.
- Yang, T., Jiao, K., Wang, Z.-J., 2005. A Thin-layer Spectroelectrochemical Study of 3, 3', 5, 5'-Tetramethylbenzidine at Optically Transparent Pt Minigrid Electrode. *Chin. J. Appl. Chem.* 22, 355-360.
- Yeh, P., Kuwana, T., 1977. Reversible electrode reaction of cyt c. *Chem. Lett.* 1145-1148.
- Zhang, X., Wang, J., Wu, W., Qian, S., Man, Y., 2007. Immobilization and electrochemistry of cytochrome c on amino-functionalized mesoporous silica thin films. *Electrochem. Commun.* 9, 2098-2104.
- Zhang, Y., Asahina, S., Yoshihara, S., Shirakashi, T., 2003. Oxygen reduction on Au nanoparticle deposited boron-doped diamond films. *Electrochim. Acta* 48, 741-747.
- Zhou, H., Xu, Y., Chen, T., Suzuki, I., Li, G., 2006. Electrochemistry of xanthine oxidase and its interaction with nitric oxide. *Anal. Sci.* 22, 337-340.

7 List of publications

- I. **Mesoporous Indium Tin Oxide as a Novel Platform for Bioelectronics**
Stefano Frasca, Till von Graberg, Jiu-Ju Feng, Arne Thomas, Bernd M. Smarsly, Inez M. Weidinger, Frieder W. Scheller, Peter Hildebrandt, Ulla Wollenberger
ChemCatChem 2 (2010) 839-845.
- II. **A new type of microemulsion consisting of two halogen-free ionic liquids and one oil component**
Oscar Rojas, Brigitte Tiersch, Stefano Frasca, Ulla Wollenberger, Joachim Koetz
Colloids and Surfaces A: Physicochemical and Engineering Aspects 369 (2010) 82-87.
- III. **A Molecular Precursor Approach to Tunable Porous *Tin-rich* Indium Tin Oxide with Durable High Electrical Conductivity for Bioelectronic Devices**
Yilmaz Aksu, Stefano Frasca, Ulla Wollenberger, Matthias Driess, Arne Thomas
Chemistry of Materials 23 (2011) 1798-1804.
- IV. **Electrochemical switchable protein-based optical device**
Stefano Frasca, Claudia Richter, Till von Graberg, Bernd M. Smarsly, Ulla Wollenberger
Engineering in Life Sciences 6 (2011) 554-558.
- V. **Human sulfite oxidase electrochemistry on gold nanoparticles modified electrode**
Stefano Frasca, Oscar Rojas, Johannes Salewski, Bettina Neumann, Konstanze Stiba, Inez M. Weidinger, Brigitte Tiersch, Silke Leimkühler, Joachim Koetz, Ulla Wollenberger.
Bioelectrochemistry (2012) doi:10.1016/j.bioelechem.2011.11.012.
- VI. **Biosensing using optical transparent conductive electrode materials**
Stefano Frasca, Anna Fischer, Ulla Wollenberger
In preparation.
- VII. **Characterization of XDH variants from *Rhodobacter capsulatus* using direct electron transfer and spectroelectrochemistry**
Stefano Frasca, Silke Leimkühler, Ulla Wollenberger
In preparation.

8 List of presentations

I. Poster presentations:

22.-25.03.2009

7th Spring Meeting of the International Society of Electrochemistry, Szczyrk (Poland):

- “Direct Protein Electrochemistry in 3D-Mesoporous ITO Electrodes”

5.-10.07.2009

6th Gordon Research Conference on Mo & W Enzymes, Barga (Italy):

- “The role of the two [2Fe2S] clusters in *Rhodobacter capsulatus* xanthine dehydrogenase”

26.-28.05.2010

Biosensors 2010, 20th Anniversary World Congress on Biosensors, Glasgow (UK):

- “Cytochrome c loaded mesoporous indium tin oxide (mpITO) superoxide biosensor”
- “Electrochemical studies and application of Molybdo-enzymes”

13.-15.09.2010

Biochemistry 2010, Bochum (Germany):

- “Electrochemical behavior of Mammalian Xanthine Oxidase Homologues”

26.09-01.10.2010

61th Annual meeting of ISE, Nizza (France):

- “Mesoporous ITO and *Tin-rich* ITO as a Novel Platform for Bioelectronics”

06.-10.03-2011

Hybrid Materials 2011, Strasbourg (France):

- “Gold Nanoparticles with Defined Size as Support for the Direct Electron Transfer and Catalysis of the human Sulfite Oxidase”

II. Oral presentations:

29.03.-01.04.2009

6. Deutschen BioSensor Symposium, Freiburg (Germany):

- “Immobilization and Bioelectrochemical Behaviour of Cytochrome c in Mesoporous ITO Electrodes”

03.-06.04.2011

7. Deutschen BioSensor Symposium, Heiligenstadt (Germany):

- “Protein-modifizierte mesoporöse Materialien für elektrochemische und optische Detektion“

08.12.-05.2011

XXI International Symposium on Bioelectrochemistry and Bioenergetics of the BES, Kraków (Poland):

- “Biosensing System based on the Electrocatalytic Activity of *human* Sulfite Oxidase supported by Ultrafine Au nanoparticles with Defined Size”

9 Acknowledgements

Zuerst möchte ich mich vor allem bei meiner Doktormutter Prof. Dr. Ulla Wollenberger für die Einführung in die interessanten und interdisziplinären Projekte, sowie in die elektrochemische Welt bedanken. Des Weiteren bedanke ich mich bei Prof. Dr. Silke Leimkühler für ihre Hilfe in der Protein- und Moco-Welt. Außerdem wurde mir, durch die Doktorarbeit, eine sehr interessante und lehrreiche Erfahrung in Deutschland ermöglicht, wofür ich beiden zu großem Dank verpflichtet bin.

Weiterhin bedanke ich mich für die angenehme Arbeitsatmosphäre, die produktive Zusammenarbeit und die erfolgreichen Diskussionen im Labor bei Arto Badalyan, Miriam Adamovski, Clement Comminges, Thomas Dietz, Andrea Kühn, Lei Peng, Roberto Spricigo, C. Merlin Tientcheu, Aysu Yarman, Cigdem Yildirim und bei allen aktuellen und ehemaligen Mitarbeitern der AG Leimkühler.

Besonderer Dank gilt meinen beiden hilfreichen und netten Studentinnen Claudia Richter und Bettina Neumann. Sie haben viel Zeit und Engagement darin verwendet, meine, nicht immer schlaun Ideen auszuprobieren und umzusetzen.

Großer Danke gebührt Patrick Schulz, der aus meinen verrückten Ideen echte und funktionierende Zellen gebaut hat, ohne diese meine Experimente unmöglich gewesen wären.

Außerdem bedanke ich mich ganz herzlich bei den vielen Kollaborationspartnern, wie Till von Graberg und Prof. Dr. Bernd M. Smarsly von der JLU Gießen, sowie Prof. Dr. Peter Hildebrandt, Dr. Inez M. Weidinger, Johannes Salewski, Dr. Jiu-Ju Feng, Dr. Anna Fischer, Dr. Fernando Pérez Caballero und Dr. Yilmaz Aksu von der TU Berlin.

Weiterer Dank gilt Prof. Dr. Frieder W. Scheller und Dr. habil. Axel Warsinke für die vielen hilfreichen Diskussionen und Ratschläge.

I acknowledge also Prof. P. V. Bernhardt from University of Queensland (Brisbane, Australia) for the scientific experience and for the terrific possibility to visit the Down Under.

¿Y come no agradecer el Tico de las nanopartículas Oscar Rojas? Sobre todo por su entusiasmo contagioso en el trabajo, la comida, en la cerveza y sin duda en el fútbol.

Un grande grazie va agli ex-compagni di casa Jörn, Mario, Viola e Manuela per l'introduzione alla Deutsche Vita e a Franziska, Valentina, Francesco per non farmi mancare mai un pezzo di casa vicino anche a 1546 km di distanza.

Per concludere ringrazio tutti gli amici Colleferrini, Romani, Fiorentini, Universitari, CERMiani, Calcistici, Fantacalcistici, PerMnganini, Capoeristi che si ricordano sempre di me.

Infine mi piacerebbe ringraziare mio padre Carlo, mia madre Luisa e mio fratello Daniele per l'affetto e il supporto morale in tutti questi anni distanti.

An alle GRAZIE!

Lebenslauf



Persönliche Angaben

Name: Stefano Frasca
Geburtsdatum: 12. Januar 1981
Geburtsort: Colleferro (Italien)
Telefon: +49 15201787561
E-Mail: stefano.frasca@uni-potsdam.de
frascas@inwind.it

Hochschulausbildung

02/2008 – heute Promotionsstudium Analytische Biochemie, Universität Potsdam im Rahmen des Exzellenzclusters "Unifying Concepts in Catalysis" (UniCat). Dissertationsthema: „Biocatalysis on Nanostructured Surfaces: Investigation and Application of Redox Proteins using Spectro-Electrochemical Methods“
02/2006 – 08/2006 Diplomarbeit an der Università di Roma „La Sapienza“
Thema: „Synthese von Berberin-basierten Alkaloiden mittels Suzuki-Kupplungsreaktion“
09/2000 – 07/2006 Diplomstudium Chemie, Spezialisierung Organische Chemie, Università di Roma „La Sapienza“ (Italien)
Abschluss: Dottore in Chimica
(Gesamtprädikat: 110 von 110 Punkten)

Praktische Tätigkeiten

02/2008 – heute Wissenschaftliche Mitarbeiter / Doktorand an der Universität Potsdam (Deutschland)
12/2010 Examens-Prüfer für iSQI GmbH International Software Quality Institute, Potsdam (Deutschland)
10/2006 – 01/2008 Wissenschaftliche Mitarbeiter am CERM (Centre of Magnetic Resonance), Università di Firenze (Italien)
09/2004 – 08/2005 Mitarbeiter im Erasmusbüro der Università di Roma „La Sapienza“ (Italien)

Auslandsaufenthalte

10/2010 – 11/2010 Forschungsaufenthalt an der University of Queensland (Australien)
08/2006 – 09/2006 Forschungsaufenthalt an der Université de Liège (Belgien)
09/2004 – 08/2005 Studienaufenthalt an der Universidad de Navarra (Spanien)

Schulbildung

09/1995 – 06/2000 ITIS S. Cannizzaro in Colleferro (Italien), Schwerpunkt Industrielle Chemie, Abschluss: Abitur (Note: 92 von 100 Punkten)

Sprachkenntnisse

Deutsch	sehr gute Kenntnisse
Italienisch	Muttersprache
Englisch	verhandlungssicher
Spanisch	verhandlungssicher
Französisch	Gute Kenntnisse

Promotionsbegleitende Aktivitäten

01/2012	Führungskompetenzen Workshop
07/2010	Entrepreneurial Postgraduate Education (EPE, Science goes Market)
02/2010	Intercultural Communication Workshop

Interessen

Mitglied im Fußballverein „FC Britische Löwen“, Salsatanzen, Reisen, Geschichte und Geopolitik.